Check for updates

Advanced Sensor Research

ADVANCED SENSOR RESEARCH Open Access

www.advsensorres.com

REVIEW OPEN ACCESS

Cortisol Dynamics at High Temporal Resolution For Wearable Biosensor Research

Munia Ferdoushi[1,2] | Tess Billings[1,3] | Wenxin Cai[1] | Yasser Khan[1,4,5]

[1]Ming Hsieh Department of Electrical and Computer Engineering, University of Southern California, Los Angeles, California, USA | [2]Department of Electrical and Electronic Engineering, Bangladesh University of Engineering and Technology, Dhaka, Bangladesh | [3]Department of Biochemistry, Vassar College, Poughkeepsie, New York, USA | [4]Alfred E. Mann Department of Biomedical Engineering, University of Southern California, Los Angeles, California, USA | [5]The Institute for Technology and Medical Systems (ITEMS), Keck School of Medicine, University of Southern California, Los Angeles, California, USA

Correspondence: Yasser Khan (yasser.khan@usc.edu)

Received: 24 May 2026 | **Revised:** 16 September 2026 | **Accepted:** 26 September 2026

Keywords: bioelectronics | cortisol | stress | wearable sensors

ABSTRACT

Cortisol is a dynamic endocrine biomarker regulated by hypothalamic–pituitary–adrenal (HPA) axis activity, and plays a central role in circadian regulation and physiological stress responsiveness. This review summarizes key aspects of cortisol dynamics, including circadian rhythms, modulatory factors, dysregulation, and acute and chronic stress responses. We further examine commonly used laboratory stress-induction paradigms, such as the Trier Social Stress Test, Cold Pressor Test, Maastricht Acute Stress Test, cognitive stressors, and multicomponent stress protocols, with an emphasis on their applicability to wearable cortisol sensor development. Particular attention is given to experimental design considerations, including the choice of sampling matrix, sensor-influenced temporal resolution, and acquisition frequency, as these parameters critically influence the interpretation of cortisol fluctuations and define the performance requirements of sensing platforms. To complement the literature review, we additionally report preliminary observations from a pilot study involving three healthy adult participants. The pilot experiments explore the feasibility of selected stress-induction protocols for eliciting measurable stress responses using a dense temporal sampling protocol. By integrating insights from prior studies with our pilot observations, we highlight methodological considerations for capturing physiologically meaningful cortisol responses to stress, with a specific focus on stress-induced dynamics and the temporal resolution necessary for continuous or near-continuous monitoring.

1 | Introduction

Cortisol, a glucocorticoid commonly referred to as the stress hormone, is one of the most important regulators of physiological homeostasis [1]. It influences a wide range of human bodily processes, including metabolism, immune function, cardiovascular regulation, and neurobehavioral processes, through its pervasive effects on glucocorticoid receptors present in nearly all human tissues. The hypothalamic–pituitary–adrenal (HPA) axis, a complex neuroendocrine network, controls cortisol secretion by integrating environmental and psychological stimuli to facilitate adaptive stress responses. Cortisol's key functions are to mobilize energy resources and maintain physiological stability in response to internal and external threats to homeostasis, thereby mediating the "fight-or-flight response." Cortisol also regulates blood glucose levels by promoting gluconeogenesis, thereby linking stress physiology to long-term metabolic health [2, 3]. Cortisol dysregulation, manifested as hypercortisolism, is associated with a wide range of neuropsychiatric and metabolic disorders, including Cushing syndrome, depression, anxiety, and increased susceptibility to epileptic seizures [4–6]. Cortisol is also closely linked to performance, often exerting a U-shaped effect

This is an open access article under the terms of the Creative Commons Attribution License, which permits use, distribution and reproduction in any medium, provided the original work is properly cited.

© 2026 The Author(s). *Advanced Sensor Research* published by Wiley-VCH GmbH

on productivity [7]. Moderate cortisol levels have been shown to support optimal motivation, alertness, and cognitive function, whereas both deficient and excessive levels can compromise performance. Low cortisol is associated with reduced drive and alertness, while elevated cortisol, particularly during chronic stress, can impair cognition and decision-making.

Given the widespread effects of cortisol on human bodily functions and behavioral responses, a comprehensive understanding of cortisol dynamics is essential for distinguishing normal physiological regulation from pathological conditions. Consequently, research into cortisol dynamics and the factors influencing them, such as circadian rhythms and stress-induced variation, has expanded across medical, psychiatric, and bioengineering fields. Despite these advances, effective integration across these domains remains limited, underscoring the need for interdisciplinary frameworks that connect physiological insights to technological applications.

The development and validation of cortisol sensors capable of quantifying cortisol concentrations in various bodily fluids often rely on laboratory-based stress-induction paradigms designed to approximate real-world psychological or physiological stressors. However, variability in individual stress responsivity, experimental conditions, sampling matrices, and temporal resolution presents significant challenges in developing robust experimental protocols. A particularly critical factor is the timing of sample acquisition, as cortisol responses exhibit characteristic delays and recovery phases following stress exposure. Insufficient sampling frequency may fail to capture key features of cortisol kinetics, including onset latency, peak magnitude, time to peak, and recovery rate. Although many studies rely on salivary cortisol measurements collected at 5–10-min intervals [8, 9], higher temporal resolution can reveal finer features of cortisol kinetics. This is especially relevant for emerging wearable or minimally invasive cortisol sensing platforms, where continuous or near-continuous monitoring could provide a more physiologically accurate representation of stress-related endocrine activity. An understanding of the required temporal resolution can inform key design parameters for sensor development, including acquisition frequency, hardware performance, data storage capacity, sample volume requirements, and operational lifetime or replacement frequency.

In this review, we investigate cortisol dynamics at high temporal resolution to inform the design and validation of wearable biosensors. We review key factors influencing cortisol dynamics, including circadian rhythms and stress, and evaluate commonly used laboratory-based stress-induction protocols. We also discuss how the interpretation of these dynamics may be influenced by sampling method, medium, and sensor characteristics. To complement the existing literature, we conduct a pilot study (n = 3) using standardized stress tests, including the Cold Pressor Test (CPT), cognitive tasks, and exercise, and descriptively compare salivary cortisol profiles over time across participants. We implement a high-frequency sampling protocol, with measurements collected at intervals of 3 or 10 min, to characterize temporal changes in cortisol and explore interindividual variability. Preliminary observations revealed distinct participant- and protocol-dependent cortisol trajectories. Following the CPT, all three participants exhibited post-stressor cortisol increases, with differences in peak magnitude, timing, and recovery. The cognitive and exercise protocols produced more variable trajectories, including early, delayed, or no distinct peaks within the observation windows. These pilot observations highlight the potential importance of stressor type, sampling time, and interindividual variability in cortisol kinetics and provide preliminary experimental guidance for the development and evaluation of wearable biosensors and multimodal stress–monitoring systems.

2 | Cortisol Dynamics

The release of cortisol is predominantly orchestrated by neural pathways (Figure 1), with the HPA axis playing a central role. Specifically, the hypothalamus secretes corticotropin-releasing hormone (CRH) from neurons in the paraventricular nucleus (PVN), with arginine vasopressin (AVP) acting together with CRH to prompt the anterior pituitary gland to release adrenocorticotropic hormone (ACTH) into the bloodstream [10]. ACTH then stimulates the adrenal cortex (the outer layer of the adrenal glands, located above the kidneys), particularly the zona fasciculata, initiating the production and secretion of glucocorticoids, of which cortisol is the most prominent, via a process called steroidogenesis [11]. As a steroid hormone, cortisol is not stored in vesicles; instead, it is synthesized as needed and promptly diffuses from the cells into the circulatory system upon production. Within the bloodstream, roughly 90% of cortisol binds to corticosteroid-binding globulin, while about 5%–7% associates with albumin, leaving only a small fraction (approximately 3%–5%) to circulate as free cortisol. To prevent excessive secretion, cortisol exerts a negative feedback effect on both the hypothalamus and the pituitary, thereby inhibiting further release of CRH and ACTH.

Cortisol regulation involves two primary mechanisms: the normal pattern, dominated by the circadian rhythm, with the highest concentrations observed upon waking and the lowest during the nocturnal hours, overlaid with cortisol secretion occurring in hourly pulses [12]. The other mechanism is HPA axis activation in response to stressful events or stimuli that disrupt homeostasis, as well as the anticipation of such events. The subsequent subsections provide a description of each of these mechanisms, as well as the external factors that lead to deviations from the typical pattern.

2.1 | Circadian Rhythm

The rhythmic oscillation of cortisol levels throughout a 24-h cycle, known as the circadian rhythm, is a fundamental aspect of HPA axis regulation and significantly influences physiological processes [13]. Liddle's early work on human adrenocortical secretory activity demonstrated a clear daily rhythm in 17-hydroxycorticosteroids, a biochemical marker associated with cortisol secretion. More broadly, circadian glucocorticoid rhythmicity is observed across many mammalian species; however, its phase depends on the organism's activity pattern. In humans and many diurnal mammals, cortisol levels are generally highest near the beginning of the active phase, producing a morning "crest" and an evening "trough." Cortisol is typically elevated upon awakening, increases further to a peak within approximately 30–45 min as part of the cortisol awakening response (CAR),

27511219, 2026, 10, Downloaded from https://advanced.onlinelibrary.wiley.com/doi/10.1002/adsr.70212 by Yasser Khan - Mount Sinai Hospital , Wiley Online Library on [14/10/2026]. See the Terms and Conditions (https://onlinelibrary.wiley.com/terms-and-conditions) on Wiley Online Library for rules of use; OA articles are governed by the applicable Creative Commons License

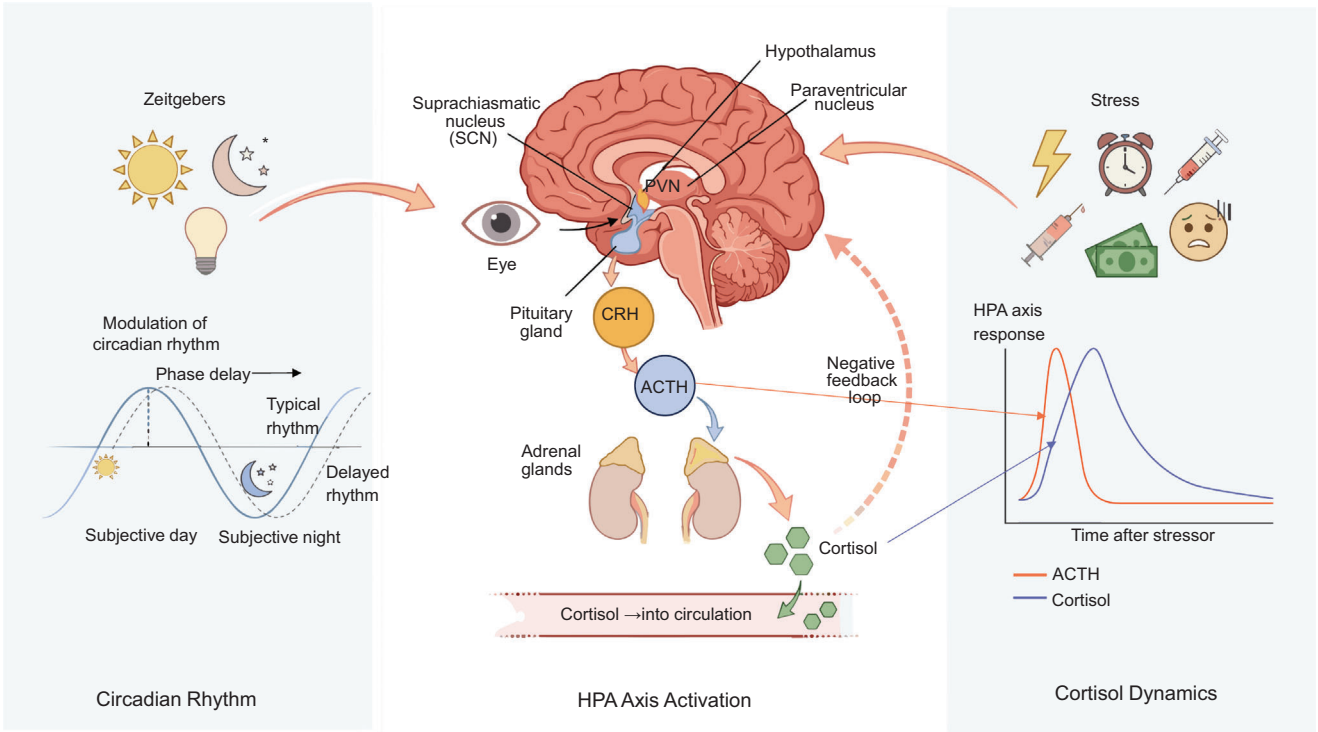


FIGURE 1 | Regulation of cortisol by circadian rhythms and stress via the HPA axis. External zeitgebers (light–dark cycles) entrain the circadian rhythm through the suprachiasmatic nucleus (SCN) of the hypothalamus, modulating basal cortisol secretion. In response to stress, activation of the neurons of the PVN triggers the release of corticotropin-releasing hormone (CRH), stimulating the pituitary gland to secrete adrenocorticotropic hormone (ACTH), which in turn activates the adrenal glands to produce cortisol. Cortisol is released into circulation, generating time-dependent stress response profiles.

and then gradually declines throughout the day. In contrast, nocturnal species often exhibit a phase-shifted glucocorticoid rhythm, with peak levels occurring near the onset of their active period during the dark phase rather than in the morning [14]. External cues, primarily the solar cycle, play a key role in regulating this rhythm. Light perceived by the retina activates the central circadian clock in the brain's suprachiasmatic nucleus (SCN), which coordinates the behavioral activity and rest periods. This central clock then synchronizes peripheral clocks in nearly every tissue, leading to increased circulating cortisol through the stimulation of the pituitary gland to produce ACTH. The circadian rhythm plays a crucial role in maintaining homeostasis and modulating responses to stressors; understanding it is essential for comprehending both normal physiological functioning and the pathogenic mechanisms underlying stress-related disorders.

2.1.1 | Modulators of Circadian Rhythm

The 24-h periodicity of the circadian rhythm has long prompted investigation into the search for its primary modulator. This rhythm is regulated by the SCN, the body's central circadian pacemaker, with secondary clocks in other brain regions and peripheral tissues, including the adrenal glands. This central clock synchronizes peripheral clocks, boosting cortisol production via ACTH from the pituitary gland. Light exposure through the retina is a major environmental cue that entrains the central circadian clock, which regulates active and rest periods and coordinates peripheral clocks throughout the body (Figure 1) [15]. However, early studies suggested that the ACTH–cortisol rhythm is not solely dependent on external light input, posture, or sleep–wake behavior. For example, investigations in bedridden and blind individuals showed that the rhythm persisted even in the absence of postural changes or visual input [16], though shifts in the sleep–wake schedule could alter the timing of cortisol metabolites [17]. Later, Orth et al. further demonstrated that even under abnormal or absent sleep cycles, plasma cortisol maintained a 24-h periodicity, establishing its origin in an endogenous circadian oscillator rather than in the sleep schedule alone [18]. Together, these findings indicate that cortisol rhythmicity is primarily driven by the SCN as the central biological clock, entrained by light, and modulated by sleep–wake patterns and stress exposure [19].

Due to the complexity of this mechanism and its underlying multifaceted nature, various studies have focused on systematically modeling the stimuli and responses via phase response curves. Light is the most commonly studied stimulus in these phase response curves, which quantify the magnitude and direction of phase shifts (advances or delays) in a circadian rhythm caused by a brief external cue (zeitgeber, or "time-giver") [20, 21]. The SCN acts as the master circadian clock, aligning physiological and behavioral oscillations to day/night (activity/inactivity) transitions, with light entraining its ventrolateral core (SCN core). This core then communicates with the dorsomedial shell (SCN shell) via vasoactive intestinal polypeptide (VIP), which in turn outputs AVP (arginine vasopressin) to entrain the HPA axis, resulting in rhythmic glucocorticoid secretion. To stimulate

27511219, 2026, 10, Downloaded from https://advanced.onlinelibrary.wiley.com/doi/10.1002/adsr.70212 by Yasser Khan - Mount Sinai Hospital , Wiley Online Library on [14/10/2026]. See the Terms and Conditions (https://onlinelibrary.wiley.com/terms-and-conditions) on Wiley Online Library for rules of use; OA articles are governed by the applicable Creative Commons License

synchronization within the SCN and between the SCN and the HPA axis under light entrainment,Li and Androulakis built a semi-mechanistic mathematical model linking these layers (light → SCN core → SCN shell → HPA axis). The model successfully replicated experimentally observed phase relationships, such as those in which light exposure during the early subjective night delays the circadian rhythm, while light exposure during the late night or early day slightly advances it [22]. Their analysis of virtual populations revealed significant interindividual variability in circadian flexibility; individuals with higher light sensitivity and stronger AVP coupling strength resynchronized their cortisol rhythms more rapidly following a jet lag perturbation, reflecting greater responsiveness of the adrenal–suprachiasmatic coupling to external light cues. In humans, the intrinsic circadian period, typically around 24.2 h, naturally favors phase delays, consistent with the notion that eastward travel is harder. In addition to air travel, night-shift simulations indicated that alternating-shift and transient-shift schedules may affect cortisol rhythmicity differently. In their simulation, some individuals with higher light sensitivity maintained approximately 24-h oscillations with a phase offset, suggesting better long-term tolerance, whereas others lost their circadian rhythm. Transient shift work was particularly detrimental to individuals with higher light sensitivity. These findings imply that circadian plasticity varies significantly among individuals due to differences in coupling strengths, and that light therapy could benefit individuals with low light sensitivity in adapting to shift work or jet lag. The broader influence of light therapy is further supported by a study by Figueiro et al., which reported that no significant differences were found between early and late chronotypes (chronotype identified via preference for activity timing) following light therapy. However, the study assessed circadian phase using melatonin rather than cortisol [23].

2.1.2 | Dysregulation of Circadian Rhythm

Circadian rhythm persists even in individuals with atypical sleep schedules, such as shift workers; however, it often becomes phase-shifted, reduced in amplitude, or desynchronized relative to environmental light–dark cycles and behavioral patterns. Night-shift and rotating-shift workers exhibit reduced or delayed CAR (cortisol awakening response), flatter diurnal slopes, and elevated evening cortisol compared to day workers, reflecting a misaligned HPA axis rhythm characterized by shift work disorder (SWD), a circadian rhythm disorder associated with working outside typical 8-to-5 shifts [24–27].

People who frequently experience jet lag, such as airline crews, often face symptoms that worsen with the number of time zones crossed and when traveling eastwards. Mood changes, particularly dysphoria, are a significant component of jet lag, with eastward travel notably disturbing sleep and increasing anxiety and depression levels [28].

In addition to jet lag and shift work, social jet lag represents a common form of circadian misalignment arising from differences in sleep timing between workdays and free days. This discrepancy reflects the conflict between an individual's biological timing and externally imposed social or occupational schedules and is often greater in individuals with later chronotypes [29, 30]. Social jet lag and other forms of circadian disruption have been associated with adverse metabolic, cardiovascular, neurological, and psychiatric outcomes [30, 31].

Flattened or phase-shifted cortisol rhythms are linked to impaired glucose tolerance, insulin resistance, and increased risk of type 2 diabetes and obesity, as well as heightened cardiovascular risks including hypertension and non-dipping blood pressure profiles [32–34]. Psychiatric outcomes are also affected: circadian misalignment and cortisol rhythm disruption increase vulnerability to depression, bipolar disorder, and seasonal affective disorder, with laboratory misalignment experiments showing heightened mood disturbances under shifted schedules [21]. Widespread circadian rhythm disruption is likely a contributing factor to the prevalence of mood disorders and mood vulnerability [35]. Furthermore, because cortisol is immunoregulatory, loss of rhythmic control can contribute to chronic low-grade inflammation and impaired immune function.

Importantly, misaligned rhythms also alter acute stress responsiveness. Shift workers and individuals with chronic HPA dysregulation frequently display blunted cortisol reactivity in laboratory stress tests, such as the Trier Social Stress Test (TSST) or CPTs [36]. Such blunting has also been documented in occupational burnout, where emotional exhaustion correlates with diminished cortisol responses to stress exposure [37]. The "non-responders" phenomenon (in which individuals show minimal cortisol response in laboratory stress tests) may be more common in those with chronically disrupted rhythms. Although the exact patterns may differ, circadian misalignment generally impairs the system's capacity to mount strong acute stress responses and diminishes the flexibility of the HPA axis, leaving baseline cortisol levels elevated or misaligned. This combination increases vulnerability to metabolic, cardiovascular, and mental health problems while decreasing resilience.

2.2 | Stress Response

The stress response represents an intricate, adaptive, and evolutionarily conserved physiological mechanism, during which the HPA axis undergoes transient activation, resulting in elevated and sustained secretory activity of CRH and ACTH. Subsequently, cortisol initiates a rapid negative feedback loop targeting both the hypothalamus and the pituitary. This action serves to attenuate the further release of CRH and ACTH, thereby preventing excessive activation of the HPA axis. The complex dynamics of the HPA axis stress response are characterized by distinct temporal phases [1].

Upon exposure to acute stress, the anterior pituitary gland rapidly secretes ACTH, typically within minutes. This surge in ACTH, which usually peaks approximately 15 min after the onset of the stressor, is transient and tightly regulated by swift, non-genomic feedback mechanisms. Rat experiments found the subsequent glucocorticoid response to be delayed, as they must be synthesized in the adrenal cortex, resulting in plasma corticosterone levels peaking 30 to 60 min after stress initiation [38]. This response lasts longer than the ACTH pulse and is regulated by the combined effects of metabolic clearance and active feedback, typically exhibiting a "rise-and-fall" pattern.

27511219, 2026, 10, Downloaded from https://advanced.onlinelibrary.wiley.com/doi/10.1002/adsr.70212 by Yasser Khan - Mount Sinai Hospital , Wiley Online Library on [14/10/2026]. See the Terms and Conditions (https://onlinelibrary.wiley.com/terms-and-conditions) on Wiley Online Library for rules of use; OA articles are governed by the applicable Creative Commons License

The rising phase begins when excitatory neural inputs stimulate CRH neurons in the PVN of the hypothalamus. These inputs carry information from circuits monitoring homeostatic threats such as cardiovascular, immune, and nociceptive signals. CRH then drives ACTH release from the anterior pituitary, which in turn stimulates adrenal steroidogenesis, leading to the synthesis and secretion of cortisol. As levels increase, cortisol supports metabolic mobilization, modulates cardiovascular activity, and exerts broad immunoregulatory effects to counter threats to homeostasis, effectively triggering the "fight-or-flight response".

The falling phase begins when circulating glucocorticoid concentrations reach a level sufficient to trigger feedback mechanisms that halt HPA axis output. Cortisol can directly suppress CRH release within the PVN by binding to the glucocorticoid receptor and promoting the release of endocannabinoids [39]. GABAergic projections to CRH neurons in the PVN also limit the HPA axis activity. Additionally, a slower and intermediate feedback process involves trans-synaptic circuits, where inhibitory signals are sent from the hippocampus and medial prefrontal cortex to the PVN. Hence, the falling phase, controlled by feedback mechanisms, is integrated through multiple pathways, and the overall inhibitory effect observed at the PVN results from a combination of inputs from the hippocampus, prefrontal cortex, and hindbrain, as well as direct cortisol binding. Diminished negative feedback caused by the depletion of glucocorticoid receptors in the corticolimbic forebrain and lesions in the ventral hippocampus have been found to prolong HPA axis responses [40]. Similarly, stimulating the prelimbic cortex reduces glucocorticoid output, causing stress inhibition [41], and alterations in the prefrontal cortex impact both the intensity and duration of stress responses.

These processes collectively create the characteristic pattern of a swift ACTH pulse, succeeded by a more gradual but sustained cortisol elevation, and ultimately a feedback-driven return to baseline (Figure 1). This integrated feedback mechanism ensures that the stress response remains both transient and self-limiting: potent enough to facilitate adaptation, yet rigorously controlled to avert the detrimental consequences associated with prolonged cortisol exposure, including excessive energy expenditure. In scenarios involving chronic stress, elevated glucocorticoid levels might amplify the expression of CRH in the central amygdala, thereby establishing a self-reinforcing cycle that exacerbates HPA axis excitability rather than inhibiting it [42]. This maladaptive loop can culminate in sustained hypercortisolemia, a condition implicated in numerous physical and psychological pathologies, representing a significant divergence from the adaptive, short-term activation of the HPA axis [1].

2.2.1 | Stressor Type

The HPA axis responds differently depending on both the modality and the intensity of a stressor. High-intensity, long-duration systemic challenges produce prolonged ACTH and glucocorticoid elevations; this extended secretion is adaptive because it helps regulate and limit potentially harmful immune activity. In contrast, psychological stressors, for example, a strange or threatening environment or situation–produce shorter, more transient responses.

The mechanism of HPA axis activation is also different. Homeostatic stressors, which signal threats to physiological balance, are communicated directly to PVN CRH neurons. This occurs generally via direct monosynaptic sensory relays from sensory organs, such as baroreceptor and chemoreceptor inputs, or signals related to fluid and energy balance, in a bottom-up manner. These are also known as reactive stressors, as glucocorticoids are released to address the perceived need [43].

In contrast, psychogenic stressors are conveyed through corticolimbic circuits in the brain, including the hippocampus, amygdala, and prefrontal cortex, that provide contextual appraisal and exert top-down modulation, shaping the magnitude and duration of HPA activation. They elicit anticipatory responses that are initiated by polysensory external stimuli that may predict a physiological challenge, rather than its actual presence, leading to glucocorticoid release in preparation for potential adverse outcomes and the need for additional resources [44]. However, the overall temporal course of the glucocorticoid response often does not depend on the modality of the stressor, as demonstrated by comparable corticosterone responses in mice to restraint (anticipatory) and hypoxia (reactive) stress [1, 45]. In humans, anticipation of a laboratory stressor has been shown to elicit a larger subsequent salivary cortisol increase [8]. Higher anticipatory stress was also associated with faster cortisol recovery after the stressor, suggesting that this preparatory response may reflect physiological readiness rather than impaired stress regulation. Conversely, positive expectations and a greater perceived ability to cope are associated with a lower cortisol response [46].

Apart from the nature of the stressor, the repetition and chronicity of stressful events also profoundly influence HPA axis regulation, often leading to habituation and heightened stress reactivity (facilitation) [47]. In habituation with repeated exposure, the glucocorticoid peak becomes lower and the response becomes shorter, though it never disappears entirely. Responses to more severe stressors have been found to be less likely to undergo habituation, as adapting to these demands requires a higher perceived effort [48].

Facilitation of the stress response refers to an amplified HPA axis reaction to a new stressor following prior stress exposure [49]. This occurs because the initial stress "primes" the axis, leading to a quicker onset and higher glucocorticoid peaks in response to a subsequent challenge, often due to increased ACTH release or heightened adrenal sensitivity. Lesions to the paraventricular thalamus disrupt such facilitation, indicating its role in integrating previous stress exposures with subsequent responses. This facilitative process primes the organism to better confront unfamiliar or severe threats, effectively overriding the usual suppressive feedback mechanisms.

Despite being evolutionarily adaptive processes, both facilitation and habituation can turn maladaptive. Habituation can contribute to blunted cortisol responses, which are linked to post-traumatic stress disorder (PTSD), chronic fatigue, and poor immune control. Exaggerated responses due to facilitation can keep the system in a state of chronic hyperactivation, increasing the risk of anxiety, depression, hypertension, and metabolic disease. It may also impair recovery if every new stressor triggers an oversized cortisol surge.

27511219, 2026, 10, Downloaded from https://advanced.onlinelibrary.wiley.com/doi/10.1002/adsr.70212 by Yasser Khan - Mount Sinai Hospital , Wiley Online Library on [14/10/2026]. See the Terms and Conditions (https://onlinelibrary.wiley.com/terms-and-conditions) on Wiley Online Library for rules of use; OA articles are governed by the applicable Creative Commons License

The distinction between homotypic (repeated, identical) and heterotypic stressors further elucidates the complexity of HPA axis adaptation, as the former typically induces habituation, while the latter can lead to sensitization, with variations observed between sexes [50]. Repeated exposure to one type of stress (white noise) leads to habituation of CRH neuron responses, but switching stress modalities (e.g., from noise to foot shock) disrupts habituation and "resets" responsiveness. Also, habituation can fade over time: after a rest period, CRH responses can revert toward initial levels, indicating that experience-driven suppression is not permanent but reversible [51].

HPA reactivity varies significantly across individuals, influenced by factors such as sex, age, and genetics [52–54]. Testosterone generally dampens HPA responsiveness, while estradiol enhances it, resulting in women demonstrating greater variability in cortisol responses across the menstrual cycle. This variability may potentially contribute to increased female vulnerability to stress-related psychopathologies like depression and PTSD. Aging is associated with prolonged elevations of glucocorticoids; prior experience (such as chronic stress exposure) can recalibrate HPA dynamics, altering the speed, magnitude, and duration of cortisol secretion.

2.2.2 | Chronic Stress

Although brief variations in the HPA axis are considered normal and beneficial reactions by the body, persistent HPA axis dysfunction, which is metabolically demanding, is linked to various diseases. Stressful events that persist over an extended duration (e.g., caring for a spouse with dementia) or brief focal events that continue to be experienced as overwhelming long after they have ended (e.g., experiencing a sexual assault) may lead to chronic stress, and exposure to chronic stress is most likely to result in long-term or permanent changes in the emotional, physiological, and behavioral responses that influence susceptibility to and the course of disease. Imbalances in cortisol caused by chronic and prolonged periods of stress can directly impact neuronal function, neurotransmitter balance, and brain regions involved in mood and cognition. In addition, they alter other physiological biomarkers [55]. Chronic stress can activate the HPA axis in various ways, with manifestations depending on the stressor's chronicity, intensity, frequency, and type. An individual's response to stress is influenced by genetics, early life experiences, environment, sex, and age, with the context determining if responses are adaptive or maladaptive. For example, psychological stress has been found to impair vagal tone, which can also increase the risk of noncommunicable diseases, particularly stroke and heart disease [10, 56].

Elevated morning cortisol levels have been associated with schizophrenia and bipolar disorder [57]. Similarly, obesity, metabolic diseases, and cardiovascular conditions have been associated with altered HPA dynamics [58]. Cortisol can also lead to Cushing's syndrome when present in excess, characterized by major depression [59], anxiety or panic disorders [60], and cognitive issues, alongside physical changes like increased body mass index, cholesterol, blood pressure, and blood sugar often associated with type 2 diabetes mellitus [10, 61]. Conversely, cortisol deficiency (Addison's disease) can manifest as irritability, mood disturbances, distress, depression, and, to a minor extent, psychosis [62, 63], and low blood pressure [55]. Endocrine dysfunction often triggers a chronic stress response, leading to alterations in the HPA axis, impacting mood, sleep, and overall well-being [55].

Stress also affects mood and motivation. The nucleus accumbens (NAc: the neural interface between motivation and action) and the ventral tegmental area (VTA) are key brain structures that form the mesolimbic pathway, a major dopaminergic circuit involved in reward, motivation, and learning, collectively constituting the reward pathway. Stress hormones reshape reward circuitry by acting through glucocorticoid receptors in the NAc, altering dopamine input and excitatory drive. Acute stress typically produces a transient increase in dopamine release within the NAc [64]. This dopaminergic burst is often viewed as an adaptive signal, as it can enhance motivation, salience, and alertness, which can aid in coping with or preparing for challenging situations [64]. While acute stress can sharpen motivation, chronic glucocorticoid exposure reprograms the NAc toward maladaptive states, thereby linking stress to mood disorders and substance abuse. Over time, repeated or chronic stress–and the elevated glucocorticoid exposure that accompanies it, can dysregulate dopaminergic circuits. Rather than simply boosting dopamine release, chronic stress can reduce the excitability of dopamine neurons, diminish reward sensitivity, or alter synaptic connectivity. This dysregulation within the reward circuitry is a significant factor in the development of various mental conditions, especially psychiatric disorders such as depression and anxiety, along with substance use disorders [65].

2.2.3 | Blunted Cortisol Response

A diminished cortisol response to acute psychological stress, characterized by blunted reactivity, has been identified in various mental health conditions and is associated with adverse health outcomes [66]. Blunted responses are often indicators of HPA strain, early-life developmental programming, circadian misalignment, and disease states, all of which impair the system's adaptive flexibility in responding to new stressors.

A blunted cortisol response indicates reduced flexibility of the HPA axis; insufficient cortisol during a challenging situation compromises metabolic fuel availability and weakens anti-inflammatory control, fostering low-grade inflammation and dysregulation of stress–immune crosstalk [67]. Inadequate acute reactivity fails to resolve challenges efficiently and promotes cumulative wear and tear on brain–body systems [68]. Clinically, blunted cortisol reactivity is documented in stress-related conditions such as PTSD, where women show reduced salivary cortisol responses to the TSST [69], and burnout, where individuals exhibit a diminished CAR, reflecting altered HPA tone [70]. Thus, stress unresponsiveness is problematic because it marks a loss of HPA axis flexibility that undermines metabolic and immune adaptation, heightens allostatic load, and co-occurs with (and may contribute to) stress-related psychopathology [68].

27511219, 2026, 10, Downloaded from https://advanced.onlinelibrary.wiley.com/doi/10.1002/adsr.70212 by Yasser Khan - Mount Sinai Hospital , Wiley Online Library on [14/10/2026]. See the Terms and Conditions (https://onlinelibrary.wiley.com/terms-and-conditions) on Wiley Online Library for rules of use; OA articles are governed by the applicable Creative Commons License

3 | Laboratory Experiments for Studying Cortisol Dynamics

Cortisol research, either for biosensor development or to gain an understanding of varied human responses, requires the emulation of stressful situations in the laboratory. Researchers employ a variety of stress-inducing methods, such as the TSST and the CPT, to examine stress responses under controlled conditions. The choice of an optimal technique depends on factors including practicality, cost, researcher expertise, and environmental constraints. Different stressor paradigms are thought to engage both the sympathetic-adrenal–medullary (SAM) and HPA axes to varying degrees. The physiological impact of these techniques can differ substantially across individuals, complicating experimental design, hypothesis development, and the interpretation of results within and across studies.

A wide range of stress induction paradigms have been employed in laboratory studies. These methods can be broadly categorized into physical, physiological, and psychological stressors. Physical stressors involve the imposition of an external environmental challenge, such as extreme noise, the threat of electric shock, or pain induced by the CPT. In contrast, physiological stressors disrupt internal homeostasis through means such as calorie restriction, sleep deprivation, or intense exercise. Psychological stressors engage cognitive and emotional processes, for example, by requiring individuals to perform demanding mental tasks, such as complex arithmetic, or by exposing them to aversive or distressing stimuli. These categories are not mutually exclusive; for example, the threat of electric shock also elicits fear and anxiety (a psychological component), while sleep deprivation amplifies psychological stress reactivity. An additional way of classifying stressors is by the presence of a social-evaluative component, as seen in the TSST and the Socially Evaluated Cold Pressor Test (SECPT), which reliably elevate cortisol levels by threatening social status [71].

Several paradigms intentionally combine stressors to elicit stronger responses across both the SAM and the HPA axes. For example, the Mannheim Multicomponent Stress Test (MMST) integrates mental arithmetic, emotional image viewing, aversive noise, and the threat of monetary loss, whereas the Maastricht Acute Stress Test (MAST) combines the SECPT with challenging mental arithmetic [72, 73]. Importantly, methodological moderators such as participant demographics (age, sex), time of day, and saliva sampling timing strongly influence the magnitude of physiological responses. Cortisol responses are typically more pronounced in men and older participants and tend to be more observable in the afternoon due to the influence of circadian rhythms [74]. In women, hormonal contraceptive use, menstrual phase, and chronic stress exposure can attenuate cortisol reactivity [75]. The timing of biomarker collection is also crucial, as salivary alpha-amylase, a reflection of SAM activity, typically peaks about 10 min after stress onset. In contrast, cortisol responses occur approximately 20–30 min after the onset of the stressor and can remain elevated for up to an hour. One important variable to consider is the time of day at which the test is administered. Cortisol reactivity tends to be blunted in the morning, when basal cortisol levels are near their circadian peak, and stronger during afternoon sessions [9, 76]. The diurnal variation highlights the need to account for circadian influences when designing experiments and interpreting stress responses. Table 1 provides an overview of widely used stress-induction methods, outlining their implementation and associated physiological and psychological outcomes.

3.1 | Trier Social Stress Test (TSST)

The TSST, developed in 1993 [77], is the most widely used protocol for inducing psychosocial stress in laboratory settings [71]. It combines a public speaking task with a mental arithmetic challenge performed before a panel of evaluators. The standard protocol includes a preparation phase, followed by a speech task and then an arithmetic task, each lasting about 5 min and conducted under conditions of social evaluation. This method effectively induces stress by leveraging humans' sensitivity to social threat, defined as situations that may diminish one's perceived social standing. Exposure to such evaluative conditions reliably boosts cortisol levels because individuals are inherently motivated to maintain their sense of belonging in social groups [78]. The TSST is shown to perform well in longitudinal studies with a 4-month interval during which habituation was not observed, and meta-analyzes often note that the TSST continues to produce reliable responses in repeated protocols, depending on the spacing between sessions [79]. The TSST can also be adapted to examine stress associated with recalled experiences of unfair treatment; in this modified protocol, cortisol and negative emotion increased while heart-rate variability decreased [80]. Similarly, the group public speaking task for adolescents has been shown to elicit a significant cortisol increase in youths, reinforcing the persistence of HPA axis activation across varied stress paradigms [81].

A caveat of the TSST is that its effectiveness in activating the HPA axis depends on methodological factors and individual participant characteristics. Sex differences and hormonal status heavily impact the stress response. Research indicates that men frequently exhibit stronger cortisol responses to the TSST compared to women [74, 77]. Within female participants, responses vary across the menstrual cycle, with enhanced reactivity reported during the luteal phase relative to the follicular phase. The use of oral contraceptives, pregnancy, and postmenopausal status has also been associated with attenuated cortisol reactivity [9, 82]. A wide body of work has also documented the role of health status and lifestyle factors. Cortisol reactivity to the TSST is reduced in individuals with psychiatric conditions such as depression and anxiety disorders, and in those using psychotropic or corticosteroid medications [83]. Night-shift workers, whose circadian rhythms are disrupted, also display irregular cortisol responses [9]. These observations indicate that participant selection and health background can strongly shape endocrine reactivity in stress paradigms.

In terms of protocol features, evidence suggests that the presence and composition of the evaluator panel are key to the TSST's effectiveness. Studies have demonstrated that a panel of two to three evaluators, particularly when the panel is mixed in gender, reliably heightens the social-evaluative threat and produces stronger cortisol increases compared to tasks conducted without an audience [77, 84]. Juster et al. demonstrated the impact of anticipatory stress on TSST induced cortisol response [8]. In their study, participants provided 10 saliva samples from 50 min before

27511219, 2026, 10, Downloaded from https://advanced.onlinelibrary.wiley.com/doi/10.1002/adsr.70212 by Yasser Khan - Mount Sinai Hospital , Wiley Online Library on [14/10/2026]. See the Terms and Conditions (https://onlinelibrary.wiley.com/terms-and-conditions) on Wiley Online Library for rules of use; OA articles are governed by the applicable Creative Commons License

TABLE 1 | Comparison of Common Laboratory Stress Tests and Their Cortisol Dynamics.

Stress Test	Definition / Procedure	Cortisol Peak Timing	Response Robustness / Resources	Recovery to Baseline	Limitations / Moderators
Trier Social Stress Test (TSST)	Public speaking + mental arithmetic in front of evaluators; socially evaluative, uncontrollable	~20–30 min after onset	Response robustness: generally strong and reproducible HPA axis activation; logistical complexity and resource requirements: high	~60–90 min post-stress	Requires trained evaluators and substantial coordination; response magnitude may be influenced by sex (men > women), age (older > younger), time of day (afternoon > morning), prior public-speaking experience, and comfort with social evaluation. Speaking during saliva collection may interfere with standardized swab placement and complicate high-frequency sampling, limiting suitability for some wearable-validation protocols.
Maastricht Acute Stress Test (MAST)	Alternating cold pressor (2 °C hand immersion) and mental arithmetic with negative feedback; unpredictable trial lengths	~20–30 min after stressor	Response robustness: generally robust and comparable to the TSST; logistical complexity and resource requirements: moderate	~60–90 min	Does not require a formal jury but combines physical, cognitive, and evaluative components. Responses may depend on cold and pain tolerance, arithmetic familiarity, question selection and difficulty, and sensitivity to negative feedback. Speaking during arithmetic tasks may complicate simultaneous saliva collection.
Cold Pressor Test (CPT)	Hand or foot submerged in ice water (0–4 °C) for 1–3 min; some versions include social evaluation (SECPT)	~15–20 min post-immersion	Response robustness: variable and generally lower than socially evaluative paradigms; logistical complexity and resource requirements: low	~60 min	Requires limited equipment and is compatible with wearable monitoring and repeated saliva sampling. Exposure duration may be limited by individual cold and pain tolerance, and responses may be affected by sex differences (men > women), prior cold exposure, acute illness, medication use, and anticipatory stress.
Mental Arithmetic / Stroop Tasks	Standalone cognitive stress (e.g., backward counting, Stroop) under time pressure	Variable; weak/absent without evaluation	Response robustness: often weak or variable without social evaluation or negative feedback; logistical complexity and resource requirements: low	If present, ~60–90 min recovery	Requires limited equipment and is compatible with wearable monitoring. Response magnitude may depend on arithmetic-question selection, task difficulty, familiarity with arithmetic or Stroop tasks, time pressure, task engagement, and the presence of evaluation or negative feedback. Verbal responses may interfere with saliva collection if speaking is required.
Exercise Stressors	Treadmill, cycle ergometer, or exhausting endurance exercise (≥10–15 min at high intensity)	~20–30 min after cessation (sometimes up to 90 min)	Response robustness: dependent on relative intensity, duration, and participant fitness; logistical complexity and resource requirements: moderate	~60–90 min (sometimes longer after exhaustive exercise)	Requires exercise equipment and control of workload. Responses depend on relative intensity, duration, sex, training status, fitness level, time of day, recent physical activity, acute illness, and medication use. Heart rate, perceived exertion, power output, or aerobic capacity may be required to compare exercise load across participants.
Other Paradigms (MMST, Montreal Imaging Stress Task (MIST), Loud Music, Firefighting Simulation)	MMST: mental arithmetic + aversive noise + negative feedback + emotional images; MIST: computerized arithmetic with time pressure; others include frightening videos, firefighter simulations, loud techno music.	Generally ~20–30 min after onset	Response robustness: variable, with stronger responses generally reported for multicomponent paradigms; logistical complexity and resource requirements: variable	~60–90 min	Standardization and resource requirements vary across laboratories. Responses may depend on task complexity, participant familiarity, social evaluation, negative feedback, acute health status, and individual sensitivity to the selected stressor; suitability for wearable validation therefore depends on the specific protocol; isolated stressors (e.g., music) mostly activate SAM, not HPA; cortisol rise depends on task complexity and evaluation.

27511219, 2026, 10, Downloaded from https://advanced.onlinelibrary.wiley.com/doi/10.1002/adsr.70212 by Yasser Khan - Mount Sinai Hospital , Wiley Online Library on [14/10/2026]. See the Terms and Conditions (https://onlinelibrary.wiley.com/terms-and-conditions) on Wiley Online Library for rules of use; OA articles are governed by the applicable Creative Commons License

through 50 min after the TSST, allowing the study to assess anticipatory activation, cortisol reactivity, and post-task recovery. Higher self-reported anticipatory stress predicted both greater cortisol reactivity and a steeper subsequent decline, showing that pre-task appraisal can meaningfully shape the measured cortisol trajectory. Thus, a cortisol elevation measured near the task may reflect both anticipation of the upcoming evaluation and reactivity to the task itself.

Duchesne et al. found that both sexes showed increased cortisol levels when evaluated by the opposite gender, but this was only observed in women during their follicular phase [85]. Additionally, video recording participants increases feelings of threat, which may enhance stress responses and influence TSST outcomes. A friendly version of the TSST, F-TSST, in which evaluators exhibited friendly behavior instead of a reserved demeanor, resulted in significantly reduced cortisol responses compared to the standard TSST, emphasizing the critical role of social-evaluative threat in HPA axis activation [86]. The virtual Trier Social Stress Test (V-TSST) presents advantages in resource conservation and standardization, demonstrating a medium effect size in eliciting a cortisol response, suggesting its potential as an alternative for stress research. However, a meta-analysis indicates that the traditional TSST achieves a large effect size in cortisol response, implying that the V-TSST may be less effective in this regard [87].

As for the temporal dynamics induced by the TSST, cortisol typically rises within 10–15 min after stress onset, peaks around 20–30 min, and begins to recover within 60–90 min [9]. To capture this trajectory, prior research has suggested saliva sampling at baseline and at multiple post–stress intervals, with six time points (–30, 0, +15, +25, +35, +45 min) recommended to encompass anticipatory activity, the peak, and the early recovery phase [9].

3.2 | Cold Pressor Test (CPT)

The CPT is one of the most frequently employed laboratory paradigms for inducing acute physiological stress, primarily through exposure to painful cold stimulation. The standard protocol involves immersing the non-dominant hand or forearm in ice-cold water, typically maintained at a temperature between 0°C and 4°C, for a duration of 1–3 min [88]. Recent variations of this test have introduced the submersion of both feet in cold water to elicit a more robust stress response [89]. The CPT effectively activates the sympathetic nervous system; however, its ability to induce significant HPA axis reactivity is generally moderate to low [90]. The magnitude of the cortisol response to the CPT depends on several methodological factors, including water temperature, immersion duration, and the presence of a social-evaluative component. A study comparing the CPT and TSST in individuals with alcohol dependence and/or PTSD found that the TSST generally elicited higher levels of ACTH and cortisol, along with lower mood ratings, compared to the CPT, indicating a stronger HPA response to the TSST [91]. However, the stronger response may also be due to the typically longer duration of the TSST (10 min) compared to the CPT (1–3 min). The study also observed variation in cortisol and ACTH peaks between these two tests; for the TSST, ACTH and cortisol typically peak immediately and within 5 min after the stress period, respectively, reflecting continuous engagement of the HPA axis during the prolonged stress. In contrast, for the CPT, the peaks occur later–around 5 and 30 min after the test, respectively–indicating that the brief, intense physical stress elicits a more delayed endocrine response.

The Socially Evaluated Cold Pressor Test (SECPT) exposes participants to a cold stimulus while simultaneously being observed by evaluators or being video-recorded, resulting in stronger HPA axis activation compared to the traditional CPT [90]. Similar to the TSST, the addition of social evaluation enhances cortisol reactivity. Participants undergoing stress experiments can be classified as cortisol responders or non-responders using the standard TSST threshold, defined as a baseline-to-peak cortisol increase of at least 1.5 nM [92]. Schwabe et al. analyzed 10 years of SECPT data, observing that approximately 60% of participants met the responder criteria, with individual study rates ranging from 48% to 84%. These findings indicate that the SECPT reliably elicits cortisol elevations, though its response rate is somewhat lower than that typically observed in the TSST, where cortisol levels often double from baseline and 70%–75% of participants qualify as responders [93].

As with other stress tests, the time of day plays a significant role in shaping cortisol responses to the CPT. Morning testing, when basal cortisol levels are high, tends to yield smaller relative increases, whereas afternoon or early-evening sessions produce more pronounced reactivity [94]. Bullock et al. reached the conclusion that repeated CPT exposure does not evoke a strong HPA axis response due to habituation [95]. They also suggested that to accurately use cortisol as an indicator of HPA axis activation in experimental designs involving the CPT, it is essential to consider both the stress potentially induced by the laboratory visit and the specific duration of the CPT. All of these results show that although the CPT is a powerful sympathetic system activator, its ability to consistently cause HPA axis activation depends on participant characteristics, social-evaluative and other uncontrolled factors, and circadian timing.

3.3 | The Maastricht Acute Stress Test (MAST)

The MAST is a proven laboratory paradigm that combines elements of psychological and physical stress to induce acute stress. The MAST was created by Smeets et al. in 2012 and combines the unpleasant cold stimulation of the CPT with a cognitive stressor that involves performing mental math under time constraints and receiving unfavorable social feedback [73]. The standard protocol alternates short, randomly timed trials of hand immersion in 2°C ice water and backward counting from 2043 in steps of 17, with participants unaware of the total number or duration of trials. Errors or delays exceeding 5 s trigger negative verbal feedback and a restart of the arithmetic task. Repeatedly alternating between physical discomfort and cognitive evaluation in an unpredictable fashion produces a strong and multidimensional stress experience [73], activating both the SAM and HPA systems.

The MAST elicits stronger cortisol responses than the CPT because of the integration of both physical pain and cognitive-evaluative stressors [73]. The MAST and the TSST are similar in their activation of the cortisol response, but differ in their

27511219, 2026, 10, Downloaded from https://advanced.onlinelibrary.wiley.com/doi/10.1002/adsr.70212 by Yasser Khan - Mount Sinai Hospital , Wiley Online Library on [14/10/2026]. See the Terms and Conditions (https://onlinelibrary.wiley.com/terms-and-conditions) on Wiley Online Library for rules of use; OA articles are governed by the applicable Creative Commons License

methods of inducing stress. While the TSST emphasizes social-evaluative threat through public speaking and observation by evaluators, the MAST focuses on performance-based cognitive and physical challenges [96]. Despite these procedural differences, the MAST and TSST have produced broadly comparable increases in subjective stress, salivary cortisol, and alpha-amylase activity under the conditions examined [73, 96]. Cortisol concentrations following the MAST generally peak approximately 20–30 min after stress induction, similar to the temporal pattern reported for the TSST [92]. Furthermore, one study found no significant differences in cortisol responses across repeated MAST sessions, suggesting that the paradigm may retain its capacity to elicit an HPA axis response when administered repeatedly [96]. Despite eliciting similar cortisol responses, the MAST offers various methodological advantages over the TSST, such as being shorter in duration (typically 10 min) and not requiring a panel of evaluators, allowing it to be conducted by an individual experimenter. These advantages make it less resource-intensive and easier to standardize across labs. Additionally, these features make the MAST desirable for studies that require rapid induction and recovery of stress responses, such as investigations of cognitive performance, emotion regulation, or pharmacological modulation under stress.

3.4 | Mannheim Multicomponent Stress Test

The Mannheim Multicomponent Stress Test (MMST) combines cognitive and evaluative stressors by integrating mental arithmetic, Stroop interference, and negative performance feedback within contexts of monetary threat or social evaluation. The approach enhances feelings of task uncontrollability and social-evaluative threat, which activate the SAM and HPA axes to a greater extent than single-task techniques [72]. Repeated administration of the MMST has demonstrated good test–retest reliability and robust cortisol responses [72]. In contrast, isolated cognitive tasks, such as computerized arithmetic or Stroop tasks without a strong social-evaluative component, primarily elicit sympathetic–adrenomedullary activation and tend to produce weaker or less consistent cortisol responses [71].

3.5 | Cognitive and Performance-Based Stressors

Cognitive stress paradigms, such as mental arithmetic, Stroop interference tasks, and unsolvable puzzles, elicit stress through cognitive load, time pressure, and evaluative feedback rather than direct physical discomfort. These tasks often appear as standalone stressors or as components within broader paradigms like the TSST or the MMST. The analysis indicates that such cognitive stressors reliably activate the SAM system, though their effects on HPA axis activity (cortisol) are often smaller or more variable than those produced by socially evaluative or physical stressors [84].

One of the most popular performance-based cognitive stressors is mental arithmetic, in which participants are typically required to complete serial subtraction problems under time constraints, with an experimenter or evaluator present. Negative feedback, such as "That's too slow, please start again," is frequently given in response to mistakes or slow answers, adding an evaluative and uncontrollable element. The stress response is primarily caused by this unpredictability rather than the cognitive load itself.

The Stroop test elicits a stress response by inducing cognitive interference and attentional conflict. In this task, participants must identify the color of the ink in which a word is printed, even when the word itself denotes a different color (e.g., the word "GREEN" printed in red ink). The test causes mental strain and frustration when responses are repeatedly incorrect, when the task is performed under time pressure, or when it is conducted in the presence of evaluators. Unsolvable problem-solving paradigms induce stress through goal frustration and perceived failure. These include tasks where the correct answer cannot be reached, regardless of how much effort is put in, such as impossible puzzles or tracing geometric figures without lifting a pen. The resulting loss of control and perceived incompetence emulate psychological stress in the real world [97]. However, most of these tests produce milder and shorter-lived physiological stress responses than the TSST or CPT [71] and heavily rely on participants' working memory and problem-solving skills.

3.6 | Stress Induction Experiments in Sensors Research

Validating cortisol biosensors used in a wearable or point-of-care format requires a robust stress-induction paradigm, and the methods used by research labs vary significantly. The targeted matrix in which cortisol is analyzed also differs, with point-of-care methods relying on urine or saliva, whereas wearables generally rely on sweat or interstitial fluid.

Wang et al. developed and validated a flexible indium oxide (In_2O_3) aptamer field-effect transistor (FET) sensor for label-free, multiplexed detection of cortisol across several biological fluids [98]. Two complementary human studies were conducted: acute stress induction using the TSST in 71 participants, and circadian rhythm sampling in 17 participants at morning (9 am) and afternoon (5 pm) time points. In the TSST, each participant underwent a 10-min stressor block preceded by baseline acclimation and followed by a 90-min recovery period. Saliva samples were collected by passive drool at baseline and at 15, 25, and 90 min post-stress to capture the temporal cortisol response profile. Sweat secretion was iontophoretically stimulated on the forearm (1.5 mA, 5 min) and collected for 40 min using absorbent micro-patches. The collected sweat and saliva samples were frozen (−20 °C) and later tested on multiple functionalized In_2O_3 FET chips to validate the sensors. These samples were analyzed via enzyme-linked immunosorbent assay (ELISA), liquid chromatography–mass spectrometry, and the developed aptamer-FET platform, all of which showed strong correlations across methods and consistent peak cortisol elevation at 15 min post-stress.

Torrente–Rodríguez et al. developed a graphene-based electrochemical biosensor (GS4) for real-time, noninvasive monitoring of cortisol in human sweat under both circadian and acute stress paradigms. The experiments encompassed 12 healthy participants (aged 18–65 years) and integrated simultaneous measurements from sweat, saliva, and blood to validate cross-fluid cortisol correlations [99]. The GS4 sensor employed a laser-induced graphene transduction platform functionalized with a cortisol-specific

27511219, 2026, 10, Downloaded from https://advanced.onlinelibrary.wiley.com/doi/10.1002/adsr.70212 by Yasser Khan - Mount Sinai Hospital , Wiley Online Library on [14/10/2026]. See the Terms and Conditions (https://onlinelibrary.wiley.com/terms-and-conditions) on Wiley Online Library for rules of use; OA articles are governed by the applicable Creative Commons License

antibody to perform a competitive electrochemical immunoassay. Collected sweat entered a microfluidic reservoir, where it interacted with HRP-labeled cortisol, generating an amperometric signal inversely correlated with cortisol concentration. They conducted three complementary experiments to examine cortisol dynamics across diurnal, physiological, and acute stress conditions. For circadian rhythm assessment, sweat, saliva, and capillary blood samples were collected at 8 am and 7 pm from four participants to capture daily variations in cortisol secretion. Iontophoretic sweat was collected using the microfluidic GS4 patch for 40 min. The patch allowed for on-body electrochemical measurement of cortisol. Saliva was collected via passive drool, and blood was collected via finger prick; both were analyzed in parallel to sweat. The cortisol measurements showed a prominent diurnal pattern where levels were significantly higher in the morning (AM) and lower in the evening (PM) across sweat, saliva, and blood samples. Their observed correlations between sweat and blood ($r = 0.87$) and sweat and saliva ($r = 0.78$) demonstrate that sweat is a reliable indicator of systemic cortisol rhythms.

To assess sensor performance under physical exertion, three untrained participants and one trained participant cycled on a stationary ergometer for 50 min at 60 rpm with a constant workload. During exercise, sweat was collected continuously from the forehead with the GS4 microfluidic patch. Serum samples were taken before and after the exercise period. The study found that during exercise, cortisol levels progressively increased and reached a maximum at approximately 40 min. The levels then gradually declined during the recovery period. They also performed the CPT, in which sweat was iontophoretically stimulated on four participants and sampled at 8-min intervals, whereas saliva and capillary-blood samples were obtained at baseline and at discrete post-CPT time points (8, 16, and 24 min). Cortisol levels were observed to increase rapidly 8–16 min after the stressor, followed by a gradual return to baseline by 24 min; however, previous research indicated a longer recovery time to baseline.

In the study by Hossain et al. [100], the authors demonstrated a flexible multimodal biosensor (StressFit) capable of tracking both circadian and stress-induced fluctuations of cortisol directly in human sweat. The platform integrates electrochemical cortisol sensing, pH and temperature monitoring, and surface electromyography (EMG) within a single laser-induced graphene substrate. The sensor's cortisol detection unit was functionalized with anti-cortisol antibodies via thiol and EDC/NHS coupling, enabling real-time amperometric measurement as sweat directly wetted the LIG–AgNP working electrode. Two experimental protocols were utilized; the diurnal variation was captured by collecting samples in the morning (8–10 am) and the evening (8–10 pm), with sweat generated through mild physical activity. In a separate session, the same participant performed 55 min of stationary cycling at 60 rpm to elicit sympathetic activation and sweating, and the device continuously measured cortisol in real-time sweat. Because the system relies on active perspiration to sustain a fluidic interface, it is best suited for exercise-based or thermogenic stress testing and is less compatible with dry-state psychological paradigms.

Singh et al. developed a non-invasive wearable microfluidic aptamer-based sweat patch for real-time cortisol monitoring during stress induction [101]. The device integrates electrochemical sensing with microfluidic sweat sampling and employs a pseudoknot-assisted conformation–switching cortisol aptamer immobilized on gold electrodes for enhanced signal specificity and regenerability. On-body validation was conducted on three healthy adult participants who underwent indoor stationary cycling while being intermittently exposed to the CPT to elicit an acute stress response. Their microfluidic sweat patch was attached to the lower neck region, chosen for its stable sweat rate, low hair density, and ease of electrode–skin contact. Further investigation is required to disentangle the superimposed effects of psychological stress testing during physiological exertion for sweat collection, as used in many contemporary studies, as exercise-induced stress may elevate pre-CPT baseline cortisol and confound the interpretation of CPT-driven cortisol changes.

4 | Sampling Matrix Induced Cortisol Dynamics

Understanding cortisol dynamics across physiological matrices is essential for selecting an appropriate sampling medium for wearable cortisol monitoring. Blood remains the main clinical reference because serum and plasma measurements are well established; however, repeated blood collection is invasive and is not suitable for continuous ambulatory monitoring. Saliva and sweat can be collected noninvasively, while interstitial fluid (ISF) can be accessed using minimally invasive methods such as microneedles or implanted platforms. Tears and cerebrospinal fluid (CSF) provide additional sources of physiological information, but their collection is currently less practical for routine wearable monitoring.

These matrices differ in their biological origins, transport pathways, binding environments, and collection requirements. Therefore, their cortisol signals should not be treated as synchronous or physiologically interchangeable. Most evidence on cortisol responses to acute stress comes from blood and saliva. However, relatively few human studies have examined how cortisol levels in interstitial fluid (ISF) change during acute stress. Cortisol concentrations also differ substantially among matrices. Published reviews frequently cite approximate cortisol concentrations of 50–230 ng/mL in blood, 8–140 ng/mL in sweat, 2–20 ng/mL in saliva, and 9–34 ng/mL in ISF [102, 103]. These values represent broad reference ranges rather than universal physiological limits because cortisol levels can vary with the time of day, stress, exercise, health status, individual characteristics, sampling method, and analytical assay [104, 105]. Differences among reviews, such as narrower salivary ranges or alternative estimates for ISF, further indicate that a single fixed range cannot represent all populations and experimental conditions [103]. The following subsections examine plasma, saliva, sweat, ISF, and tears, with emphasis on cortisol dynamics and cross-matrix correspondence.

4.1 | Serum and Plasma

Plasma cortisol remains the conventional reference matrix for assessing HPA axis activity, but its interpretation depends on whether total or free cortisol is measured [106]. In

27511219, 2026, 10, Downloaded from https://advanced.onlinelibrary.wiley.com/doi/10.1002/adsr.70212 by Yasser Khan - Mount Sinai Hospital , Wiley Online Library on [14/10/2026]. See the Terms and Conditions (https://onlinelibrary.wiley.com/terms-and-conditions) on Wiley Online Library for rules of use; OA articles are governed by the applicable Creative Commons License

healthy individuals, most circulating cortisol is bound to corticosteroid–binding–globulin (CBG) and albumin. Only the unbound fraction is readily available for tissue diffusion and glucocorticoid–receptor activation [107].

Plasma measurements can resolve cortisol dynamics at relatively high temporal resolution when blood is collected repeatedly through an indwelling venous catheter [108]. Nevertheless, blood sampling remains invasive, restricts participant mobility, and is difficult to incorporate into ambulatory or wearable monitoring [109]. The collection procedure itself may also activate the HPA axis and confound the response being measured. In laboratory animals, Spencer and Deak describe a brief "window of opportunity" before handling-induced HPA axis activation produces a measurable rise in circulating glucocorticoids, emphasizing that baseline samples must be obtained rapidly or through procedures that minimize sampling-related stress [110]. This method is particularly relevant when plasma cortisol is used as the temporal reference against which less invasive matrices are compared.

Although plasma provides the most established reference trajectory, total cortisol does not always represent biologically active cortisol accurately. This limitation becomes especially important when corticosteroid–binding globulin or albumin concentrations are altered. For example, Hamrahian et al. found that nearly 40% of critically ill patients with hypoproteinemia had apparently subnormal total serum cortisol despite having normal adrenal function [111]. Free cortisol has been found to reflect illness severity more accurately than total cortisol, and it often increases more markedly than total cortisol following stimulation [112, 113]. Similarly, patients with sepsis and septic shock can have lower concentrations of cortisol–binding proteins and a higher free-to-total cortisol ratio [114]. These findings demonstrate that cross-matrix comparisons should specify whether total cortisol or free cortisol is used as the reference, particularly because cortisol in saliva, sweat, and ISF is generally interpreted to reflect the unbound circulating fraction [107].

4.2 | Interstitial Fluid

Interstitial fluid (ISF) contains cortisol within the extracellular space surrounding tissue cells and is therefore a physiologically relevant matrix for minimally invasive monitoring. Predominantly unbound cortisol can diffuse from the circulation into tissues, making ISF cortisol more directly comparable with circulating free cortisol than with total plasma cortisol. However, collecting ISF remains more technically demanding than collecting saliva or sweat. Microdialysis enables repeated measurement of subcutaneous free cortisol but requires catheter insertion, while microneedles provide a less invasive interface that is potentially better suited to wearable monitoring. With either approach, the observed response may include delays introduced by vascular-to-interstitial transport, ISF extraction, transport through the sampling device, and sensor equilibration. A scaffolded hydrogel microneedle study estimated ISF free cortisol at approximately 10% of total blood cortisol, illustrating why plasma and ISF concentrations should not be compared without considering binding and matrix-specific calibration [115]. This difference in concentration reflects physiological partitioning and does not, by itself, indicate a fixed temporal delay.

Human microdialysis studies provide more direct evidence regarding the temporal correspondence between circulating and subcutaneous cortisol. Bhake et al. studied 42 healthy men under Synacthen–stimulation, dexamethasone-suppression, and placebo conditions. Serum total cortisol and microdialysis-derived free cortisol in blood and subcutaneous tissue were measured at 10-min intervals beginning 1 h before and continuing for 4 h after administration. The authors found good correspondence between circulating and subcutaneous free cortisol in the Synacthen and dexamethasone groups, with no significant delay and an estimated offset of less than 5 min. However, this result was obtained under pharmacological stimulation and suppression and does not establish that the same temporal relationship occurs during acute psychological stress [116].

More recent ambulatory microdialysis studies demonstrate why the sampling process must also be considered when interpreting ISF timing. Isherwood et al. compared simultaneous plasma and subcutaneous microdialysate profiles across a broad panel of hormones and metabolites [117]. For two participants, the median offsets across correlated analytes were 32.3 min and 12.9 min, whereas only 3 of 20 metabolite profiles were correlated in a third participant. Although cortisol was detected, these aggregate values were calculated across analytes and should not be interpreted as cortisol–specific plasma-to-ISF delays. Instead, the findings demonstrate that apparent plasma-ISF offsets can vary among analytes and individuals.

Upton et al. further used portable automated microdialysis to measure 24-h subcutaneous adrenal-steroid profiles in 214 healthy participants. Consecutive 20-min samples captured circadian and ultradian variation in tissue cortisol and revealed substantial interindividual differences in the timing and magnitude of these rhythms. Plasma–tissue validation, however, was performed in only seven additional participants, not the full cohort of 214 [118]. Each reported microdialysate concentration also represented cortisol accumulated over a 20-min collection interval rather than an instantaneous ISF concentration [119]. Consequently, rapid changes may be temporally averaged, meaning that a single ISF measurement or a sparsely sampled profile may not accurately represent the underlying cortisol trajectory.

Plasma-tissue correspondence may be further altered under pathological conditions. Microdialysis studies involving severe burns, sepsis, and traumatic brain injury have reported partial or inconsistent agreement between tissue and circulating cortisol [120–122]. These differences may reflect changes in perfusion, inflammation, local cortisol metabolism, and plasma-binding proteins rather than a limitation inherent to microdialysis itself. Therefore, the applicability of tissue ISF measurements should be carefully considered before use in different clinical or physiological settings.

Collectively, the available evidence does not support the application of a universal plasma-to-ISF delay. The observed temporal relationship may depend on tissue perfusion, anatomical site, participant physiology, the rate and magnitude of the cortisol change, sampling interval, extraction method, and device architecture. Importantly, direct human evidence describing ISF cortisol responses to standardized psychological stressors such as the Trier Social Stress Test, Cold Pressor Test, or cognitive

27511219, 2026, 10, Downloaded from https://advanced.onlinelibrary.wiley.com/doi/10.1002/adsr.70212 by Yasser Khan - Mount Sinai Hospital , Wiley Online Library on [14/10/2026]. See the Terms and Conditions (https://onlinelibrary.wiley.com/terms-and-conditions) on Wiley Online Library for rules of use; OA articles are governed by the applicable Creative Commons License

stress remains limited. Dedicated paired plasma-ISF studies are therefore needed to establish whether acute stress-related cortisol changes are delayed, attenuated, or temporally averaged in ISF. For wearable microneedle platforms, delays in plasma-to-ISF transport should be distinguished from additional delays introduced by ISF uptake, transport through the microneedle or hydrogel, molecular-recognition kinetics, and signal equilibration [123].

4.3 | Saliva

Saliva is the most established noninvasive matrix for repeated cortisol assessment and, therefore, provides a practical comparator for emerging sweat, tear, and ISF-based sensing platforms. Saliva collection does not require venipuncture, can be repeated during laboratory or field protocols, and has been used to validate emerging sweat-sensing platforms. However, saliva remains a discretely collected fluid rather than a continuously available matrix. Consequently, the temporal resolution of a salivary profile depends primarily on collection frequency rather than assay speed.

Cortisol enters saliva principally from the unbound circulating fraction and is therefore generally interpreted as a surrogate for free, rather than total, plasma cortisol. This distinction is important because changes in cortisol-binding globulin, including those associated with estrogen-containing oral contraceptives, can alter total serum cortisol without producing an equivalent change in salivary cortisol. In a 24-h study involving hourly paired samples from nine adults, serum and salivary cortisol rhythms were synchronous in seven participants; the two exceptions were oral-contraceptive users [124]. In septic-shock patients, salivary cortisol also correlated more strongly with measured free serum cortisol than with total serum cortisol ($r \approx 0.79$), although the clinical setting and small study populations limit generalization [125].

The interpretation of salivary cortisol is further influenced by the cortisol-cortisone conversion. Within the salivary glands, 11-hydroxysteroid dehydrogenase type 2 converts a substantial proportion of cortisol to cortisone. Therefore, salivary cortisol and salivary cortisone represent related but noninterchangeable measurements. As cortisone is more abundant in saliva and remains measurable when cortisol concentrations are low, it may sometimes correspond more closely to serum free–cortisol exposure than salivary cortisol does [126]. Consistent with this, salivary cortisone has been reported to track serum and subcutaneous free cortisol more consistently, especially at low cortisol concentrations [127].

The principal strength of saliva is its suitability for repeated characterization of circadian and stress-related trajectories. Dorn et al. reported temporal synchrony between serum and salivary cortisol over 24 h in most participants, although oral-contraceptive use altered this relationship [124]. Juster et al. collected ten salivary samples from 50 min before until 50 min after the TSST, allowing anticipatory activity, post-stressor reactivity, and recovery to be distinguished [8]. Saliva is therefore substantially more informative when collected at several defined time points than when represented by a single pre and post-event measurement.

The timing of salivary responses relative to blood is stimulus and protocol-dependent. Sampling density, circadian phase, stressor type and duration, exercise intensity, and individual cortisol responsiveness all affect the observed onset, peak, and recovery profile [128, 129]. In 12 endurance-trained men completing 30 min of cycling at different intensities, serum and salivary cortisol increased significantly only after exercise at 80% of maximal oxygen uptake. Serum cortisol peaked immediately after exercise, while the highest salivary cortisol value was observed at the next and final sampling point, 30 min into recovery [130]. Similarly, an insulin–tolerance study found that the highest observed salivary cortisol value occurred at least 30 min after the serum maximum [131]. These findings demonstrate delayed salivary maxima under those particular experimental conditions, but they do not establish a universal 30-min lag between blood and saliva cortisol measurements. The apparent delay depends on the stimulus, circadian phase, response magnitude, sampling schedule, and temporal averaging introduced by sample collection. For example, measurements obtained only before exercise, immediately afterward, and 30 min into recovery cannot determine whether the actual delay was 10, 20, or 30 min.

Cross-matrix comparisons are further constrained when the matrices are sampled at different frequencies. Bhake et al. collected subcutaneous and intravenous microdialysate samples every 10 min for 1 h before and 4 h after administration of placebo, Synacthen, or dexamethasone. Saliva was collected less frequently, at 30-min intervals. Although saliva was included in the comparison, it was sampled less frequently. This limited the ability to detect short-term changes and determine the precise timing of the blood-to-saliva delay [116].

Saliva also presents important preanalytical constraints. Collection time and awakening time must be documented because cortisol has pronounced circadian and awakening-related variation. Eating, drinking, smoking, toothbrushing, oral bleeding, recent exercise, glucocorticoid exposure, collection-device material, sample volume, and storage conditions can all affect the measured value or its interpretation [132]. Absorbent devices and passive drool should not automatically be treated as equivalent because cortisol recovery from swabs can depend on both the swab material and the volume of saliva absorbed. McKinlay et al. found that cortisol recovery was affected by the volume of saliva recovered, with smaller volumes potentially leading to measurement bias. They reported that at least 2 mL of saliva should be absorbed onto swabs to achieve adequate cortisol recovery [133]. The saliva collection process has also been shown to add noise. Consecutive same-time-point samples still differed by 9%–14% for cortisol and 5%–10% for cortisone, while 17% of participants provided insufficient material for at least one analysis [134]. These issues are particularly relevant for wearable or frequent-sampling applications, where a nominally rapid assay cannot compensate for an inadequately controlled or intermittently obtained saliva sample.

Saliva collection can be particularly difficult in critically ill or mechanically ventilated patients. Kim et al. obtained insufficient saliva from 15 of 49 mechanically ventilated participants (30.6%), likely reflecting factors such as ventilation, poor oral hygiene and lack of oral intake [135]. Oral bleeding, secretions, medication residue, and impaired oral care can further contaminate samples

27511219, 2026, 10, Downloaded from https://advanced.onlinelibrary.wiley.com/doi/10.1002/adsr.70212 by Yasser Khan - Mount Sinai Hospital , Wiley Online Library on [14/10/2026]. See the Terms and Conditions (https://onlinelibrary.wiley.com/terms-and-conditions) on Wiley Online Library for rules of use; OA articles are governed by the applicable Creative Commons License

[135, 136]. Thus, saliva is a practical and well-validated matrix for repeated cortisol measurements in healthy stress studies. However, its relationship to blood should be interpreted as a physiological correspondence that varies with timing and context rather than as a fixed, real-time equivalence.

4.4 | Sweat

Sweat is an attractive matrix for wearable cortisol monitoring because it can be collected at the skin surface without venipuncture and coupled directly to an on-body sampling interface. The presence of cortisol in human eccrine sweat has been analytically confirmed using liquid chromatography–tandem mass spectrometry (LC–MS/MS), establishing that cortisol is a measurable constituent of this matrix [104]. Nevertheless, sweat cortisol should not be treated as an interchangeable proxy for plasma, saliva, or ISF cortisol. Its measured concentration can be influenced by systemic cortisol availability, transport into the sweat gland, local steroid metabolism, sweat rate, evaporation, anatomical collection site, and the interval over which the sample accumulates.

Repeated-sampling studies demonstrate that sweat cortisol changes over time during exercise, although the observed trajectory varies across participants and collection conditions. Runyon et al. measured cortisol, cortisone, and downstream metabolites in repeated sweat samples from four healthy participants during a 60-min exercise period. Cortisol and metabolite profiles were highly individualized, indicating that sweat can capture dynamic changes but that a single pattern cannot be generalized across individuals [137]. In another study, King et al. collected sweat from eight participants during 90 min of cycling in a heated chamber. Mean sweat cortisol increased across the exercise periods, from approximately 0.34 ng/mL during the first collection interval to 1.27 ng/mL during the final interval [138]. These studies show that sweat cortisol can change over the course of sustained exercise, but they do not establish a universal response profile or a fixed biological delay relative to blood or saliva.

Published exercise studies have reported differing sweat–cortisol trajectories, ranging from an immediate post-exercise maximum to a progressive increase during continuous cycling [100]. This inconsistency reinforces that apparent sweat timing depends on both cortisol physiology and sweat collection history rather than a fixed biological lag. Paired-matrix studies provide evidence of association but do not yet establish a fixed sweat delay. Torrente–Rodríguez et al. reported a positive matched-sample relationship between sweat and serum cortisol across morning and evening measurements [99]. Sweat–saliva associations have also been reported. Russell et al. found a significant correlation after intensive exercise in 17 participants, with sweat cortisol varying significantly with time of day. Wang et al. reported a sweat-saliva correlation of $r = 0.73$ in 17 healthy participants sampled in the morning and afternoon [98, 139]. Continuous passive-perspiration monitoring has also shown strong sweat–saliva agreement ($r = 0.92$) and low Bland–Altman mean bias, while passive–sweat concentration categories aligned with paired salivary reference intervals in a subsequent study [140, 141].

Correlation at a small number of matched time points does not demonstrate that sweat, saliva, and blood respond simultaneously. No available study has defined a validated, generalizable minute-scale sweat-to-serum or sweat-to-saliva lag during acute stress. An apparent sweat–cortisol trajectory may combine systemic cortisol secretion and transport into sweat with the time required to generate, collect, deliver, and replace the sample at the sensor. Correlation between matrices can therefore coexist with differences in onset, peak time, or recovery. Determining a true biological sweat delay will require repeated, closely spaced measurements from sweat and a reference matrix under a standardized stress protocol.

Sweat availability and the method used to stimulate secretion also affect temporal interpretation. Some individuals produce insufficient passive sweat under resting or low-intensity conditions, whereas exercise or thermal stimulation performed to generate sweat may itself alter cortisol physiology. Passive sweat and sweat stimulated by exercise, heat, or iontophoresis can differ in secretion rate, local stimulation conditions, and collection history. Iontophoresis can increase sample availability, but iontophoretically stimulated sweat should not be assumed to be directly equivalent to unstimulated sweat without experimental validation.

Anatomical collection site is a major determinant of sweat cortisol measurement. In the cycling study by King et al., sweat cortisol differed among the forehead, dorsal forearm, scapula, and triceps; the forehead showed higher concentrations than the dorsal forearm and triceps. Although cortisol increased over time at all sites, the site-dependent concentrations and excretion rates demonstrate that a sweat–cortisol value should always be reported with its anatomical collection location [142]. Wearable studies should therefore avoid treating values from different body sites as directly interchangeable unless this equivalence has been established for the specific device, sweat-induction method, and sampling interval. Precollection skin cleaning, control of evaporation, and documentation of cosmetics or topical products are also necessary because residual sweat and surface contamination can alter the recovered sample. Where possible, cortisol concentration should be interpreted alongside local sweat rate or cortisol excretion rate. Concentration alone may increase or decrease because of changes in fluid secretion even when the amount of cortisol delivered to the skin does not change proportionally.

These limitations become particularly important for long-duration collection. A continuously worn patch integrates sweat produced over time, so its final cortisol content may not reproduce the timing of a salivary or plasma trajectory. Meyer et al., for example, found that cortisol recovered from a week-long sweat patch did not consistently correspond to the diurnal salivary cortisol area under the curve [143]. Pearlmutter et al. also reported that limited sweat volume and the small number of quantifiable eccrine samples constrained direct comparison between sweat and saliva [144]. Such studies demonstrate a practical distinction between cumulative cortisol exposure and time-resolved endocrine monitoring.

Overall, current evidence supports associations between sweat cortisol and cortisol measured in other matrices, but it does not establish a universal biological delay. Biological transport into sweat must therefore be distinguished from delays caused by

27511219, 2026, 10, Downloaded from https://advanced.onlinelibrary.wiley.com/doi/10.1002/adsr.70212 by Yasser Khan - Mount Sinai Hospital , Wiley Online Library on [14/10/2026]. See the Terms and Conditions (https://onlinelibrary.wiley.com/terms-and-conditions) on Wiley Online Library for rules of use; OA articles are governed by the applicable Creative Commons License

sweat generation, sample accumulation, microfluidic transport, incomplete fluid replacement, and sensor response, which are considered further in Section 5.

4.5 | Tears

Tear fluid is an emerging peripheral cortisol matrix with potential relevance to ocular wearable sensing. Its principal attraction is direct access to a small, continuously renewed surface fluid through contact lenses or other ocular interfaces. However, tear cortisol should not be assumed to be equivalent to plasma, saliva, sweat, or ISF. Tear composition is influenced by lacrimal secretion, tear-flow rate, ocular-surface condition, and the collection procedure. Therefore, both concentration and apparent response timing may depend on how tears are obtained.

Direct acute–stress evidence remains limited but is physiologically informative. Barmpari et al. reported that tear cortisol increased following stress induction, correlated with salivary cortisol, and reached its observed peak earlier than salivary cortisol. Tear cortisol also showed acceptable test– retest reliability across sessions, whereas tear alpha–amylase was more variable and did not show a reliable stress-related response [145]. These findings indicate that tear cortisol may respond earlier than salivary cortisol under the specific protocol used by Barmpari et al. They do not establish a universal tear-to-saliva delay or demonstrate that tear cortisol changes simultaneously with blood cortisol.

The small sample volume and risk of reflex tearing are important limitations. Schirmer strips can irritate the ocular surface and stimulate reflex tearing. In contrast, microcapillary tubes and soft contact lenses produced less observable irritation in the study by Roden et al., although their performance may depend on operator skill [146]. Reflex tearing can alter tear-flow rate and dilute some tear constituents, while collection and processing methods can also affect analyte recovery [147]. Moreover, basal, reflex, and flush tears differ in lipid concentration and composition, demonstrating that collection procedure can influence the biochemical characteristics of the resulting sample [148]. Therefore, the collection method needs to be treated as part of the measurement definition rather than as a neutral procedural detail.

For temporal studies, investigators should report collection method, tear volume, whether tears were basal or reflex-stimulated, sampling duration, ocular irritation, contact-lens use, eye drops or topical medication, and the interval between stress exposure and sample acquisition. These controls are particularly important because the observed timing of a tear-cortisol peak could reflect true biological dynamics, changes in tear secretion, or collection-related variation in tear flow and sample dilution. Thus, tears are promising for high-temporal-resolution cortisol research, but dense paired studies with saliva and blood are required before their timing can be quantitatively compared across matrices.

5 | Cortisol Dynamics Influenced by Sensors and Sampling Method

Wearable cortisol measurements are influenced not only by underlying physiology but also by sensor performance, sample-collection methods, and the biological matrix in which cortisol is measured. Wearable cortisol–sensing platforms frequently demonstrate limits of detection (LODs) and dynamic ranges that span physiologically relevant concentrations. However, these analytical characteristics are often acquired in simplified buffer systems or artificial biofluids rather than the native biological matrix. Aptamer-based platforms have reported detection ranges extending from sub-picomolar to micromolar, including an LOD of 0.2 pM for the regenerative sweat patch of Singh et al. [101] and practical detection near 1 pM for the aptamer-FET smartwatch of Wang et al. [98]. Similarly, broad analytical performance has been reported for molecularly imprinted polymer (MIP) based sensors, including a range of 0.1 pM–1 μM [149] and 0.1 pM–5 μM [150]. Nevertheless, a low LOD or a broad benchtop calibration range does not, by itself, imply suitability for continuous physiological monitoring.

Temporal performance remains under-characterized and inconsistently defined across the published literature. Response time may be used to describe the intrinsic recognition or transduction process, the time required to obtain a quantitative measurement, or the total interval from sample acquisition to signal generation. For instance, while the aptasensor reported by An et al. [151] demonstrated a 5s sensor response under idealized analytical testing conditions with an LOD of 10 pM, detecting cortisol in actual sweat required several minutes. Thus, the reported electronic or analytical response time should not automatically be interpreted as the effective temporal resolution of the fully integrated wearable platform. Matrix-specific biological delays and latency introduced by sweat microfluidics and ISF microneedle sampling are discussed separately in Sections 5.1 and 5.2, respectively.

Continuous monitoring also demands the sensing interface to track both decreasing and increasing cortisol concentrations while maintaining reliable performance during repeated or prolonged operation. Here, a fundamental distinction should be clearly addressed between reversibility and regeneration. Reversibility denotes spontaneous, thermodynamic equilibrium-driven tracking of analyte concentration fluctuations, whereas regeneration requires exogenous intervention (e.g., thermal, chemical, or electrostatic release) to restore occupied binding pockets. Regenerative or reversible monitoring has been demonstrated most clearly by the pseudoknot-assisted aptamer-based sensing patch of Singh et al. [101], which tracked sweat cortisol for up to 90 min; the MIP sensor of Chen et al. [150], which exhibited less than 3.76% signal attenuation over 120 regeneration cycles; and the in situ regenerative MIP–OECT platform of Liu et al. [152]. Neither reversible binding nor cycle endurance guarantees drift resistance. Storage stability must also be interpreted separately: Chen et al. retained approximately 96.1% of the initial response after 30 days [150], whereas Fande et al. retained approximately 80% over the same period [153]. These results characterize performance after storage rather than continuous on-body operation and therefore do not establish low operational drift.

Human validation bridges controlled analytical performance and practical translational utility by exposing devices to native-matrix composition, interindividual variability, motion, temperature, or changing sample availability. Human acute–stress validation remains less common than analytical or proof-of-concept testing

27511219, 2026, 10, Downloaded from https://advanced.onlinelibrary.wiley.com/doi/10.1002/adsr.70212 by Yasser Khan - Mount Sinai Hospital , Wiley Online Library on [14/10/2026]. See the Terms and Conditions (https://onlinelibrary.wiley.com/terms-and-conditions) on Wiley Online Library for rules of use; OA articles are governed by the applicable Creative Commons License

and is concentrated primarily among sweat–sensing platforms, including the exercise and cold-pressor experiments of Torrente–Rodriguez et al. [99]. Studies have demonstrated on-body measurements, diurnal variation, exercise-associated changes, or agreement with reference assays without establishing a complete acute–stress trajectory. Therefore, these different validation levels should be distinguished when assessing whether a platform can resolve physiologically meaningful cortisol dynamics.

Table S1 provides a paper-specific comparison of representative wearable cortisol platforms, in terms of the sensing mechanism, analytical range, and LOD, validation matrices, sampling matrix and method, intrinsic response and recovery, sampling-related delays, regeneration or reversibility, drift and stability, human or animal validation, stress experiment, and principal finding. Values absent from the original reports are designated as not reported (NR) rather than inferred. Moreover, the available evidence indicates that few studies characterize analytical sensitivity, bidirectional reversibility, operational drift, long-term stability, native-matrix performance, and in vivo stress tracking within the same platform. The suitability for high-temporal-resolution continuous monitoring should therefore be evaluated based on the combined evidence across these characteristics.

5.1 | Sweat Sampling and Microfluidic Interfaces

Wearable sweat microfluidics can achieve temporal resolutions spanning sub-minute to multi-minute; however, the actual duration of a measurement is determined by the complete sampling pathway rather than sensor response time alone. Factors such as sweat availability, flow rate, effective fluid volume, channel geometry, hydraulic resistance, and sample replacement collectively determine the age of sweat reaching the sensor [154].

Although lower dead volume and higher flow generally improve temporal resolution, channel miniaturization alone may not guarantee accelerated transport, as narrow channels increase capillary pressure while also increasing hydraulic resistance. Moreover, changes in sweat secretion rates produce variable transport velocities. These tradeoffs may contribute to diverse channel dimensions and materials, including silicone, thermoplastics, and paper. From a design perspective, low-dead-volume sensing regions, directional flow, and a defined outlet are therefore preferable when the objective is the rapid replacement of old sweat with newly secreted fluid.

5.1.1 | Sweat Generation and Sampling Delay

Sweat generation itself is a primary determinant of microfluidic timing as it directly governs channel filling rates, sample residence time, and sensor-refresh frequency. Perspiration rates vary substantially across individuals, anatomical locations, environmental conditions, and stimulation methods. Consequently, a fixed-volume chamber may yield differing temporal resolutions between users and over the course of a single monitoring session. Natural resting sweat rates are typically very low and highly variable, approximately 0–0.25 nL min^{-1} $gland^{-1}$ [155], whereas physical exercise and thermal stress can increase secretion to approximately 10–100 nL $min^{-1}gland^{-1}$or more [155, 156].

For non-exercise sweat collections, transdermal iontophoresis provides an alternative means of stimulation. A bioinspired Janus–membrane platform was reported to demonstrate sweat emergence within approximately 10 min after stimulation and maintained continuous sampling for over 2 days [157]. Among iontophoretic agents, pilocarpine produces a rapid initial sweat response of approximately 1–10 nL $min^{-1}gland^{-1}$, but this effect declines within approximately 1–2 h [155]. In contrast, carbachol can sustain secretion rates of approximately 1–15 nL min^{-1} $gland^{-1}$ for 24–48 h or longer, offering superior durability for prolonged monitoring [155]. Importantly, sweat-generation rate and the actual rate collected by the microfluidic device are not necessarily equivalent.

5.1.2 | Microfluidic Transport Dynamics and System Latency

Due to variations in sweat generation complicating the interpretation of on-body filling times, microfluidic filling and renewal are commonly characterized first under controlled benchtop conditions using artificial sweating systems. These experiments isolate transport at the device level from variations in physiological sweat onset and secretion. For example, Yin et al. [158] visualized and quantified fluid routing across microchannel-connected chambers using dye tracking. The system yielded 15.7 μL over 1200 s, corresponding to an average device-level collection rate of approximately 0.79 μL/min.

Although artificial sweating systems enable controlled characterization of filling and renewal at device-level, they do not reproduce the variable sweat onset and secretion rates encountered during actual human body application. Therefore, on-body studies provide a more practical measure of the latency between the beginning of the stimulation and the generation of a usable sensor signal. An epidermal microfluidic platform filled its reservoir approximately 8 min after exercise onset [159], whereas another wearable patch initiated sensing approximately 13 min into a cycling trial [160]. In a more complex integrated platform, the initial measurements remained unreliable for approximately 18–27 min, reflecting the time required for sufficient sweat to reach the electrodes [161]. These values represent practical delays that combine sweat onset, device priming, microfluidic transport, chamber filling, electrode wetting, and, in some cases, signal stabilization rather than simply microfluidic transit times.

The initial chamber filling does not necessarily indicate that the sample represents newly secreted sweat. As demonstrated by Martín et al. [159], a large initial glucose response was attributed to residual glucose on the skin surface and within sweat pores before continuous fresh-sweat generation. Continuous flushing was required to remove and replace this initially contaminated sample, and analytically useful glucose measurements were obtained only approximately 15–20 min after the detection chamber was initially filled. Continuous renewal and adequate flushing are therefore important in reducing surface contamination and sample-age effects, although they do not eliminate the biological delay associated with the transport of analyte into sweat. The extent of carryover and sample averaging depends on the effective sensing volume, channel length and cross-section, sweat flow rate, and the presence of stagnant regions. Directional flow, low-

27511219, 2026, 10, Downloaded from https://advanced.onlinelibrary.wiley.com/doi/10.1002/adsr.70212 by Yasser Khan - Mount Sinai Hospital , Wiley Online Library on [14/10/2026]. See the Terms and Conditions (https://onlinelibrary.wiley.com/terms-and-conditions) on Wiley Online Library for rules of use; OA articles are governed by the applicable Creative Commons License

dead-volume sensing chambers, and explicit outlet pathways can promote sample replacement, whereas passive valves and isolated reservoirs can prevent mixing by physically separating sequential samples [162].

Continuous renewal also creates a capacity requirement. Some volume-constrained microfluidic devices saturate within approximately 8 min at typical exercise-associated sweat rates, causing subsequent sweat to mix indiscriminately or overflow [163]. Thus, although a device can exhibit a rapid initial filling rate, it can still be unsuitable for prolonged continuous monitoring. Long-term operation may further require fluidic robustness, given that accumulated salts, skin debris, air bubbles, delamination, or changes in surface wettability can cause irregular filling, partial channel blockage, and eventual measurement failure [164].

The opposite limitation occurs under low-flow or resting conditions, where passive fluid collection can substantially increase sample age. At the extreme end of passive collection, a granular hydrogel scaffold based on osmotic uptake may require up to approximately 60 min to harvest analytical volumes [165]. Low flow increases the residence time of sample and slows the replacement of previously collected sweat. Under these conditions, diffusion, surface adsorption, and mixing within the collection pathway may broaden or shift the measured trajectory; however, these contributions have rarely been quantified separately in wearable sweat devices. Modeling of approximately 100-μm-wide channels indicates that diffusive flux may become comparable to convective transport under low-flow conditions, while smaller channels and faster filling reduce diffusion-related temporal smearing [164]. Surface interactions and dispersion effects can further delay or attenuate concentration changes during analyte transport [166]. Therefore, evaluating material compatibility under dynamic laminar flow is essential to prevent artificial peak broadening.

Efforts to minimize dead volume or incorporate spontaneous capillary driving forces can drastically accelerate fluid delivery. Fully printed microfluidic channels delivered sweat to the sensing electrodes in approximately 40 s [167], while a self-driven platform based on dropwise Laplace–capillary transport reported fluidic response in approximately 100 ms [168]. However, this 100-ms value characterizes local mechanical movement of the fluid front rather than complete physiological sample-to-result timing and should not be interpreted as 100-ms biomarker temporal resolution. Thus, reported microfluidic sweat-sampling times appear to span from sub-seconds to nearly an hour depending on whether the reported metric represents capillary actuation, transport to the sensor, chamber filling, active sweat induction, or passive collection under low-flow conditions.

Sequential or chrono-sampling architectures provide another strategy for addressing mixing and sample-age limitations associated with slow sampling by physically segregating successive sweat fractions into discrete microchambers. Choi et al. [169] used capillary bursting valves to passively route incoming sweat through individual microreservoirs and collected approximately 1.8 μL in 0.8 min from a collection area of 0.03 cm^2. Sweat-gland pressure drove the fluid through interconnected microchannels containing capillary bursting valves that opened at progressively higher pressure thresholds, producing sequential routing without external actuation. By isolating consecutive samples instead of allowing unrestricted mixing within one reservoir, such architectures can better preserve temporal information in the collected sweat. This improved sample definition comes at the cost of finite compartment capacity and, in some implementations, greater fabrication and control complexity along with power requirements for active circuits.

Sweat-activated galvanic cells offer a parallel mechanism to timestamp segregated sweat volumes without active external electronics [170]. Bandodkar et al. incorporated galvanic cells into soft microfluidic devices as passive "stopwatches" to determine when individual chambers were filled. The anodes and cathodes behave as open circuits in the absence of sweat. Once sweat enters the corresponding channel, it electrically connects the electrodes, completes the circuit, and generates a voltage that decays according to a characterized temporal profile. Because the microchambers are filled sequentially, their corresponding galvanic stopwatches are activated at different times, allowing the voltage readings to provide a temporal reference for each harvested volume [170].

A more recent example of time-resolved sample isolation is the Cap–Sweat platform, in which sweat was captured and fractionated into 18 discrete, fixed-volume sequential compartments using passive capillary circuits. The platform reported sub-minute temporal resolution and captured a transient early cortisol increase that could be obscured by averaging or mixing in continuous-flow collection architectures [171]. An optimized venting structure suppressed evaporation and back-contamination, allowing the device to resolve characteristic sweat-rate behavior that included an initial transient peak during the first 3–5 min of exertion, followed by a lower and more fluctuating secretion phase [171]. These results illustrate why preventing backflow, evaporation, and mixing is part of temporal design rather than simply a packaging consideration.

Active fluidic control provides an alternative route to enhance sample definition. By pairing thermally actuated expansion valves with passive capillary gates in a dual-valve configuration, previously harvested sweat can be physically sealed before fresh fluid enters the manifold, eliminating internal mixing and assigning each volume to a verified collection interval [172]. Together, chrono-sampling, passive valves, active valves, and explicit sample-isolation strategies suggest that temporal resolution may depend not only on sweat-transport velocity but also on the physical distinguishability of successive samples after collection.

5.1.3 | Sweat Sampling in Cortisol Research

Cortisol-sensing platforms directly illustrate how microfluidic latency can affect the interpretation of dynamic and continuous hormonal profiles. In the aptamer-FET smartwatch developed by Wang et al. [98], channel filling required 5–15 min after iontophoretic stimulation. This filling period should therefore be distinguished from both the biological appearance of cortisol in sweat and the intrinsic electrical response of the aptamer-FET sensor.

27511219, 2026, 10, Downloaded from https://advanced.onlinelibrary.wiley.com/doi/10.1002/adsr.70212 by Yasser Khan - Mount Sinai Hospital , Wiley Online Library on [14/10/2026]. See the Terms and Conditions (https://onlinelibrary.wiley.com/terms-and-conditions) on Wiley Online Library for rules of use; OA articles are governed by the applicable Creative Commons License

The MIP-based cortisol sensing platform reported by Garg et al. [149] provides a particularly useful example because both filling and clearance were characterized clearly. At an average sweat rate of approximately 2 μL/min, its 2.4 μL sensing chamber filled within 2 min, while complete sweat removal required approximately 3 min through a 0.5-mm-wide paperfluidic channel. The analytical signal itself increased over the first 2 min and reached a plateau after approximately 3 min. Because chamber filling, sample clearance, and sensor equilibration occurred on similar timescales, the measured temporal response could not be assigned to any one of these processes. Nevertheless, the platform demonstrated that minute-scale sample renewal is feasible when sensing-chamber volume and sweat flow are appropriately matched. It also illustrates an important continuous-monitoring design criterion: chamber volume must be small enough to permit rapid replacement but sufficiently stable to maintain consistent sensor contact.

Interface geometry can generate additional delays that may otherwise be incorrectly attributed to recognition chemistry. Parlak et al. [173] reported a geometric artifact when comparing skin-contact interfaces: a simple hole-punch acquisition layer produced no significant sensor signal until approximately 6 min later. In contrast, the laser-patterned capillary architecture produced a much earlier response and subsequently maintained a stable signal for approximately 10 min. Although the study did not report a complete microfluidic transport-lag constant, the comparison proves that apparent sensor delay can originate from inefficient fluid delivery. Thus, the fluidic interface should be characterized independently before temporal changes are assigned to sensor kinetics.

Longer-duration cortisol monitoring requires sustained sample renewal while limiting carryover from previously collected sweat. Singh et al. [101] integrated multiple inlets, microfluidic channels, a sensing reservoir, and an outlet to support continuous cortisol monitoring for up to 90 min. Sweat reached the sensing reservoir within approximately 6–10 min, and continuous replacement through the outlet began after the chamber was filled. By contrast, platforms such as MicroSweat [174] directed sweat generated at successive time points into separate absorbent storage chambers, enabling chronological sampling instead of continuous sensing. These contrasting architectures suggest two strategies for preserving temporal information: continuous renewal of the sensing volume and physical separation of sequential samples. Designs intended for extended monitoring must therefore address not only total collection capacity but also sample replacement, stagnant volumes, channel contamination, changes in wettability, and physical separation of successive samples.

As an alternative to conventional microfluidic routing, porous materials can harvest sweat directly at the sensing interface. Tang et al. [175] used a permeable hydrogel to collect fingertip sweat without stimulation or a separate microfluidic conduit, enabling a cortisol assay with a total analysis time of approximately 3.5 min. Similarly, Wang et al. [176] used a porous chitosan hydrogel as both the sweat-collection medium and, after carbon-nanotube incorporation, a conductive interface between accumulated fingertip sweat and the MIP electrode. The on-body measurements required only a 30-s fingertip contact period prior to electrochemical interrogation.

Accordingly, time-resolved wearable studies would ideally characterize the sweat-induction condition, anatomical collection site and area, time to first sweat, volumetric or area-normalized sweat rate, inlet and chamber volumes, channel dimensions, time to reach the sensor, chamber-filling time, sample-clearance or washout time, effective sample age, sampling interval, total device capacity, saturation time, and whether old and new sweat are physically separated. Latency induced via biological transport into sweat, microfluidic transport and renewal, and intrinsic sensor response should be reported as distinct quantities. Although favorable microfluidic architectures may achieve sub-minute to minute-scale handling, practical on-body delays can extend to tens of minutes when sweat induction, low secretion rates, initial filling, flushing, and sample replacement are accounted for. The physiological fidelity of a wearable sweat-based cortisol measurement therefore depends not only on sensor sensitivity but also on whether the microfluidic interface delivers a fresh, time-defined, and adequately renewed sample.

5.2 | Microneedle-Based Interstitial Fluid Sampling

Microneedle-based interstitial-fluid (ISF) sensing provides minimally invasive access to cortisol and has potential for wearable, time-resolved monitoring, particularly due to the strong correlation between plasma and ISF cortisol levels. However, the temporal performance of a microneedle platform cannot be inferred solely from the response time of its sensing element. Depending on the device architecture, the measured response may reflect vascular-to-interstitial transport, diffusion within the dermis, ISF extraction or uptake by the microneedles, analyte transport through hydrogel or microfluidic components, molecular-recognition kinetics, and signal equilibration. These biological, sampling, transport, and sensing contributions should therefore be distinguished when determining whether a platform can resolve physiologically relevant cortisol fluctuations.

Mechanistic studies show that microneedle sampling is governed by tissue hydraulic resistance, microneedle geometry, and the pressure gradient applied across the skin [177]. Dermal ISF turnover has been estimated at approximately 60 nL min^{-1} cm^{-2}, equivalent to approximately 3.6 μL h^{-1} cm^{-2} [178]. This relatively slow replenishment places a physiological constraint on continuous extraction: increasing the applied pressure or number of microneedles may improve the recovered volume, but extraction that is too rapid relative to local replenishment could produce depletion of the sampled region.

Abbasiasl et al. demonstrated this pressure-driven approach using a touch-activated wearable device comprising laser-drilled hollow microneedles, a microfluidic collection chamber, and a finger-actuated vacuum generator. The system maintained pressures as low as approximately −53 kPa and collected ISF at approximately 2 μL $needle^{-1}$ h^{-1}, with the recovered fluid directed to electrochemical glucose and pH sensors [178]. The platform established that an integrated vacuum can support sustained ISF withdrawal without an external pump, although the reported collection rate represents bulk fluid extraction rather than biomarker–specific temporal resolution.

27511219, 2026, 10, Downloaded from https://advanced.onlinelibrary.wiley.com/doi/10.1002/adsr.70212 by Yasser Khan - Mount Sinai Hospital , Wiley Online Library on [14/10/2026]. See the Terms and Conditions (https://onlinelibrary.wiley.com/terms-and-conditions) on Wiley Online Library for rules of use; OA articles are governed by the applicable Creative Commons License

Hydrogel microneedles collect ISF through swelling rather than through continuous pressure-driven flow [179]. Laszlo et al. developed superabsorbent acrylate-based microneedle arrays that recovered up to 6 μL of dermal ISF within 10 min in vivo, thereby enabling the identification of 176 clinically relevant biomarkers by proteomic analysis [180]. The study also showed that the molecular profile of the recovered ISF depended strongly on hydrogel composition, indicating selective partitioning of biomarkers into different microneedle formulations. Thus, sampling performance depends not only on the volume absorbed but also on interactions between the analyte and the hydrogel network. For cortisol applications, diffusion, partitioning, and nonspecific retention within the selected polymer would need to be characterized before the extracted concentration could be considered representative of native ISF. Rapid fluid recovery has also been demonstrated using pressure-gradient-based sampling. Hung et al. collected an average of approximately 15.5 mg of human dermal ISF within 5 min by designing the spatial pressure gradient that drives fluid from microneedle-created pores into the collection chamber [181]. Together, the Laszlo and Hung studies show that microneedle systems can obtain analytically useful sample volumes within several minutes. However, the time required to collect bulk ISF does not necessarily equal the time required for a specific biomarker to reach and equilibrate with an integrated sensor.

This distinction was demonstrated by the Wearable Aptalyzer developed by Bakhshandeh et al., which coupled methacrylated hyaluronic–acid hydrogel microneedles to electrochemical aptamer sensors for glucose and lactate [182]. The hydrogel transported analytes from the skin to aptamer-functionalized electrodes positioned behind the microneedle array. Although the microneedles approached maximum swelling within approximately 6 min, the electrochemical response in ex vivo porcine skin stabilized only after approximately 20 min. The effective time resolution was therefore limited primarily by analyte diffusion through the hydrogel and binding at the aptamer interface rather than by swelling or electrochemical measurement alone. Some platforms have proposed computational compensation for these effects. Dai et al. integrated hydrogel microneedles with a predictive model intended to account for signal delay during ISF sensing [183]. Such modeling may improve temporal alignment, but its accuracy depends on whether the underlying delay is stable across concentration direction, anatomical site, participant, and physiological state. It cannot substitute for experimental separation of physiological transport, device transport, and transducer response.

5.2.1 | ISF Sampling in Cortisol Sensor Research

Direct characterization of cortisol dynamics with microneedle sensors remains limited. In rats, a 3D-printed scaffolded hydrogel microneedle array recorded an ISF cortisol time-to-peak of 61.6 $\pm$ 27.5 min after retro-orbital hydrocortisone administration [115]. This interval represents an end-to-end response that includes systemic hydrocortisone distribution, vascular-to-interstitial transfer, local dermal transport, and transport and equilibration within the cortisol-responsive hydrogel and optical sensing system. Because these contributions were not measured independently, the reported peak time cannot be interpreted as a physiological blood-to-ISF delay. The animal model and pharmacological administration route also limit its direct extrapolation to endogenous cortisol responses following acute stress in humans.

Other cortisol platforms further illustrate the temporal averaging introduced by finite collection periods. A europium-based metal–organic framework hydrogel microneedle patch recovered up to approximately 5 μL of ISF during a 1-h application and distinguished stress-associated cortisol states [184]. However, the resulting measurement integrates cortisol accumulated over the collection interval rather than resolving a continuous trajectory. Similarly, the aptamer-based hybridization chain reaction microneedle patch distinguished resting and exercise-fatigue cortisol levels in mice but did not quantify the corresponding blood-to-ISF delay [185]. The Sharkey et al. system combined hydrogel-forming microneedles with a hydrogel osmotic pump and a paper microfluidic collection layer [186]. The osmotic gradient transported ISF through the swollen microneedles and along the paper collection layer. After 15 min, cortisol recovery varied across the paper segments despite complete wetting, indicating incomplete analyte equilibration. Recovery improved at longer durations and closer to the microneedle interface. Thus, the paper pathway may have introduced additional transport delay [186], suggesting placement of the sensor near the extraction site with minimal intervening volume. These platforms demonstrate cortisol-detection feasibility but do not yet establish the temporal resolution required to reconstruct rapid endocrine dynamics.

Future studies should characterize the complete delay from systemic cortisol changes to sensor response, distinguishing vascular-to-ISF transport, local replenishment, extraction, hydrogel uptake, analyte transport, and transducer equilibration. Rising and falling kinetics should be assessed separately, alongside key device parameters such as hydrogel composition, microneedle area, extraction pressure, collection volume, sensor position, dead volume, drift, and stability.

Cortisol–specific validation should synchronize plasma and ISF measurements during controlled physiological or pharmacological perturbations, using sampling intervals shorter than the expected delay. Until these factors are independently characterized, "real-time" microneedle signals may reflect delayed or time-averaged ISF cortisol concentrations rather than instantaneous endocrine responses.

6 | Preliminary Observations of Cortisol Dynamics at High Temporal Resolution

6.1 | Experimental Method

The objective of this exploratory pilot study was to evaluate whether common, resource-efficient laboratory stress paradigms could produce cortisol dynamics that could be resolved using high-frequency sampling. The study was designed to approximate the temporal profiling envisioned for wearable cortisol–monitoring systems, which seek to characterize changes over time rather than provide only isolated pre- and post-stressor measurements. The TSST, MIST, and MAST were not selected because of their greater experimental complexity and, in some cases, their requirement for trained evaluators or social evaluation. Instead,

27511219, 2026, 10, Downloaded from https://advanced.onlinelibrary.wiley.com/doi/10.1002/adsr.70212 by Yasser Khan - Mount Sinai Hospital , Wiley Online Library on [14/10/2026]. See the Terms and Conditions (https://onlinelibrary.wiley.com/terms-and-conditions) on Wiley Online Library for rules of use; OA articles are governed by the applicable Creative Commons License

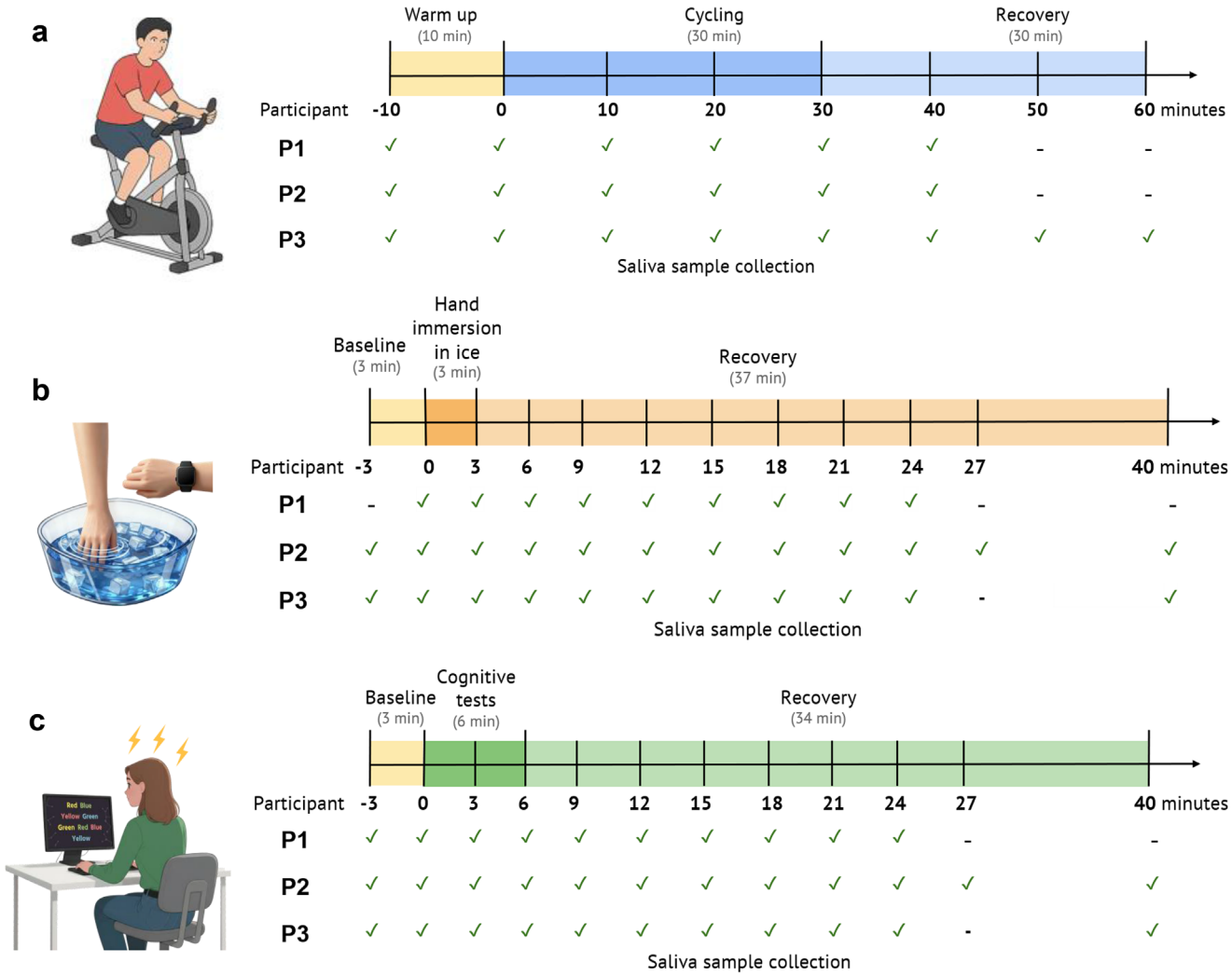


FIGURE 2 | Experimental protocol and data collection protocol used in this work. Participants completed three acute stress paradigms: (a) Stationary Bike exercise, (b) Cold Pressor Test (CPT), and (c) Cognitive (Math/Stroop) task, in separate sessions. Salivary cortisol was collected prior to each protocol (at baseline or during warm up) and at repeated intervals during the protocol and recovery periods. Exact collection timing and total duration varied across paradigms and participants due to protocol refinements made during the study.

three experimentally distinct stress paradigms were evaluated: stationary bike exercise, the CPT, and a computerized cognitive task combining mental arithmetic and the Stroop test.

Three healthy adult participants (one undergraduate, one master's student, and one Ph.D. student; age range 21–29 years) were recruited under an Institutional Review Board (IRB)-approved experimental protocol (HS-25-00142). Participants were non-smokers and reported normal sleep–wake schedules (further information is available in Table S2). Participant 3 reported antibiotic use for strep throat. Written informed consent was obtained before participation. Each participant completed circadian sampling in the morning and at night and all three acute stress paradigms, with the experimental sessions conducted on separate days (Figure 2). Acute stress experiments were conducted during the afternoon to reduce time-of-day variability in cortisol concentrations. The CPT sessions were conducted at approximately 5:30 pm. Morning-to-evening cortisol variation governed by circadian rhythm was assessed by collecting saliva at 10 am and 10 pm across three consecutive days, resulting in six circadian samples per participant. The small cohort was selected in a manner consistent with proof-of-concept wearable cortisol studies, which commonly use a limited number of participants for initial human validation [99–101, 149, 173]. The study combined repeated morning-and-evening sampling with dense sampling across multiple stress paradigms to characterize time-dependent cortisol dynamics and inform future wearable cortisol research, rather than support population-level inference.

Saliva was selected as the cortisol-testing matrix because it avoided invasive finger-prick blood collection and the collection latency associated with sweat-based measurements. Saliva was collected using a SalivaBio Oral Swab (SOS; Salimetrics), which was placed under the participant's tongue for 2 min. Samples were collected every 3 min during the CPT and cognitive protocols and every 10 min during the stationary bike protocol. Thus, each 3-min sampling cycle comprised a 2-min swab-collection period followed by a 1-min interval, whereas each 10-min cycle comprised a 2-min collection period followed by an 8-min interval. This dense sampling schedule was intended to provide

27511219, 2026, 10, Downloaded from https://advanced.onlinelibrary.wiley.com/doi/10.1002/adsr.70212 by Yasser Khan - Mount Sinai Hospital , Wiley Online Library on [14/10/2026]. See the Terms and Conditions (https://onlinelibrary.wiley.com/terms-and-conditions) on Wiley Online Library for rules of use; OA articles are governed by the applicable Creative Commons License

temporal resolution approaching that envisioned for wearable biomarker-monitoring systems and to capture cortisol changes that could be missed by conventional protocols employing less frequent sampling.

Because this was an iterative pilot study, participants were enrolled and tested sequentially. P1 was evaluated using the initial sampling schedules, whereas the schedules for subsequent participants were extended by adding later time points when the initial observation windows did not adequately characterize the recovery phase. Thus, the protocol refinements were intended to improve temporal coverage rather than facilitate direct comparisons among participants (Figure 2).

For the stationary bike exercise, all participants completed a 30-min session on an Exerpeutic Therapeutic Fitness bike. Participants maintained a cadence of 60 rpm, and the bike tension was held constant at level 4 of a maximum of 8 throughout the exercise period. P1 was trained and reported exercising an average of 10 h per week, whereas P2 and P3 were untrained and reported averages of 3 and 0 h per week, respectively. Heart rate, perceived exertion, power output, and aerobic capacity were not measured; therefore, although the prescribed cadence and bike-tension setting were standardized, the physiological and perceived exercise intensity could not be quantified. Saliva samples were collected at −10, 0, 10, 20, 30, and 40 min relative to the start of exercise for P1 and P2. The exercise ended at 30 min, making the 40-min collection the first post-exercise recovery measurement. The initial sampling window did not capture a clear declining phase and included only one post-exercise measurement, limiting characterization of the recovery trajectory. Therefore, collections at 50 and 60 min were added for P3 to better characterize post-exercise cortisol dynamics. In total, six samples were collected from P1 and P2 and eight from P3 (Figure 2a).

The CPT was conducted under controlled laboratory conditions at approximately 5:30 pm to avoid the potentially blunted cortisol response observed during the first half of the day. Participants immersed their non-dominant hand up to the wrist in a plastic tank containing water maintained at 2°C for 3 min. For P1, saliva was collected at 0, 3, 6, 9, 12, 15, 18, 21, and 24 min, resulting in 9 samples (Figure 2b). This initial observation window did not clearly capture the complete declining phase. The subsequent sampling schedules were therefore extended to determine whether the pre-test baseline and expected post-peak decline could be more clearly observed. Collection at −3 and 40 min was added for P3, resulting in 11 samples, whereas collections at −3, 27, and 40 min were added for P2, resulting in 12 samples.

The cognitive stress protocol consisted of a computerized mental-arithmetic task followed by a color-word Stroop task. Participant information was collected using the computerized intake interface shown in Figure S1, and participants completed a timed resting period before the task (Figure S2). Representative arithmetic, Stroop, and post-task feedback screens are shown in Figure S3. Each component lasted approximately 3 min, resulting in a total task duration of approximately 6 min. Participants completed both tasks individually while seated, without an evaluator or audience; therefore, the protocol did not include social evaluation. Both components incorporated time pressure through limited response periods, computer-controlled task progression, a visible countdown, and a ticking-clock sound. During the arithmetic task, participants were instructed to respond quickly and accurately. The software recorded the selected answer, response accuracy, and response time for each question. Immediate feedback identified correct responses and displayed the correct answer following an incorrect or missed response. Question difficulty was adjusted automatically according to participant performance. During the Stroop task, participants identified the displayed font color rather than the incongruent color word. The stimulus-presentation rate increased progressively, and correct, incorrect, and missed responses and their relative timestamps were recorded. Immediate correctness feedback was not displayed during the Stroop component. Thus, the cognitive protocol incorporated time pressure, computer-controlled progression, and negative performance feedback during the arithmetic component, but it did not include social evaluation or an explicit manipulation of uncontrollability. For P1, saliva was collected every 3 min from −3 to 24 min during the cognitive protocol and recovery period (Figure 2c). The subsequent sampling schedules were extended to better characterize the declining phase. A collection at 40 min was added for P3, whereas collections at 27 and 40 min were added for P2.

Participants were instructed to refrain from eating, chewing gum, smoking, drinking anything other than water, and brushing their teeth for at least 30 min before each experimental session. Immediately after collection, each sample was placed in an individually barcoded SalivaBio Swab Storage Tube and frozen at or below −20°C. Samples were subsequently shipped to the Salimetrics laboratory and analyzed for cortisol using ELISA.

6.2 | Pilot Observations

The morning and evening cortisol measurements showed the expected decrease from 10 am to 10 pm across all three consecutive days and participants (Figure 3). This consistent morning–to–evening difference is compatible with the expected diurnal pattern of cortisol secretion. In all participants, cortisol concentrations were highest on the morning of Day 1 compared with the morning measurements on subsequent days, potentially reflecting anticipatory activation of the HPA axis in response to a new experimental paradigm. While Participants 1 and 3 displayed relatively similar cortisol values, Participant 2 exhibited the largest morning–to–evening fluctuation and consistently higher cortisol levels, a pattern also observed in the other experiments.

Figure 5 summarizes both the morning-to-evening variation in cortisol levels and the quantified responses to different stress-induction experiments. Figure 5a illustrates the morning–to–night cortisol ratio across participants, with an average ratio of approximately 3.3, highlighting the expected diurnal decline in cortisol levels. Figure 5b–d presents the quantified stress responses using two parameters, r_{20} and r_{40}, defined as the ratio of cortisol concentrations measured at approximately 20 and 40 min after stressor onset, respectively, to the corresponding baseline cortisol concentration. These metrics were used to compare cortisol response magnitudes across the different stress paradigms.

27511219, 2026, 10, Downloaded from https://advanced.onlinelibrary.wiley.com/doi/10.1002/adsr.70212 by Yasser Khan - Mount Sinai Hospital , Wiley Online Library on [14/10/2026]. See the Terms and Conditions (https://onlinelibrary.wiley.com/terms-and-conditions) on Wiley Online Library for rules of use; OA articles are governed by the applicable Creative Commons License

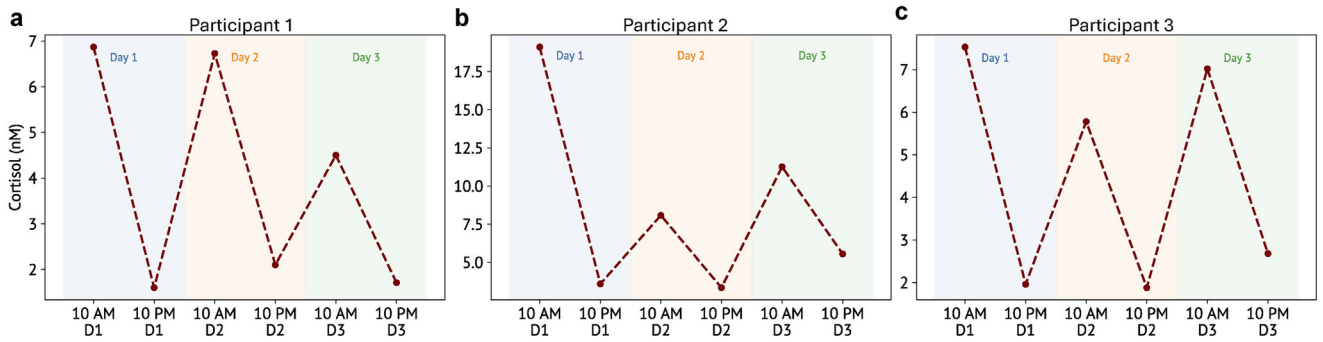


FIGURE 3 | Morning-to-evening variation in salivary cortisol across three consecutive days for participants 1, 2 and 3 in (a–c).

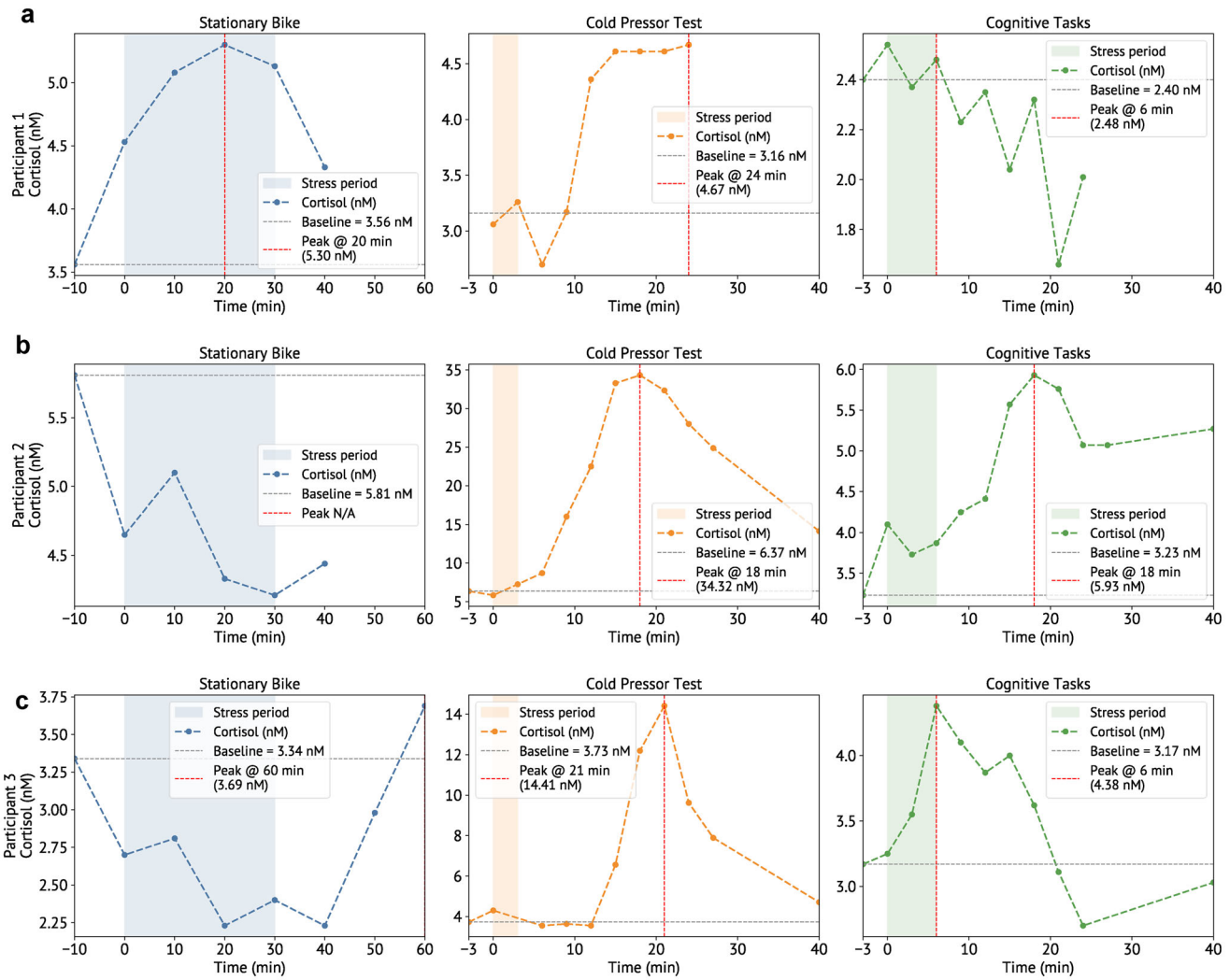


FIGURE 4 | Cortisol reactivity across the stationary-bike exercise, Cold Pressor Test (CPT), and cognitive stress-induction paradigms for Participants 1–3, shown in panels (a–c), respectively.

Following the CPT, cortisol concentrations reached their maximum measured values 18–24 min after stressor onset (Figure 4), with r_{20} values ranging from 1.5 to 5.3 (Figure 5b). For exploratory purposes, we applied the baseline-to-peak increase of at least 1.5 nM proposed by Miller et al. for distinguishing salivary cortisol responders from non-responders following the TSST protocol [92]. Participant 2 exhibited the largest response, with cortisol increasing from a baseline of 6.37 nM to a maximum of 34.32 nM at 18 min, corresponding to a peak-to-baseline increase of 27.95 nM and an approximately 5.4-fold peak concentration relative to baseline (Figure 4b). Participant 3 reached a maximum of 14.41 nM at 21 min from a baseline of 3.73 nM, corresponding

27511219, 2026, 10, Downloaded from https://advanced.onlinelibrary.wiley.com/doi/10.1002/adsr.70212 by Yasser Khan - Mount Sinai Hospital , Wiley Online Library on [14/10/2026]. See the Terms and Conditions (https://onlinelibrary.wiley.com/terms-and-conditions) on Wiley Online Library for rules of use; OA articles are governed by the applicable Creative Commons License

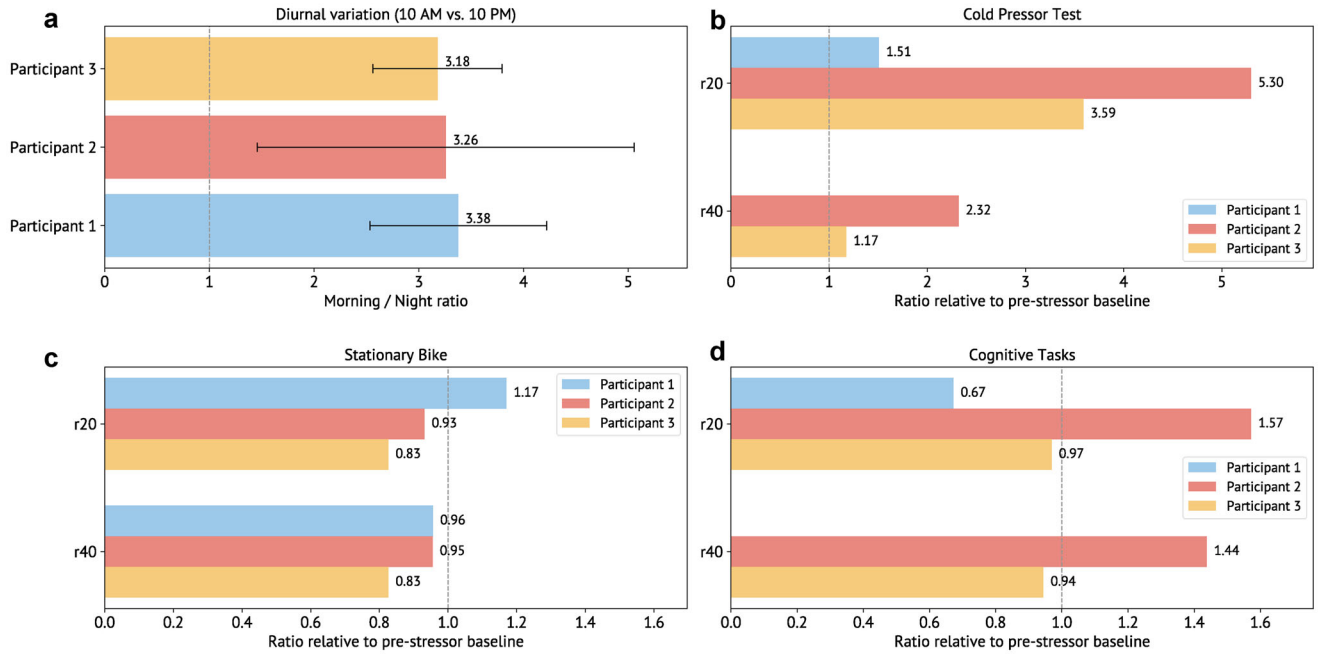


FIGURE 5 | Cortisol reactivity metrics across daily variation and stress-induction paradigms. Horizontal grouped bar plots displaying the ratios of cortisol concentrations between morning and night (a), and at 20 min (r_{20}) and 40 min (r_{40}) after stressor onset relative to baseline for each participant under three paradigms: (b) CPT, (c) stationary bike, and (d) cognitive (Math/Stroop) task. The dashed line at a ratio of 1.0 marks the baseline level.

to an increase of 10.68 nM and an approximately 3.9-fold peak concentration relative to baseline (Figure 4c). Both participants, therefore, clearly exceeded the exploratory reference threshold.

Participant 1 exhibited a smaller and more sustained response. Cortisol remained near its maximum from 15 to 24 min, with concentrations ranging from 4.61 nM at 15 min to a maximum of 4.67 nM at 24 min. Relative to the calculated baseline of 3.16 nM, the maximum increase was 1.51 nM, narrowly meeting the reference threshold (Figure 4a). However, selecting any of the near-maximum measurements from 15 to 21 min would yield an increase of 1.45 nM, which falls slightly below the threshold. Participant 1's classification was therefore sensitive to the selected peak time and should be interpreted cautiously. Based on the maximum measured concentrations, all three participants met the exploratory threshold. Because this criterion was developed for the TSST and has not been validated specifically for the CPT, its application here is descriptive and should not be interpreted as establishing a CPT responder rate or demonstrating universal effectiveness.

Cortisol response and recovery patterns also varied among participants. Participant 1, who was evaluated using the initial sampling schedule, remained near the maximum through the final measurement at 24 min, and no declining phase was observed within this sampling window. Consequently, the timing of recovery could not be determined. This incomplete recovery profile motivated the addition of later sampling points for subsequently tested participants as part of the iterative pilot design. Participants 2 and 3 were therefore monitored for 40 min, allowing for a more complete characterization of their post-peak trajectories. They exhibited distinct maxima at 18 and 21 min, respectively, followed by progressive decreases through 40 min. Neither participant had fully returned to baseline by the end of the extended observation period, although Participant 3 approached the baseline more closely and exhibited a more rapid post-peak decline. Previous research, however, has reported that sweat cortisol returned to baseline within 24–27 min after stress induction [99].

The difference between that finding and the recovery trajectories observed here may have arisen from participant characteristics, stress-induction protocols, or sampling matrices. Studies involving larger cohorts and standardized protocols are needed to characterize generalizable recovery patterns and identify factors contributing to interindividual variation.

During the 30-min stationary-bike experiment, Participant 1, who was a trained athlete reporting approximately 10 h of exercise per week, exhibited a cortisol elevation at 20 min that gradually declined thereafter (Figure 4a). Participants 2 and 3, who were not trained athletes and reported approximately 3 and 0 h of exercise per week, respectively, did not exhibit distinct exercise-associated cortisol peaks during the initial observation period. Participant 3 showed an increase between 40 and 60 min during the extended recovery period. Although all participants exercised at the same cadence and bike-tension setting, their different training backgrounds and BMIs–20.8, 21.0, and 31.5 kg/m^2 for Participants 1, 2, and 3, respectively–suggest that the standardized workload may have represented different relative exercise intensities. This interindividual variability qualitatively resembles the patterns reported by Pearlmutter et al., who observed relatively stable salivary cortisol concentrations in athletes and decreases in non-athletes following exercise [144]. In both studies, cortisol trajectories may have reflected interactions among training status, relative exercise intensity, physical characteristics, and the underlying time-of-day decrease in cortisol. However, because heart rate, perceived exertion, power output, and aerobic capacity

27511219, 2026, 10, Downloaded from https://advanced.onlinelibrary.wiley.com/doi/10.1002/adsr.70212 by Yasser Khan - Mount Sinai Hospital , Wiley Online Library on [14/10/2026]. See the Terms and Conditions (https://onlinelibrary.wiley.com/terms-and-conditions) on Wiley Online Library for rules of use; OA articles are governed by the applicable Creative Commons License

were not measured in the present study, the respective contributions of training status, BMI, and exercise intensity could not be separated.

Variable response patterns were also observed during the cognitive-stressor experiments. Participant 2 exhibited a profile similar to that observed following the CPT, with cortisol peaking at 18 min at approximately 1.83 times the baseline concentration. For Participant 3, cortisol peaked at 6 min, with a baseline-to-peak increase of 1.21 nM. The early timing of this peak, together with an r_{20} value of approximately 1, suggests that it may not represent the delayed cortisol response typically expected after stressor onset and could instead reflect anticipatory stress or endogenous variability.

The aim of this pilot was to achieve high-frequency endocrine profiling to capture finer details of cortisol dynamics. However, the small sample size limits the broader interpretation of these findings. Additionally, there were several potential sources of interindividual variability that were not controlled during experimentation, such as caffeine intake, sleep, recent stress, and medication use. Given the small sample size, the potential influence of these factors on cortisol dynamics could not be reliably evaluated. Despite these limitations, the dense temporal sampling successfully captured early post-stressor changes that could be overlooked by conventional salivary protocols, which typically employ sampling intervals of approximately 10–30 min, or only before and after an experimental intervention [9, 144]. The observations showed the expected morning–to–evening decrease in cortisol across all participants, as well as marked interindividual and protocol-dependent variability in acute stress reactivity. Following the CPT, all three participants exhibited observable cortisol increases, although the magnitude, timing, and recovery patterns differed among participants. The findings illustrate interindividual and protocol-dependent variability and indicate that factors such as physical conditioning, task engagement, anticipatory stress, circadian decline, and endogenous cortisol pulsatility should be considered when designing wearable-sensor experiments and recruiting participants. Thus, these preliminary observations may assist biosensor research groups in designing future studies to evaluate wearable-sensor performance while accounting for interindividual differences in participant characteristics.

7 | Conclusion

This study consolidates the current understanding of cortisol physiology by linking circadian regulation, acute stress reactivity, and laboratory paradigms to practical applications in biosensor research. Variability in individual stress responses is influenced by the type and intensity of the stressor, as well as by lifestyle factors that modulate cortisol profiles and baseline concentrations. Stress-induction paradigms reported in the literature were compared in terms of ease of implementation, efficacy, reproducibility, and potential for habituation. Socially evaluative and multicomponent paradigms often elicit robust responses; however, these protocols involve greater complexity and may introduce additional variability. The impact of sampling-matrix selection on recovering cortisol dynamics was also analyzed. Recent advances in wearable cortisol sensors and the temporal-resolution requirements for these devices were discussed. Alongside advances in cortisol–specific sensors, improvements in sampling techniques for wearable-accessible matrices such as sweat and interstitial fluid are necessary milestones for continuous monitoring. Based on preliminary observations from this pilot study with temporally dense sample collection, the CPT produced observable cortisol increases across participants, with differences in peak magnitude, timing, and recovery. Morning and evening measurements also showed a consistent morning–to–evening decrease in cortisol. These observations are particularly relevant given the delays introduced by wearable measurements, including matrix–specific physiological delays, sample collection, microfluidic transport, and sensor response time. Characterizing cortisol dynamics at high temporal resolution can inform the selection of sampling intervals and observation windows needed to capture the rising phase, peak, and return toward baseline. The results also suggest that optimal sampling requirements may vary among participants and stressor types, requiring different sampling frequencies, monitoring durations, and sensor dynamic ranges. Future work should combine cortisol measurements with physiological signals such as heart rate, skin conductance, and temperature to support a more comprehensive, real-time assessment of human stress physiology.

Acknowledgments

Yasser Khan thanks support from NIH 1R61MH135407-03. Munia Ferdoushi acknowledges the Schlumberger Foundation Faculty for the Future Fellowship. During the preparation of this work, the authors used ChatGPT to improve grammar, clarity, and readability of the manuscript. After using this tool, the authors reviewed and edited the content as needed and take full responsibility for the final content of the publication. ChatGPT was not used to generate scientific data, perform data analysis, or formulate conclusions.

Conflicts of Interest

The authors declare no conflicts of interest.

Data Availability Statement

The data that support the findings of this study are available from the corresponding author upon reasonable request.

References

1. J. P. Herman, J. M. McKlveen, S. Ghosal, et al., "Regulation of the Hypothalamic-Pituitary-Adrenocortical Stress Response," *Comprehensive Physiology* 6, no. 2 (2016): 603–621.

2. R. M. Reynolds, J. Labad, M. W. J. Strachan, et al., "Elevated Fasting Plasma Cortisol Is Associated with Ischemic Heart Disease and Its Risk Factors in People with Type 2 Diabetes: The Edinburgh Type 2 Diabetes Study," *The Journal of Clinical Endocrinology and Metabolism* 95, no. 4 (2010): 1602–1608.

3. M. K. Kwok, I. Kawachi, D. Rehkopf, and C. M. Schooling, "The Role of Cortisol in Ischemic Heart Disease, Ischemic Stroke, Type 2 Diabetes, and Cardiovascular Disease Risk Factors: A Bi-Directional Mendelian Randomization Study," *BMC Medicine* 18, no. 1 (2020): 363.

4. I. Cano-López and E. González-Bono, "Cortisol Levels and Seizures in Adults with Epilepsy: A Systematic Review," *Neuroscience and Biobehavioral Reviews* 103 (2019): 216–229.

27511219, 2026, 10, Downloaded from https://advanced.onlinelibrary.wiley.com/doi/10.1002/adsr.70212 by Yasser Khan - Mount Sinai Hospital , Wiley Online Library on [14/10/2026]. See the Terms and Conditions (https://onlinelibrary.wiley.com/terms-and-conditions) on Wiley Online Library for rules of use; OA articles are governed by the applicable Creative Commons License

5. E. Knezevic, K. Nenic, V. Milanovic, and N. N. Kneževic, "The Role of Cortisol in Chronic Stress, Neurodegenerative Diseases, and Psychological Disorders," *Cells* 12 (2023): 2726.

6. M. Chesnut, S. Harati, P. Paredes, et al., "Stress Markers for Mental States and Biotypes of Depression and Anxiety: A Scoping Review and Preliminary Illustrative Analysis," *Chronic Stress* 5 (2021): 24705470211000338.

7. J. M. Mateo, "Inverted-U Shape Relationship between Cortisol and Learning in Ground Squirrels," *Neurobiology of Learning and Memory* 89, no. 4 (2008): 582–590.

8. R.-P. Juster, A. Perna, M.-F. Marin, S. Sindi, and S. J. Lupien, "Timing Is Everything: Anticipatory Stress Dynamics among Cortisol and Blood Pressure Reactivity and Recovery in Healthy Adults," *Stress* 15, no. 6 (2012): 569–577.

9. N. F. N. Linares, V. Charron, A. J. Ouimet, P. Labelle, and H. Plamondon, "A Systematic Review of the Trier Social Stress Test Methodology: Issues in Promoting Study Comparison and Replicable Research," *Neurobiology of Stress* 13 (2020): 100235.

10. C. Jones and C. Gwenin, "Cortisol Level Dysregulation and Its Prevalence—Is It Nature's Alarm Clock?" *Physiological Reports* 8, no. 24 (2020): e14644.

11. M. Balbo, R. Leproult, and E. V. Cauter, "Impact of Sleep and Its Disturbances on Hypothalamo-Pituitary-Adrenal Axis Activity," *International Journal of Endocrinology* 2010 (2010): 1–16.

12. J. H. van Dalfsen and C. R. Markus, "The Influence of Sleep on Human Hypothalamic–Pituitary–Adrenal (HPA) Axis Reactivity: A Systematic Review," *Sleep Medicine Reviews* 39 (2017): 187–194.

13. G. W. Liddle, "An Analysis of Circadian Rhythms in Human Adrenocortical Secretory Activity," *Transactions of the American Clinical and Climatological Association* 77 (1966): 151–160.

14. E. Challet, "Minireview: Entrainment of the Suprachiasmatic Clockwork in Diurnal and Nocturnal Mammals," *Endocrinology* 148, no. 12 (2007): 5648–5655.

15. H. Oster, E. Challet, V. Ott, et al., "The Functional and Clinical Significance of the 24-Hour Rhythm of Circulating Glucocorticoids," *Endocrine Reviews* 38, no. 1 (2017): 3–45.

16. F. H. Katz, "Adrenal Function during Bed Rest," *Aerospace Medicine* 35, no. 9 (1964): 848–851.

17. G. T. Perkoff, K. Eik-Nes, C. A. Nugent, et al., "Studies of the Diurnal Variation of Plasma 17-Hydroxycorticosteroids in Man," *Journal of Clinical Endocrinology and Metabolism* 19, no. 4 (1959): 432–443.

18. D. N. Orth, D. P. Island, and G. W. Liddle, "Experimental Alteration of the Circadian Rhythm in Plasma Cortisol (17-OHCS) Concentration in Man," *Journal of Clinical Endocrinology and Metabolism* 27, no. 4 (1967): 549–555.

19. N. A. O'Byrne, F. Yuen, W. Z. Butt, and P. Y. Liu, "Sleep and Circadian Regulation of Cortisol: A Short Review," *Current Opinion in Endocrine and Metabolic Research* 18 (2021): 178–186.

20. R. Van Drunen and K. Eckel-Mahan, "Circadian Rhythms of the Hypothalamus: From Function to Physiology," *Clocks and Sleep* 3 (2021): 189–226.

21. W. H. Walker, J. C. Walton, A. C. DeVries, and R. J. Nelson, "Circadian Rhythm Disruption and Mental Health," *Translational Psychiatry* 10 (2020): 28.

22. Y. Li and I. P. Androulakis, "Light Entrainment of the SCN Circadian Clock and Implications for Personalized Alterations of Corticosterone Rhythms in Shift Work and Jet Lag," *Scientific Reports* 11 (2021): 17929.

23. M. G. Figueiro, B. Plitnick, and M. S. Rea, "The Effects of Chronotype, Sleep Schedule and Light/Dark Pattern Exposures on Circadian Phase," *Sleep Medicine* 15 (2014): 1554–1564.

24. L. Grosser, S. Knayfati, C. Yates, J. Dorrian, and S. Banks, "Cortisol and Shiftwork: A Scoping Review," *Sleep Medicine Reviews* 64 (2021): 101581.

25. D. B. Boivin, P. Boudreau, and A. Kosmadopoulos, "Disturbance of the Circadian System in Shift Work and Its Health Impact," *Journal of Biological Rhythms* 37 (2021): 3–28.

26. K. Burek, S. Rabstein, T. Kantermann, et al., "Night Work, Chronotype and Cortisol at Awakening in Female Hospital Employees," *Scientific Reports* 12 (2022): 2090.

27. A. Andreadi, S. Andreadi, F. Todaro, et al., "Modified Cortisol Circadian Rhythm: The Hidden Toll of Night-Shift Work," *International Journal of Molecular Sciences* 26 (2025): 2090.

28. M. F. Montange, E. V. Cauter, S. Refetoff, D. Désir, J. Tourniaire, and G. Copinschi, "Effects of 'Jet Lag' on Hormonal Patterns. II. Adaptation of Melatonin Circadian Periodicity*," *The Journal of Clinical Endocrinology and Metabolism* 52 (1981): 642–649.

29. M. Wittmann, J. Dinich, M. Merrow, and T. Roenneberg, "Social Jetlag: Misalignment of Biological and Social Time," *Chronobiology International* 23, no. 1–2 (2006): 497–509.

30. A. B. Fishbein, K. L. Knutson, and P. C. Zee, "Circadian Disruption and Human Health," *Journal of Clinical Investigation* 131 (2021): e148286.

31. R. Caliandro, A. A. Streng, L. W. M. van Kerkhof, G. T. J. van der Horst, and I. Chaves, "Social Jetlag and Related Risks for Human Health: A Timely Review," *Nutrients* 13, no. 12 (2021): 4543.

32. C. J. Morris, T. E. Purvis, K. Hu, and F. A. J. L. Scheer, "Circadian Misalignment Increases Cardiovascular Disease Risk Factors in Humans," *Proceedings of the National Academy of Sciences* 113 (2016): E1402–E1411.

33. R. Crowthers, T. Nguyen, and D. Martínez, "Circadian Disruptions and Their Role in the Development of Hypertension," *Frontiers in Neuroscience* 18 (2024): 1433512.

34. S. James, K. A. Honn, S. Gaddameedhi, and H. P. A. V. Dongen, "Shift Work: Disrupted Circadian Rhythms and Sleep—Implications for Health and Well-Being," *Current Sleep Medicine Reports* 3 (2017): 104–112.

35. S. L. Chellappa, C. J. Morris, and F. A. J. L. Scheer, "Circadian Misalignment Increases Mood Vulnerability in Simulated Shift Work," *Scientific Reports* 10 (2020): 18614.

36. I. Carson, M. Batson, J. Tranmer, T. D. Scribbans, B. J. Gurd, and K. E. Pyke, "Cardiovascular and Cortisol Reactivity to Acute Mental Stress in Female Shift and Non-Shift Workers," *SAGE Open Nursing* 3 (2017): 2377960817709181.

37. C. Zuccarella-Hackl, M. Princip, S. A. Holzgang, et al., "Cortisol Reactivity to Acute Psychosocial Stress in Physician Burnout," *Biomedicines* 12 (2024): 335–335.

38. T. P. Vahl, Y. M. Ulrich-Lai, M. M. Ostrander, et al., "Comparative Analysis of ACTH and Corticosterone Sampling Methods in Rats," *American Journal of Physiology-Endocrinology and Metabolism* 289, no. 5 (2005): E823–E828.

39. N. K. Evanson, J. G. Tasker, M. N. Hill, C. J. Hillard, and J. P. Herman, "Fast Feedback Inhibition of the HPA Axis by Glucocorticoids Is Mediated by Endocannabinoid Signaling," *Endocrinology* 151, no. 10 (2010): 4811–4819.

40. M. P. Boyle, B. J. Kolber, S. K. Vogt, D. F. Wozniak, and L. J. Muglia, "Forebrain Glucocorticoid Receptors Modulate Anxiety-Associated Locomotor Activation and Adrenal Responsiveness," *The Journal of Neuroscience* 26, no. 7 (2006): 1971–1978.

41. K. R. Jones, B. Myers, and J. P. Herman, "Stimulation of the Prelimbic Cortex Differentially Modulates Neuroendocrine Responses to Psychogenic and Systemic Stressors," *Physiology and Behavior* 104, no. 2 (2011): 266–271.

42. S. Makino, T. Shibasaki, N. Yamauchi, et al., "Psychological Stress Increased Corticotropin-Releasing Hormone mRNA and Content in the Central Nucleus of the Amygdala but Not in the Hypothalamic Paraventricular Nucleus in the Rat," *Brain Research* 850, no. 1–2 (1999): 136–143.

27511219, 2026, 10, Downloaded from https://advanced.onlinelibrary.wiley.com/doi/10.1002/adsr.70212 by Yasser Khan - Mount Sinai Hospital , Wiley Online Library on [14/10/2026]. See the Terms and Conditions (https://onlinelibrary.wiley.com/terms-and-conditions) on Wiley Online Library for rules of use; OA articles are governed by the applicable Creative Commons License

43. C. Dayas, K. Buller, J. Crane, Y. Xu, and T. Day, "Stressor Categorization: Acute Physical and Psychological Stressors Elicit Distinctive Recruitment Patterns in the Amygdala and in Medullary Noradrenergic Cell Groups," *European Journal of Neuroscience* 14, no. 7 (2001): 1143–1152.

44. C. V. Dayas, K. M. Buller, and T. A. Day, "Neuroendocrine Responses to an Emotional Stressor: Evidence for Involvement of the Medial but Not the Central Amygdala," *European Journal of Neuroscience* 11, no. 7 (1999): 2312–2322.

45. J. P. Herman, H. Figueiredo, N. K. Mueller, et al., "Central Mechanisms of Stress Integration: Hierarchical Circuitry Controlling Hypothalamo–Pituitary–Adrenocortical Responsiveness," *Frontiers in Neuroendocrinology* 24, no. 3 (2003): 151–180.

46. M. M. Pulopulos, C. Baeken, and R. De Raedt, "Cortisol Response to Stress: The Role of Expectancy and Anticipatory Stress Regulation," *Hormones and Behavior* 117 (2020): 104587.

47. M. Gray, B. Bingham, and V. Viau, "A Comparison of Two Repeated Restraint Stress Paradigms on Hypothalamic–Pituitary–Adrenal Axis Habituation, Gonadal Status and Central Neuropeptide Expression in Adult Male Rats," *Journal of Neuroendocrinology* 22, no. 2 (2010): 92–101.

48. H. F. Figueiredo, B. Bodie, M. Tauchi, C. M. Dolgas, and J. P. Herman, "Stress Integration after Acute and Chronic Predator Stress: Differential Activation of Central Stress Circuitry and Sensitization of the Hypothalamo-Pituitary-Adrenocortical Axis," *Endocrinology* 144 (2003): 5249–5258.

49. S. Bhatnagar and M. Dallman, "Neuroanatomical Basis for Facilitation of Hypothalamic-Pituitary-Adrenal Responses to a Novel Stressor after Chronic Stress," *Neuroscience* 84, no. 4 (1998): 1025–1039.

50. J. O. Vieira, J. O. Duarte, W. Costa-Ferreira, and C. C. Crestani, "Influence of Pre-Existing Hypertension on Neuroendocrine and Cardiovascular Changes Evoked by Chronic Stress in Female Rats," *Psychoneuroendocrinology* 97 (2018): 111–119.

51. J. S. Kim, S. Y. Han, and K. J. Iremonger, "Stress Experience and Hormone Feedback Tune Distinct Components of Hypothalamic CRH Neuron Activity," *Nature Communications* 10 (2019): 5696.

52. K. Putnam, G. P. Chrousos, L. K. Nieman, and D. R. Rubinow, "Sex-Related Differences in Stimulated Hypothalamic-Pituitary-Adrenal Axis during Induced Gonadal Suppression," *The Journal of Clinical Endocrinology and Metabolism* 90, no. 7 (2005): 4224–4231.

53. S. K. Butcher and J. M. Lord, "Stress Responses and Innate Immunity: Aging as a Contributory Factor," *Aging Cell* 3, no. 4 (2004): 151–160.

54. M. Ising and F. Holsboer, "Genetics of Stress Response and Stress-Related Disorders," *Dialogues in Clinical Neuroscience* 8, no. 4 (2006): 433–444.

55. J. Salvador, G. Gutierrez, M. Llavero, J. Gargallo, J. Escalada, and J. López, "Endocrine Disorders and Psychiatric Manifestations," in *Endocrinology and Systemic Diseases. Endocrinology*, ed. P. Portincasa, G. Frühbeck, and H. Nathoe (Springer International Publishing, 2021).

56. S. Cohen, D. Janicki-Deverts, and G. E. Miller, "Psychological Stress and Disease," *JAMA* 298 (2007): 1685–1685.

57. E. F. Walker, H. D. Trotman, B. D. Pearce, et al., "Cortisol Levels and Risk for Psychosis: Initial Findings from the North American Prodrome Longitudinal Study," *Biological Psychiatry* 74, no. 6 (2013): 410–417.

58. P. Björntorp and R. Rosmond, "Obesity and Cortisol," *Nutrition* 16, no. 10 (2000): 924–936.

59. S. Conner and S. Solomon, "Psychiatric Manifestations of Endocrine Disorders," *Journal of Human Endocrinology* 2 (2017): 1–7.

60. M. Starkman, "Neuropsychiatric Findings in Cushing's Syndrome and Exogenous Glucocorticoid Administration," *Endocrinology and Metabolism Clinics* 42 (2013): 477–488.

61. R. Fraser, M. C. Ingram, N. H. Anderson, C. Morrison, E. Davies, and J. M. C. Connell, "Cortisol Effects on Body Mass, Blood Pressure, and Cholesterol in the General Population," *Hypertension* 33, no. 6 (1999): 1364–1368.

62. G. Fava, N. Sonino, and M. Morphy, "Psychosomatic View of Endocrine Disorders," *Psychotherapy and Psychosomatics* 59 (1993): 20–33.

63. R. Anglin, P. Rosebush, and M. Mazurek, "The Neuropsychiatric Profile of Addison's Disease: Revisiting a Forgotten Phenomenon," *The Journal of Neuropsychiatry and Clinical Neurosciences* 18 (2006): 450–459.

64. D. C. Lowes and A. Z. Harris, "Stressed and Wired: The Effects of Stress on the VTA Circuits Underlying Motivated Behavior," *Current Opinion in Endocrine and Metabolic Research* 26 (2022): 100388.

65. V. A. L. Juliano, K. A. Albernaz-Mariano, L. H. H. Covre, et al., "Neurobiological Intersections of Stress and Substance Use Disorders," *Frontiers in Neuroscience* 19 (2025): 1548372.

66. J. Gecaite-Stonciene, B. M. Hughes, N. Kažukauskiene, et al., "Cortisol Response to Psychosocial Stress, Mental Distress, Fatigue and Quality of Life in Coronary Artery Disease Patients," *Scientific Reports* 12 (2022): 19373.

67. X. Chen, D. Gianferante, L. Hanlin, et al., "HPA-Axis and Inflammatory Reactivity to Acute Stress Is Related with Basal HPA-Axis Activity," *Psychoneuroendocrinology* 78 (2017): 168–176.

68. B. S. McEwen and H. Akil, "Revisiting the Stress Concept: Implications for Affective Disorders," *The Journal of Neuroscience* 40 (2020): 12–21.

69. S. Metz, M. Duesenberg, J. Hellmann-Regen, et al., "Blunted Salivary Cortisol Response to Psychosocial Stress in Women with Posttraumatic Stress Disorder," *Journal of Psychiatric Research* 130 (2020): 112–119.

70. J. C. Pruessner, D. H. Hellhammer, and C. Kirschbaum, "Burnout, Perceived Stress, and Cortisol Responses to Awakening," *Psychosomatic Medicine* 61 (1999): 197–204.

71. T. T. Brunyé, S. A. Goring, E. Navarro, et al., "Identifying the Most Effective Acute Stress Induction Methods for Producing SAM- and HPA-Related Physiological Responses: A Meta-Analysis," *Anxiety, Stress, & Coping* 38 (2025): 263–285.

72. T. Reinhardt, C. Schmahl, S. Wüst, and M. Bohus, "Salivary Cortisol, Heart Rate, Electrodermal Activity and Subjective Stress Responses to the Mannheim Multicomponent Stress Test (MMST)," *Psychiatry Research* 198 (2012): 106–111.

73. T. Smeets, S. Cornelisse, C. W. Quaedflieg, T. Meyer, M. Jelícic, and H. Merckelbach, "Introducing the Maastricht Acute Stress Test (MAST): A Quick and Non-Invasive Approach to Elicit Robust Autonomic and Glucocorticoid Stress Responses," *Psychoneuroendocrinology* 37 (2012): 1998–2008.

74. B. M. Kudielka and C. Kirschbaum, "Sex Differences in HPA Axis Responses to Stress: A Review," *Biological Psychology* 69 (2004): 113–132.

75. A. Y. Herrera, S. E. Nielsen, and M. Mather, "Stress-Induced Increases in Progesterone and Cortisol in Naturally Cycling Women," *Neurobiology of Stress* 3 (2016): 96–104.

76. B. M. Kudielka and S. Wüst, "Human Models in Acute and Chronic Stress: Assessing Determinants of Individual Hypothalamus–Pituitary–Adrenal Axis Activity and Reactivity," *Stress* 13, no. 1 (2010): 1–14.

77. C. Kirschbaum, K. M. Pirke, and D. H. Hellhammer, "The 'Trier Social Stress Test'—A Tool for Investigating Psychobiological Stress Responses in a Laboratory Setting," *Neuropsychobiology* 28, no. 1–2 (1993): 76–81.

78. J. A. Bosch, E. J. C. de Geus, D. Carroll, et al., "A General Enhancement of Autonomic and Cortisol Responses during Social Evaluative Threat," *Psychosomatic Medicine* 71 (2009): 877–885.

79. A.-K. Kexel, B. Kluwe-Schiavon, M. Visentini, L. M. Soravia, C. Kirschbaum, and B. B. Quednow, "Stability and Test-Retest Reliability of Different Hormonal Stress Markers upon Exposure to Psychosocial Stress at a 4-Month Interval," *Psychoneuroendocrinology* 132 (2021): 105342.

27511219, 2026, 10, Downloaded from https://advanced.onlinelibrary.wiley.com/doi/10.1002/adsr.70212 by Yasser Khan - Mount Sinai Hospital , Wiley Online Library on [14/10/2026]. See the Terms and Conditions (https://onlinelibrary.wiley.com/terms-and-conditions) on Wiley Online Library for rules of use; OA articles are governed by the applicable Creative Commons License

80. K. Keenan, J. Berona, A. E. Hipwell, S. D. Stepp, and M. Romito, "Validity of the Trier Social Stress Test in Studying Discrimination Stress," *Stress* 24 (2021): 113–119.

81. D. A. Katz and M. K. Peckins, "Cortisol and Salivary Alpha-Amylase Trajectories Following a Group Social-Evaluative Stressor with Adolescents," *Psychoneuroendocrinology* 86 (2017): 8–16.

82. C. Kirschbaum, B. M. Kudielka, J. Gaab, N. C. Schommer, and D. H. Hellhammer, "Impact of Gender, Menstrual Cycle Phase, and Oral Contraceptives on the Activity of the Hypothalamus-Pituitary-Adrenal Axis," *Psychosomatic Medicine* 61 (1999): 154–162.

83. G. E. Miller, E. Chen, and E. S. Zhou, "If It Goes Up, Must It Come Down? Chronic Stress and the Hypothalamic-Pituitary-Adrenocortical Axis in Humans," *Psychological Bulletin* 133 (2007): 25–45.

84. S. S. Dickerson and M. E. Kemeny, "Acute Stressors and Cortisol Responses: A Theoretical Integration and Synthesis of Laboratory Research," *Psychological Bulletin* 130 (2004): 355–391.

85. A. Duchesne, E. Tessera, K. Dedovic, V. Engert, and J. Pruessner, "Effects of Panel Sex Composition on the Physiological Stress Responses to Psychosocial Stress in Healthy Young Men and Women," *Biological Psychology* 89, no. 1 (2012): 99–106.

86. U. S. Wiemers, D. Schoofs, and O. T. Wolf, "A Friendly Version of the Trier Social Stress Test Does Not Activate the HPA Axis in Healthy Men and Women," *Stress* 16 (2013): 254–260.

87. E. C. Helminen, M. Morton, Q. Wang, and J. C. Felver, "A Meta-Analysis of Cortisol Reactivity to the Trier Social Stress Test in Virtual Environments," *Psychoneuroendocrinology* 110 (2019): 104437–104437.

88. W. R. Lovallo, "The Cold Pressor Test and Autonomic Function: A Review and Integration," *Psychophysiology* 12 (1975): 268–282.

89. P. Bachmann, X. Zhang, M. F. Larra, et al., "Validation of an Automated Bilateral Feet Cold Pressor Test," *International Journal of Psychophysiology* 124 (2017): 62–70.

90. L. Schwabe, L. Haddad, and H. Schachinger, "HPA Axis Activation by a Socially Evaluated Cold-Pressor Test," *Psychoneuroendocrinology* 33, no. 6 (2008): 890–895.

91. A. L. McRae, M. E. Saladin, K. T. Brady, H. Upadhyaya, S. E. Back, and M. A. Timmerman, "Stress Reactivity: Biological and Subjective Responses to the Cold Pressor and Trier Social Stressors," *Human Psychopharmacology: Clinical and Experimental* 21, no. 6 (2006): 377–385.

92. R. Miller, F. Plessow, C. Kirschbaum, and T. Stalder, "Classification Criteria for Distinguishing Cortisol Responders from Nonresponders to Psychosocial Stress," *Psychosomatic Medicine* 75 (2013): 832–840.

93. L. Schwabe and H. Schächinger, "Ten Years of Research with the Socially Evaluated Cold Pressor Test: Data from the Past and Guidelines for the Future," *Psychoneuroendocrinology* 92 (2018): 155–161.

94. A. P. J. van Eekelen, G. Kerkhof, and J. van Amsterdam, "Circadian Variation in Cortisol Reactivity to an Acute Stressor," *Chronobiology International* 20 (2003): 863–878.

95. T. Bullock, M. H. MacLean, T. Santander, et al., "Habituation of the Stress Response Multiplex to Repeated Cold Pressor Exposure," *Frontiers in Physiology* 13 (2023): 752900.

96. C. W. Quaedflieg, T. Meyer, P. van Ruitenbeek, and T. Smeets, "Examining Habituation and Sensitization across Repetitive Laboratory Stress Inductions Using the MAST," *Psychoneuroendocrinology* 77 (2017): 175–181.

97. R. S. Lewis, A. Nikolova, D. J. Chang, and N. Y. Weekes, "Examination Stress and Components of Working Memory," *Stress* 11 (2008): 108–114.

98. B. Wang, C. Zhao, Z. Wang, et al., "Wearable Aptamer-Field-Effect Transistor Sensing System for Noninvasive Cortisol Monitoring," *Science Advances* 8 (2022): eabk0967.

99. R. M. Torrente-Rodríguez, J. Tu, Y. Yang, et al., "Investigation of Cortisol Dynamics in Human Sweat Using a Graphene-Based Wireless mHealth System," *Matter* 2, no. 4 (2020): 921–937.

100. N. I. Hossain, T. Noushin, and S. Tabassum, "StressFit: A Hybrid Wearable Physicochemical Sensor Suite for Simultaneously Measuring Electromyogram and Sweat Cortisol," *Scientific Reports* 14 (2024): 29667.

101. N. K. Singh, S. Chung, A. Chang, J. Wang, and D. A. Hall, "A Non-Invasive Wearable Stress Patch for Real-Time Cortisol Monitoring Using a Pseudoknot-Assisted Aptamer," *Biosensors and Bioelectronics* 227 (2023): 115097–115097.

102. R. Pandey, "Perspective—Electrochemical Bio-Wearables for Cortisol Monitoring," *ECS Sensors Plus* 3 (2024): 27002.

103. V. Vignesh, B. Castro-Dominguez, T. D. James, J. M. Turner-Cobb, S. L. Lightman, and N. M. Reis, "Advancements in Cortisol Detection: From Conventional Methods to Next-Generation Technologies for Enhanced Hormone Monitoring," *ACS Sensors* 9 (2024): 1666–1681.

104. M. Jia, W. M. Chew, Y. Feinstein, P. Skeath, and E. Sternberg, "Quantification of Cortisol in Human Eccrine Sweat by Liquid Chromatography–Tandem Mass Spectrometry," *The Analyst* 141 (2016): 2053–2060.

105. E. Aardal and A.-C. Holm, "Cortisol in Saliva—Reference Ranges and Relation to Cortisol in Serum," *cclm* 33, no. 12 (1995): 927–932.

106. C. W. le Roux, G. A. Chapman, W. M. Kong, W. S. Dhillo, J. Jones, and J. Alaghband-Zadeh, "Free Cortisol Index Is Better than Serum Total Cortisol in Determining Hypothalamic-Pituitary-Adrenal Status in Patients Undergoing Surgery," *The Journal of Clinical Endocrinology and Metabolism* 88 (2003): 2045–2048.

107. N. El-Farhan, A. Rees, and C. Evans, "Measuring Cortisol in Serum, Urine and Saliva—Are Our Assays Good Enough?" *Annals of Clinical Biochemistry International Journal of Laboratory Medicine* 54 (2017): 308–322.

108. G. Russell, D. Henley, J. A. Leendertz, et al., "Rapid Glucocorticoid Receptor-Mediated Inhibition of Hypothalamic–Pituitary–Adrenal Ultradian Activity in Healthy Males," *Journal of Neuroscience* 30 (2010): 6106–6115.

109. P. Pandit, B. T. Crewther, C. J. Cook, C. Punyadeera, and A. K. Pandey, "Sensing Methods for Stress Biomarker Detection in Human Saliva: A New Frontier for Wearable Electronics and Biosensing," *Materials Advances* 5 (2024): 5339–5350.

110. R. L. Spencer and T. Deak, "A Users Guide to HPA Axis Research," *Physiology and Behavior* 178 (2017): 43–65.

111. A. H. Hamrahian, T. S. Oseni, and B. M. Arafah, "Measurements of Serum Free Cortisol in Critically Ill Patients," *New England Journal of Medicine* 350 (2004): 1629–1638.

112. J. T. Ho, H. S. Almusalhi, M. J. Chapman, et al., "Septic Shock and Sepsis: A Comparison of Total and Free Plasma Cortisol Levels," *The Journal of Clinical Endocrinology and Metabolism* 91 (2006): 105–114.

113. J. Cohen, M. L. Smith, R. V. Deans, et al., "Serial Changes in Plasma Total Cortisol, Plasma Free Cortisol, and Tissue Cortisol Activity in Patients with Septic Shock," *Shock* 37 (2011): 28–33.

114. H. Pai, C. Qualls, F. K. Urban, et al., "Numerical Solution for Cortisol Equilibrium and Maximal Cortisol Secretion Rates in Human Septic Shock and Healthy Control Subjects," *Journal of Investigative Medicine* 55 (2007): S85.

115. J. W. Kwak, T. Trinh, A. D. White, et al., "A 3D-Printed Scaffolded Hydrogel Microneedle Array Biosensor for Real-Time, Continuous Monitoring," *Advanced Materials* (2026): e73325.

116. R. Bhake, G. Russell, Y. M. Kershaw, et al., "Continuous Free Cortisol Profiles in Healthy Men," *The Journal of Clinical Endocrinology & Metabolism* 105 (2020): dgz002.

117. C. Isherwood, D. R. van der Veen, N. R. Chowdhury, S. Lightman, T. Upton, and D. J. Skene, "Simultaneous Plasma and Interstitial Profiles of Hormones and Metabolites Using uRhythm: A Novel Ambulatory Collection Device," *Proceedings of the Nutrition Society* 83 (2024): E242.

27511219, 2026, 10, Downloaded from https://advanced.onlinelibrary.wiley.com/doi/10.1002/adsr.70212 by Yasser Khan - Mount Sinai Hospital , Wiley Online Library on [14/10/2026]. See the Terms and Conditions (https://onlinelibrary.wiley.com/terms-and-conditions) on Wiley Online Library for rules of use; OA articles are governed by the applicable Creative Commons License

118. T. Upton, E. Zavala, P. Methlie, et al., "High-Resolution Daily Profiles of Tissue Adrenal Steroids by Portable Automated Collection," *Science Translational Medicine* 15 (2023): eadg8464.

119. T. Upton, E. Zavala, P. Methlie, et al., "OR30-03 High Resolution Daily Profiles of Tissue Adrenal Steroids by Portable Automated Collection," *Journal of the Endocrine Society* 7 (2023): bvad114.353.

120. J. Cohen, R. Deans, A. J. Dalley, J. Lipman, M. S. Roberts, and B. Venkatesh, "Measurement of Tissue Cortisol Levels in Patients with Severe Burns: A Preliminary Investigation," *Critical Care* 13 (2009): R189.

121. D. A. Vassiliadi, I. Ilias, M. Tzanela, et al., "Interstitial Cortisol Obtained by Microdialysis in Mechanically Ventilated Septic Patients: Correlations with Total and Free Serum Cortisol," *Journal of Critical Care* 28 (2012): 158–165.

122. J. A. Llompart-Pou, G. Pérez, J. Pérez-Bárcena, et al., "Correlation between Brain Interstitial and Total Serum Cortisol Levels in Traumatic Brain Injury. A Preliminary Study," *Journal of Endocrinological Investigation* 33 (2010): 368–372.

123. L. van Smeden, A. M. de Jong, and M. Prins, "Integrated Sampling-and-Sensing Using Microdialysis and Biosensing by Particle Motion for Continuous Cortisol Monitoring," *Sensors and Diagnostics* 2 (2023): 1638–1648.

124. L. D. Dorn, J. F. Lucke, T. L. Loucks, and S. L. Berga, "Salivary Cortisol Reflects Serum Cortisol: Analysis of Circadian Profiles," *Annals of Clinical Biochemistry International Journal of Laboratory Medicine* 44 (2007): 281–284.

125. R. M. Estrada-y-Martin and P. R. Orlander, "Salivary Cortisol Can Replace Free Serum Cortisol Measurements in Patients with Septic Shock," *CHEST Journal* 140 (2011): 1216–1222.

126. I. Perogamvros, B. Keevil, D. Ray, and P. Trainer, "Salivary Cortisone Is a Potential Biomarker for Serum Free Cortisol," *The Journal of Clinical Endocrinology and Metabolism* 95 (2010): 4951–4958.

127. E. Danese, A. Padoan, D. Negrini, et al., "Diurnal and Day-to-Day Biological Variation of Salivary Cortisol and Cortisone," *Clinical Chemistry and Laboratory Medicine (CCLM)* 62 (2024): 2287–2293.

128. L. D. Hayes, N. Sculthorpe, B. Cunniffe, and F. Grace, "Salivary Testosterone and Cortisol Measurement in Sports Medicine: A Narrative Review and User's Guide for Researchers and Practitioners," *International Journal of Sports Medicine* 37 (2016): 1007–1018.

129. F. Dong, J. S. Sefcik, E. Euiler, and N. Hodgson, "Measuring Salivary Cortisol in Biobehavioral Research: A Systematic Review and Methodological Considerations," *Brain Behavior and Immunity - Health* 43 (2024): 100936.

130. M. VanBruggen, A. C. Hackney, R. G. McMurray, and K. S. Ondrak, "The Relationship between Serum and Salivary Cortisol Levels in Response to Different Intensities of Exercise," *International Journal of Sports Physiology and Performance* 6 (2011): 396–407.

131. E. Aardal-Eriksson, B. E. Karlberg, and A.-C. Holm, "Salivary Cortisol—An Alternative to Serum Cortisol Determinations in Dynamic Function Tests," *Clinical Chemistry and Laboratory Medicine (CCLM)* 36 (1998): 215–222.

132. Å. M. Hansen, A. H. Garde, and R. Persson, "Sources of Biological and Methodological Variation in Salivary Cortisol and Their Impact on Measurement among Healthy Adults: A Review," *Scandinavian Journal of Clinical and Laboratory Investigation* 68 (2008): 448–458.

133. C. J. D. McKinlay, E. B. Thorstensen, W. S. Cutfield, M. Battin, S. R. Dalziel, and J. E. Harding, "Effect of Collection Methods on Salivary Cortisol," *Journal of Diagnostic Techniques and Biomedical Analysis* 6 (2017): 1000121.

134. S. Ahmadian, C. A. V. Torres, V. Fell, et al., "SUN-474 Time-Point Intra-Individual Variability in Salivary Cortisol and Cortisone: A Cross-Sectional Study," *Journal of the Endocrine Society* 9 (2025): bvaf149.440.

135. J. H. Kim, Y. J. Kim, S. Lee, and J. Lee, "Comparison of Salivary and Serum Cortisol Levels in Mechanically Ventilated Patients and Non-Critically Ill Patients," *Acute and Critical Care* 35 (2020): 149–155.

136. J. J. Zimmerman, A. Donaldson, R. M. Barker, et al., "Real-Time Free Cortisol Quantification among Critically Ill Children," *Pediatric Critical Care Medicine* 12 (2010): 525–531.

137. J. R. Runyon, M. Jia, M. R. Goldstein, et al., "Dynamic Behavior of Cortisol and Cortisol Metabolites in Human Eccrine Sweat," *International Journal of Prognostics and Health Management* 10 (2019): 1–11.

138. M. A. King, S. Brown, K. A. Barnes, P. J. D. D. Chavez, and L. B. Baker, "Regional and Time Course Differences in Sweat Cortisol, Glucose, and Select Cytokine Concentrations during Exercise," *European Journal of Applied Physiology* 123 (2023): 1727–1738.

139. E. Russell, G. Koren, M. Rieder, and S. V. Uum, "The Detection of Cortisol in Human Sweat," *Therapeutic Drug Monitoring* 36 (2013): 30–34.

140. A. Ramasubramanya, P. Singh, K.-C. Lin, S. Prasad, and S. Muthukumar, "CIRCA: Circadian Inference of Rhythmicity Using Comparative Analysis from Non-Invasive Continuous Measurements of Cortisol and Melatonin in Passive Perspiration," *Biosensors and Bioelectronics X* 26 (2025): 100656.

141. A. Ramasubramanya, P. Singh, A. Kumar, K. Lin, S. Prasad, and S. Muthukumar, "A Wearable Biosensing Platform for Continuous Monitoring of Inflammatory and Metabolic Biomarkers for Real-Time Health Tracking and Personalized Care," *Bioengineering and Translational Medicine* 11 (2026): e70104.

142. M. A. King, S. Brown, and L. B. Baker, "Regional and Time Course Differences in Sweat Cortisol and Glucose during Steady State Exercise," *The FASEB Journal* 35 (2021): e21893.

143. J. S. Meyer, J. P. Blain, and K. A. Kalmakis, "A Method for Assessing Week-Long Cortisol Output Using a Continuously Worn Sweat Patch," *Methods and Protocols* 9 (2026): 13.

144. P. Pearlmutter, G. Derose, C. Samson, et al., "Sweat and Saliva Cortisol Response to Stress and Nutrition Factors," *Scientific Reports* 10 (2020): 19050.

145. D. A. Barmpari, W. van Deurse, C. W. Quaedflieg, T. A. van Amelsvoort, M. Gijs, and D. Hernaus, "Tear Fluid Cortisol as a Marker of Acute Stress Reactivity: A Validation Study against Salivary Measures," *Psychoneuroendocrinology* 191 (2026): 107942.

146. R. K. Roden, N. R. Zuniga, J. Wright, et al., "Human Tear Film Protein Sampling Using Soft Contact Lenses," *Clinical Proteomics* 21 (2024): 23.

147. F. Bachhuber, A. Huss, M. Şenel, and H. Tumani, "Diagnostic Biomarkers in Tear Fluid: From Sampling to Preanalytical Processing," *Scientific Reports* 11 (2021): 10064.

148. A. Rohit, F. Stapleton, S. H. J. Brown, T. W. Mitchell, and M. D. P. Willcox, "Comparison of Tear Lipid Profile among Basal, Reflex, and Flush Tear Samples," *Optometry and Vision Science* 91 (2014): 1391–1395.

149. M. Garg, H. Guo, E. Maclam, et al., "Molecularly Imprinted Wearable Sensor with Paper Microfluidics for Real-Time Sweat Biomarker Analysis," *ACS Applied Materials and Interfaces* 16 (2024): 46113.

150. Y. Chen, Z. He, Y. Wu, et al., "A Wearable Molecularly Imprinted Electrochemical Sensor for Cortisol Stable Monitoring in Sweat," *Biosensors* 15 (2025): 194.

151. J. E. An, K. H. Kim, S. J. Park, et al., "Wearable Cortisol Aptasensor for Simple and Rapid Real-Time Monitoring," *ACS Sensors* 7 (2022): 99–108.

152. Y. Liu, X. Su, P. Fan, X. Liu, Y. Pan, and J. Ping, "Computationally-Assisted Wearable System for Continuous Cortisol Monitoring," *Science Bulletin* 70 (2025): 2004–2013.

153. S. Fande, D. Sriram, and S. Goel, "Flexible Electrochemical Biosensor for Non-Invasive, On-Site Cortisol Monitoring in Sweat and Saliva," *ACS Measurement Science Au* 6 (2026): 170–178.

27511219, 2026, 10, Downloaded from https://advanced.onlinelibrary.wiley.com/doi/10.1002/adsr.70212 by Yasser Khan - Mount Sinai Hospital , Wiley Online Library on [14/10/2026]. See the Terms and Conditions (https://onlinelibrary.wiley.com/terms-and-conditions) on Wiley Online Library for rules of use; OA articles are governed by the applicable Creative Commons License

154. S. Shin and W. Gao, "Making Sweat Measurable: Induction, Sampling, and Refreshment in Wearable Biofluid Sensing," *Advanced Science* (2026): e75684.

155. P. Simmers, S. K. Li, G. B. Kasting, and J. Heikenfeld, "Prolonged and Localized Sweat Stimulation by Iontophoretic Delivery of the Slowly-Metabolized Cholinergic Agent Carbachol," *Journal of Dermatological Science* 89 (2017): 40–51.

156. Z. Sonner, E. Wilder, J. Heikenfeld, et al., "The Microfluidics of the Eccrine Sweat Gland, Including Biomarker Partitioning, Transport, and Biosensing Implications," *Biomicrofluidics* 9 (2015): 31301.

157. S. Shin, R. Liu, Y. Yang, et al., "A Bioinspired Microfluidic Wearable Sensor for Multiday Sweat Sampling, Transport, and Metabolic Analysis," *Science Advances* 11 (2025): eadw9024.

158. Y. Yin, Z. Tan, W. Zhu, et al., "A Wearable Microfluidic System for Efficient Sweat Collection and Real-Time Detection," *Talanta* 274 (2024): 125967.

159. A. Martín, J. Kim, J. Kurniawan, et al., "Epidermal Microfluidic Electrochemical Detection System: Enhanced Sweat Sampling and Metabolite Detection," *ACS Sensors* 2 (2017): 1860–1868.

160. H. Y. Y. Nyein, L. Tai, Q. P. Ngo, et al., "A Wearable Microfluidic Sensing Patch for Dynamic Sweat Secretion Analysis," *ACS Sensors* 3 (2018): 944–952.

161. X. Xuan, C. Chen, Á. Molinero-Fernández, et al., "Fully Integrated Wearable Device for Continuous Sweat Lactate Monitoring in Sports," *ACS Sensors* 8 (2023): 2401–2409.

162. F. Gao, C. Liu, L. Zhang, et al., "Wearable and Flexible Electrochemical Sensors for Sweat Analysis: A Review," *Microsystems and Nanoengineering* 9 (2023): 1.

163. M. Bariya, N. Davis, L. Gillan, et al., "Resettable Microfluidics for Broad-Range and Prolonged Sweat Rate Sensing," *ACS Sensors* 7 (2022): 1156–1164.

164. R. F. R. Ursem, A. Steijlen, M. Parrilla, J. Bastemeijer, A. Bossche, and K. D. Wael, "Worth Your Sweat: Wearable Microfluidic Flow Rate Sensors for Meaningful Sweat Analytics," *Lab on a Chip* 25 (2025): 1296–1315.

165. F. Lorestani, X. Zhang, Z. Ataie, et al., "A Granular Hydrogel-Enabled Wearable Electrochemical Biosensing Platform for Continuous Non-Invasive Sweat Lactate Detection," *Small* 21 (2025): 2502655.

166. H. Y. Y. Nyein, M. Bariya, B. Tran, et al., "A Wearable Patch for Continuous Analysis of Thermoregulatory Sweat at Rest," *Nature Communications* 12 (2021): 1823.

167. R. Vinoth, T. Nakagawa, J. Mathiyarasu, and A. M. V. Mohan, "Fully Printed Wearable Microfluidic Devices for High-Throughput Sweat Sampling and Multiplexed Electrochemical Analysis," *ACS Sensors* 6 (2021): 1174–1186.

168. W. Wang, Y. Jin, Y. Huang, et al., "A Self-Driven Multifunctional Microfluidic Sweat Analysis System for Efficient Sweat Collection and Real-Time Monitoring," *Sensors and Actuators B Chemical* 414 (2024): 135920.

169. J. Choi, D. Kang, S. Han, S. B. Kim, and J. A. Rogers, "Thin, Soft, Skin-Mounted Microfluidic Networks with Capillary Bursting Valves for Chrono-Sampling of Sweat," *Advanced Healthcare Materials* 6 (2017): 1601355.

170. A. J. Bandodkar, J. Choi, S. P. Lee, et al., "Soft, Skin-Interfaced Microfluidic Systems with Passive Galvanic Stopwatches for Precise Chronometric Sampling of Sweat," *Advanced Materials* 31 (2019): 1902109.

171. P. Jalali and A. S. Nezhad, "Cap-Sweat: A Capillary Microfluidic Platform for Digitized Sweat Sampling and Time-Resolved Biomarker Analysis," *Lab on a Chip* 26 (2026): 2734–2746.

172. J. H. Yang, U. David, Y. S. Noh, and A. Koh, "Dual-Valved Skin-Interfaced Microfluidic Device for Programmed Time-Control Sweat Collection," *Sensors and Actuators B Chemical* 395 (2023): 134441.

173. O. Parlak, S. T. Keene, A. Marais, V. F. Curto, and A. Salleo, "Molecularly Selective Nanoporous Membrane-Based Wearable Organic Electrochemical Device for Noninvasive Cortisol Sensing," *Science Advances* 4 (2018): eaar2904.

174. S. Shajari, R. Salahandish, A. Zare, et al., "Microsweat: A Wearable Microfluidic Patch for Noninvasive and Reliable Sweat Collection Enables Human Stress Monitoring," *Advanced Science* 10, no. 7 (2022): 2204171.

175. W. Tang, L. Yin, J. R. Sempionatto, J. Moon, H. Teymourian, and J. Wang, "Touch-Based Stressless Cortisol Sensing," *Advanced Materials* 33, no. 18 (2021): 2008465.

176. C. Wang, Z. Wang, W. Wei, et al., "High-Precision Flexible Sweat Self-Collection Sensor for Mental Stress Evaluation," *npj Flexible Electronics* 8 (2024): 47.

177. P. P. Samant and M. R. Prausnitz, "Mechanisms of Sampling Interstitial Fluid from Skin Using a Microneedle Patch," *Proceedings of the National Academy of Sciences* 115 (2018): 4583–4588.

178. T. Abbasiasl, F. Mirlou, H. Mirzajani, et al., "A Wearable Touch-Activated Device Integrated with Hollow Microneedles for Continuous Sampling and Sensing of Dermal Interstitial Fluid," *Advanced Materials* 36 (2023): 2304704.

179. A. F. Aroche, H. E. Nissan, and M. A. Daniele, "Hydrogel-Forming Microneedles and Applications in Interstitial Fluid Diagnostic Devices," *Advanced Healthcare Materials* 14 (2024): 2401782.

180. E. Laszlo, G. D. Crescenzo, A. Nieto-Argüello, X. Banquy, and D. Brambilla, "Superswelling Microneedle Arrays for Dermal Interstitial Fluid (Prote)Omics," *Advanced Functional Materials* 31 (2021): 2106061.

181. A. H. Hung, N. U. Kamat, A. Bermudez, et al., "A Microneedle Device for Rapid Dermal Interstitial Fluid Sampling," *Science Advances* 11 (2025): eadx5492.

182. F. Bakhshandeh, H. Zheng, N. G. Barra, et al., "Wearable Aptalyzer Integrates Microneedle and Electrochemical Sensing for In Vivo Monitoring of Glucose and Lactate in Live Animals," *Advanced Materials* 36 (2024): e14242.

183. Y. Dai, J. K. Nolan, E. Madsen, et al., "Wearable Sensor Patch with Hydrogel Microneedles for In Situ Analysis of Interstitial Fluid," *ACS Applied Materials and Interfaces* 15 (2023): 56760–56773.

184. K. Liu, H. Wang, F. Zhu, et al., "Lab on the Microneedles: A Wearable Metal–Organic Frameworks-Based Sensor for Visual Monitoring of Stress Hormone," *ACS Nano* 18 (2024): 14207–14217.

185. Y. Zhou, L. He, L. He, et al., "An Aptamer-Responsive Microneedle Patch Sensor Platform Combining with Hybridization Chain Reaction Amplification for Detection of Steroid Hormone Cortisol in Skin Interstitial Fluid," *Biosensors and Bioelectronics* 269 (2024): 116935.

186. C. T. Sharkey, A. F. Aroche, I. G. Agusta, et al., "Design and Characterization of a Self-Powered Microneedle Microfluidic System for Interstitial Fluid Sampling," *Lab on a Chip* 25 (2025): 4577–4587.

Supporting Information

Additional supporting information can be found online in the Supporting Information section.

Supporting File: adsr70212-sup-0001-SuppMat.pdf.

27511219, 2026, 10, Downloaded from https://advanced.onlinelibrary.wiley.com/doi/10.1002/adsr.70212 by Yasser Khan - Mount Sinai Hospital , Wiley Online Library on [14/10/2026]. See the Terms and Conditions (https://onlinelibrary.wiley.com/terms-and-conditions) on Wiley Online Library for rules of use; OA articles are governed by the applicable Creative Commons License

Table S1: Comparison of wearable and minimally invasive cortisol-sensing platforms, including analytical performance, sampling and assay timing, regeneration, stability, and biological validation. NR, not reported; NA, not applicable.

Study	Sensor / recognition element	Analytical range and LOD	Sampling matrix and collection method	Intrinsic sensor response / recovery	Sampling-interface and assay timing	Regeneration / reversibility	Drift / stability / duration	Measured cortisol / temporal result	Main finding / limitation
Torrente-Rodríguez et al. (2020) [1]	Laser-induced graphene electrochemical immunosensor	Competitive immunosensor dynamic range (20–80% inhibition): 0.43–50.2 ng/mL; LOD: 0.08 ng/mL.	Sweat; iontophoresis at rest and naturally generated sweat during exercise	Competitive recognition was significant after 1 min at 5 ng/mL; 15-min incubation was used for accurate real-sample quantification. Wireless electronic readings stabilized within 10 s; 15-min incubation was used for quantification.	Sample volume <10 μL. Sweat was collected at protocol-specific intervals (10 min during cycling; 8 min for cold-pressor profiling); no separate chamber-clearance time was reported.	Continuously reversible binding not established	>90% analytical response retained after 7 days at 4 °C (storage stability). Electronics supported ∼330 min continuous amperometric acquisition	Cycling (3 untrained + 1 trained): 50 min at 60 rpm; sweat sampled every 10 min; all profiles peaked at 40 min and declined slightly by 50 min; the trained athlete showed a blunted response. Cold-pressor (4 subjects): 3-min ice-water exposure; mean sweat-cortisol peak occurred 8–16 min afterward. Circadian AM/PM ratio: 1.35–2.00.	Acute and diurnal sweat-cortisol profiles were obtained; sensor response and sampling-related timing were not fully separated.
Wang et al. (2022) [2]	Aptamer-functionalized In_2O_3 FET smartwatch	Dynamic range: 1 pM–1 μM. Lowest practically detectable concentration: 1 pM.	Sweat; iontophoresis followed by thin-film microfluidic delivery	Aptamer-FET response occurred on the scale of seconds. Recovery time during decreasing cortisol: NR.	Iontophoretic sweat induction and sweat collection required ∼5–15 min, separate from the seconds-scale FET response.	Dynamic tracking of increasing concentrations was shown; explicit decreasing-concentration recovery or regeneration-cycle validation was NR.	Baseline normalization reduced device-to-device variation from ∼50% to ∼30%; calibrated variation was <10%. Long-duration operational drift NR.	Human: TSST saliva study (71 participants; baseline and 15, 25, 90 min). Separate paired sweat–saliva AM/PM study: N=17, r=0.73. TSST saliva peaked at 15 min and recovered by 90 min. Paired AM/PM sweat–saliva correlation r=0.73 (N=17). Participant concentrations were presented graphically rather than tabulated.	Repeated wearable measurements and on-body iontophoretic sweat collection were reported; the TSST cortisol measurements used saliva, not sweat.
An et al. (2022) [3]	Aptamer-functionalized PEDOT–PAN nanofiber FET	Full range: NR; LOD: 10 pM; approximately 1 nM detected in native sweat	Sweat; swab transfer or direct placement on skin	Analytical response <5 s; recovery NR. Native-sweat measurement took several minutes and is listed separately.	Swab transfer or direct skin placement; native-sweat detection required several minutes.	Reversibility and regeneration NR	Short-term performance reported; drift and prolonged duration NR	Controlled stress experiment NR	The reported ¡5-s FET response was separate from the several-minute native-sweat measurement.
Fiore et al. (2023) [4]	Competitive magnetic-bead electrochemical immunosensor	Range: 10–140 ng/mL; LOD: approximately 3 ng/mL in standard solutions; native sweat evaluated separately by standard addition	Sweat; wax-patterned paper microfluidics with NFC readout	Complete measurement time less than 15 min, including sweat collection	Approximately 10 min for sweat to wet the paper microfluidic device, followed by two sequential 90-s processing periods before electrochemical detection	Disposable competitive assay; regeneration NR	Reproducibility and 7-day room-temperature storage stability evaluated; operational drift NR	One participant completed two 10-min cycling sessions at 16:00 and 17:00; measured cortisol concentrations were 90 and 93 ng/mL, respectively; two endpoint concentrations only	On-body cortisol measurement used a disposable paper assay with discrete sample collection and endpoint detection.

Continued on next page

Table S1 – continued from previous page

Study	Sensor / recognition element	Analytical range and LOD	Sampling matrix and collection method	Intrinsic sensor response / recovery	Sampling-interface and assay timing	Regeneration / reversibility	Drift / stability / duration	Measured cortisol / temporal result	Main finding / limitation
Singh et al. (2023) [5]	Electrochemical pseudoknot-assisted structure-switching aptamer	Linear dynamic range: 1 pM–1 μM. LOD: 0.17 pM in buffer and 0.20 pM in artificial sweat.	Sweat; flexible PDMS microfluidic sampler	Intrinsic response and recovery NR.	PDMS sampler isolated older from newly generated sweat; quantitative volume, filling, exchange, and clearance times NR.	Pseudoknot-assisted aptamer was designed for reversible binding; repeated on-body signal regeneration was demonstrated during monitoring.	On-body monitoring for up to 90 min; quantitative drift NR	Human: three participants; exercise-generated sweat and cold-pressor stress protocols; monitoring extended up to 90 min.	Repeated on-body signal regeneration was reported; microfluidic renewal time and operational drift were not quantified.
Garg et al. (2024) [6]	MIP-modified laser-induced graphene impedance sensor	Tested range: 0.1 pM–1 μM in pH 6.5 artificial sweat. After oxygen-plasma treatment, reliable quantification was demonstrated down to 1 pM.	Sweat; iontophoresis and paper microfluidic pumping	Combined sensor-exposure response rose over $\sim$2 min and plateaued at $\sim$3 min; impedance acquired every 27 s; isolated recovery NR.	$\sim$2.4-μL chamber; $\sim$2-min filling and $\sim$3-min clearance; $\sim$0.5-mm paper channel; average sweat rate $\sim$2 μL/min.	Sequential measurements reported; regeneration-cycle retention NR	Short-term repeated operation demonstrated; extended drift NR	One participant cycled at three times of day. The on-body concentrations are shown graphically and were not stated numerically in the text; exact values were not reported in the text.	Filling, measurement, and sample-removal times were reported, although transport and sensor equilibration remained coupled.
Chen et al. (2025) [7]	Flexible Au-electrode MIP sensor	Tested range: 0.1 pM–5 μM. Formal calculated LOD: NR	Sweat; directional transport through an SF/PVDF membrane	Intrinsic response/recovery NR; Measurements were acquired at 1-min intervals; intrinsic response and recovery times were not reported.	Volume, area, flow, filling, and renewal NR.	120 regeneration cycles with less than 3.76% attenuation	Approximately 96.1% response retained after 30-day storage; approximately 1.38% RSD under 20% strain; operational drift NR	Human exercise and diurnal profiles were reported for three participants.	The sensor retained its response over repeated regeneration and storage tests; sampling delay and continuous operational drift were NR.
Liu et al. (2024) [8]	Eu-MOF-loaded hydrogel microneedle fluorescence sensor	Eu-MOF detection limit: 1 nM; microneedle-patch quantitative range: 100 nM–1 mM	ISF; swellable hydrogel microneedle extraction	Intrinsic fluorescence response/recovery NR; 1 h is ISF-collection duration.	Maximum extraction capacity of approximately 5 μL per patch within 1 h; cortisol measurements used a 10-min patch application	Endpoint fluorescence measurement; regeneration NR	Batch reproducibility and storage stability evaluated; continuous operational drift NR	Animal study using an acute restraint-stress mouse model; microneedles were applied for 10 min after stress induction. Reported plasma cortisol concentrations were 200.98 $\pm$ 17.67 ng/mL at rest and 294.38 $\pm$ 32.15 ng/mL under stress.	ISF extraction and fluorescence detection produced time-integrated endpoint measurements.
Zhou et al. (2025) [9]	Aptamer–hybridization-chain-reaction fluorescence microneedle patch	In-vitro linear response: 0–0.5 μM (R^2=0.9992). Formal LOD: NR.	ISF; direct microneedle sampling and in-patch fluorescence detection	Intrinsic sensor response/recovery NR; microneedle collection and HCR reaction times were not isolated.	Microneedle collection plus in-patch HCR amplification caused temporal averaging; volume, transport rate, and blood-to-ISF delay NR.	Endpoint amplified assay; regeneration NR	Short-term analytical stability reported; continuous drift NR	Mouse ISF cortisol was approximately 127 nM after running fatigue versus approximately 75 nM at rest (figure/text-reported approximate comparison).	Mouse rest and running-fatigue conditions were differentiated by endpoint ISF measurements; continuous and reversible tracking were NR.

Continued on next page

Table S1 – continued from previous page

Study	Sensor / recognition element	Analytical range and LOD	Sampling matrix and collection method	Intrinsic sensor response / recovery	Sampling-interface and assay timing	Regeneration / reversibility	Drift / stability / duration	Measured cortisol / temporal result	Main finding / limitation
Sharkey et al. (2025) [10]	Sampling-only platform; no integrated cortisol sensor	Range and LOD: NA; cortisol recovery evaluated as a representative analyte	ISF; hydrogel-forming microneedles, osmotic pump and paper collector	NA (sampling study without an integrated cortisol sensor).	Cortisol recovery was evaluated after 15 min, 45 min, and 24 h. Spatial equilibration along the paper channel was incomplete after 15 min despite complete visible wetting and improved after 45 min, particularly nearer the microneedle extraction site. Recovery after 24 h was less consistent because of possible cortisol degradation, evaporation, or diffusion limitations.	NA	Sampling performance characterized; sensor drift NA	In vitro agarose and synthetic-skin models; no human or animal stress experiment and no cortisol trajectory	Complete visible wetting preceded quantitative equilibration along the paper collector.
Kwak et al. (2026) [11]	Cortisol-responsive fluorescent aptamer-hydrogel microneedle array housed within a 3D-printed scaffold	MAB-system LOD: 500 nM; responses demonstrated at 0.5, 1, and 10 μM cortisol	ISF; direct dermal sensing using a scaffolded aptamer-hydrogel microneedle array	In a vascularized skin phantom, the signal reached 90% of steady state within 5 min after introducing 500 nM cortisol; in vivo time-to-peak: 61.6 $\pm$ 27.5 min after hydrocortisone administration	The 61.6 $\pm$ 27.5-min in vivo peak combines hydrocortisone pharmacokinetics, blood-to-ISF transport, diffusion into the hydrogel, aptamer binding, and optical response; it is not an isolated transport or sensor-response time	Reversible response demonstrated through sequential measurements and wash steps; regeneration-cycle retention NR	Minimal photobleaching over 90 min, no meaningful change in concentration-dependent response over 3 days in vitro, and unchanged calibration after in vivo use; longer-term in vivo drift NR	Three female rats received 2.3 mg/kg hydrocortisone by retro-orbital injection and were monitored for up to 4 h; mean time-to-peak was 61.6 $\pm$ 27.5 min	Time-resolved in vivo measurements were obtained; the 61.6-min peak combined pharmacokinetics, transport, hydrogel equilibration, and optical response.
Sheibani et al. (2021) [12]	Pt/aptamer-functionalized graphene extended-gate FET	Tested range: 1 nM–10 μM; LOD: 0.2 nM	Cortisol solutions in physiological incubation buffer; proposed for sweat sensing but not tested with human sweat	Intrinsic response and recovery times NR; measurements were performed after a 30-min cortisol incubation	The modified electrode was incubated in each cortisol solution for 30 min, rinsed five times with DI water, dried with nitrogen, and then electrically measured in 0.05$\times$ PBS; this was an ex situ assay; continuous sampling was not performed	Hysteresis-free FET operation reported; reversible cortisol tracking and sensor-regeneration protocol not demonstrated	No significant response drift was observed over 1.5 h in buffer; prolonged or on-body stability not demonstrated	No human or animal cortisol or stress experiment; wearable sweat monitoring was proposed	Low-drift cortisol detection was reported in physiological buffer; real-time native-sweat and on-body measurements were NR.

Continued on next page

Table S1 – continued from previous page

Study	Sensor / recognition element	Analytical range and LOD	Sampling matrix and collection method	Intrinsic sensor response / recovery	Sampling-interface and assay timing	Regeneration / reversibility	Drift / stability / duration	Measured cortisol / temporal result	Main finding / limitation
Mei et al. (2023) [13]	MIP electrochemical sensor integrated with a nanofiber-based microfluidic chip	Tested range: 1 nM–1 μM in PBS; LOD: 0.35 nM. Artificial sweat recoveries: 95.3%–104.6%	Sweat; nanofiber-based microfluidic collection and in situ electrochemical measurement	Intrinsic MIP response and recovery times NR; on-body measurement required 18 min of exercise for sweat accumulation followed by 3 min of incubation	Nanofiber capillary transport through a 0.7-mm-wide channel from a 5.2-mm inlet chamber to a 7.2-mm sensing chamber; quantitative flow rate, transported volume, filling time independent of sweat production, and sample-replacement time NR	Successive measurements using one sensor were evaluated, but a defined regeneration procedure and cycle-retention value were not reported	Repeatability RSD: 3.56%; intersensor reproducibility RSD: 4.87%; 97.8% of the initial response retained after 20 days at 4 °C; mechanical and temperature performance evaluated; continuous operational drift NR	Five healthy volunteers cycled while wearing the sensor. Cortisol was measured at 8:00 am and 6:00 pm; morning concentrations were 125.2–270.6 nM and afternoon concentrations were 30.1–123.4 nM. This was exercise-associated monitoring; a controlled psychological-stress test was not performed.	On-body measurement combined exercise-driven sweat accumulation with a subsequent 3-min incubation.
Cheng et al. (2023) [14]	Dual-readout paper-based wearable sensor; cortisol measured electrochemically alongside colorimetric measurements of glucose, lactate, uric acid, Mg(II), and pH	Tested cortisol range: 1 nM–10 μM; formal calculated LOD NR	Sweat; patch-based 3D origami paper microfluidic collection	Cortisol incubation time: 10 min; intrinsic binding, electrical-response, and recovery times NR	Calibration used a 5 μL cortisol sample with 10-min incubation. The complete chip experiment required a minimum liquid volume of 160 μL. During on-body testing, approximately 30 min of exercise was required for sweat to reach the sensing area.	Disposable paper assay; regeneration and reversible cortisol measurement not demonstrated	Triplicate calibration measurements reported; storage stability and continuous operational drift NR	Exercise-associated morning and evening cortisol changes were shown graphically for five volunteers; exact individual cortisol concentrations were not numerically tabulated	Multiplexed on-body sweat analysis used discrete cortisol measurements requiring sweat collection and 10-min incubation.
Chakoma et al. (2024) [15]	Battery-free MIP–radio-frequency resonant sensor with LC transduction	Tested range: 0.025–1 μM; sensitivity: 160.936 kHz/log(μM) with NFC readout and 166.852 kHz/log(μM) with an impedance spectroscope; formal calculated LOD NR	Sweat; MIP-RF sensor integrated with a 3D-printed PDMS microfluidic channel	Wireless resonant response demonstrated; intrinsic molecular-recognition and recovery times NR	Microfluidic reservoir: approximately 150 μL, 12.6 mm diameter, and 1.2 mm depth; inlet and outlet channels: 1 mm wide and 1.2 mm deep. Approximately 15 min of treadmill exercise was required to fill the channel; sweat rate and sample-renewal time NR	Reuse employed methanol/acetic acid solution (1:2, v/v), followed by DI-water rinsing, repeated three times; negligible differences in resonant-frequency response were reported between washes, but extended reuse-cycle retention NR	Approximately 96.8% of the initial response was retained after 28 days of storage; 100-cycle bending stability evaluated; continuous on-body drift NR	Three subjects completed approximately 15 min of treadmill exercise for measurements at 10 am and 7 pm; all showed higher morning than evening cortisol levels. No controlled acute-stress challenge was performed.	Passive wireless cortisol measurements and chemical sensor reuse were reported; the 28-day result was a storage-stability test.

Continued on next page

Table S1 – continued from previous page

Study	Sensor / recognition element	Analytical range and LOD	Sampling matrix and collection method	Intrinsic sensor response / recovery	Sampling-interface and assay timing	Regeneration / reversibility	Drift / stability / duration	Measured cortisol / temporal result	Main finding / limitation
Hossain et al. (2024) [16]	StressFit hybrid patch combining an anti-cortisol antibody-functionalized PANI–AuNP–MWCNT electrochemical sensor with EMG, temperature, and pH sensing	Tested calibration concentrations: 0.1 pM–1 μM in artificial sweat, based on the calibration figure; formal calculated LOD NR	Sweat; medical gauze wicked sweat from the skin to the electrochemical sensor	Real-time acquisition reported; intrinsic binding, response, recovery, and total sample-to-signal times NR	Skin-interfaced multilayer patch with gauze-mediated sweat delivery; sample volume, sweat-generation and collection times, flow rate, and sample-renewal time NR	Cortisol-sensor regeneration and bidirectional reversibility NR	Cortisol-sensor repeatability and reproducibility were evaluated using three sensors at three concentrations over three consecutive days; mechanical and multimodal operation evaluated; long-term cortisol drift NR	One healthy individual completed stationary cycling measurements over four days, with cortisol assessed every 5 min during nominal 55-min sessions, although the statistical analysis included a 60-min cortisol point. Plotted cortisol increased from approximately 0.25 ng/mL at 5 min to approximately 1.9 ng/mL near 50 min and then decreased to approximately 1.0 ng/mL at 60 min. Differences were significant between 5 and 40 min ($p = 0.0071$) and between 40 and 60 min ($p = 0.0271$).	Physicochemical and electrophysiological signals were acquired simultaneously; cortisol validation involved one self-participating investigator, and sweat-transport timing was NR.
Wang et al. (2024) [17]	MIP-based high-precision flexible sensor using porous chitosan hydrogel as both sweat collector and conductive interface	Tested range: 10^{-3}–10^{4} nM (1 pM–10 μM); formal LOD NR. Sensitivity with the porous chitosan-hydrogel interface: 189.2 nA/log10(nM). Calibration experiments used 100 μL per concentration; 1 pM was the lowest tested concentration, not a formally calculated LOD.	Palm/fingertip touch sweat; direct self-collection using porous chitosan hydrogel	Electronic readout and transmission were described as real time, but physiological measurements used discrete 30-s fingertip contacts; intrinsic MIP response and recovery times NR	Fingertip sweat was contacted with the hydrogel-covered electrode for 30 s before measurement. Bench calibration used 100 μL solution; this volume does not represent the sweat volume collected during on-body testing.	Reuse, regeneration, and bidirectional reversibility NR; template elution occurred during fabrication rather than during sensor operation	Electrodes stored at 5 °C for 4 weeks and tested weekly at 100 nM lost approximately 5 nA/week. Five repeated 100-nM tests with the hydrogel-covered sensor produced signals near 550 nA. Multi-hour on-body drift NR.	Circadian study: three volunteers measured every 2 h from 7 am to 7 pm; mean sweat cortisol decreased from 350 to 30 nM. Exercise study: two volunteers performed rope skipping; cortisol measured 1 h later was 180 nM above the mean of resting volunteers. Exercise/CPT responses reached approximately 250 nM. CPT: three volunteers immersed one hand in 0 °C water for 3 min; baseline was below 50 nM, cortisol rose sharply at 10–15 min, and returned to the pre-CPT level by 20 min.	Hydrogel-assisted touch sampling supported diurnal, exercise, and cold-pressor measurements using discrete fingertip samples.

Continued on next page

Table S1 – continued from previous page

Study	Sensor / recognition element	Analytical range and LOD	Sampling matrix and collection method	Intrinsic sensor response / recovery	Sampling-interface and assay timing	Regeneration / reversibility	Drift / stability / duration	Measured cortisol / temporal result	Main finding / limitation
Tu et al. (2025) [18]	Stressomic multiplexed competitive electrochemical immunosensor for cortisol, epinephrine, and norepinephrine using Au-nanodendrite-decorated laser-engraved graphene electrodes	Cortisol calibration range: 0–100 ng/mL; LOD: 2.70 ng/mL. The corresponding LODs for epinephrine and norepinephrine were 2.73 and 9.14 pg/mL, respectively. The cortisol LOD was distinct from the picogram-per-milliliter LODs reported for the catecholamines.	Sweat; iontophoresis-assisted wearable sequential-sampling microfluidic patch	Cortisol measurements stabilized after 15 min of incubation irrespective of the tested flow rate. Isolated antibody association and dissociation times were not reported.	Sample volumes greater than 5 μL produced stable current, and a 10-min incubation was selected during analytical optimization. The five chambers filled sequentially at approximately 6-min intervals at 1.5 μL/min. Flow rates of 0.5–3 μL/min were evaluated. Each chamber represents the hormone level when sweat entered it, although electrical readout may occur later.	Five separate detection chambers underwent sequential filling, incubation, release, and refreshing. This provided time-separated samples; regeneration of the same immunosensor surface NR.	Sequential measurements and negligible current drift under the tested physiological-temperature conditions were reported. Measurement duration is limited by the number of chambers; prolonged continuous operational drift was not established.	Human: HIIT (n=10), emotional-picture/IAPS stress (n=11), and stress-modulating supplement intervention (n=10); measurements at 0, 10, 20, 30, and 40 min. HIIT: cortisol increased at 10 min and gradually declined toward baseline by 40 min. IAPS: cortisol showed a slight, nonsignificant change at 10 min and remained stable through 40 min. Supplement intervention: cortisol gradually declined. Individual concentrations were presented graphically rather than tabulated.	Sequential chambers provided time-stamped hormone measurements under physical, emotional, and supplement conditions; each chamber used a separate sample aliquot.
Liu et al. (2025) [19]	Computationally assisted, in-situ regenerative molecularly imprinted polymer organic electrochemical transistor (MIP-OECT) wearable system	Tested range: 1 nM–10 μM in PBS, artificial sweat, and artificial saliva. LOD: 0.69 nM in PBS, 0.36 nM in artificial sweat, and 0.82 nM in artificial saliva.	Sweat; carbachol iontophoresis with integrated microfluidic collection and delivery	After the sweat chamber was filled, the OECT current stabilized in approximately 150 s. This is the sensor-level signal stabilization time reported by the authors; regeneration and sweat induction required substantially longer.	The microfluidic chamber held a fixed sweat volume of 9.4 μL. Sweat generally appeared approximately 4 min after application of a 1-mA iontophoresis current, and the chamber was nearly filled after approximately 8 min. The authors recommended 10 min of sweat induction before biosensing.	The MIP was regenerated in situ by applying -0.2 V for approximately 1200 s (20 min), followed by another 10-min sweat-induction step to refresh the channel. Regeneration was demonstrated for up to eight cycles without washing; numerical signal retention across the eight cycles was not stated in the main text.	The device retained 92.1% of its initial current response after 7 days. The 7-day result describes retained response; continuous on-body drift NR.	Human; one participant underwent one-day diurnal monitoring from 7 am to 11 pm at 2-h intervals, including a 45-min running intervention before the 5 pm measurement. No controlled psychological-stress challenge was performed.	Repeated regenerative measurements were obtained at 2-h intervals; each cycle included sweat induction, signal stabilization, regeneration, and channel refreshing.

Continued on next page

Table S1 – continued from previous page

Study	Sensor / recognition element	Analytical range and LOD	Sampling matrix and collection method	Intrinsic sensor response / recovery	Sampling-interface and assay timing	Regeneration / reversibility	Drift / stability / duration	Measured cortisol / temporal result	Main finding / limitation
Zhao et al. (2026) [20]	Cortisol-aptamer-functionalized soft and intrinsically stretchable electrolyte-gated organic field-effect transistor (EG-OFET)	Tested cortisol range: 1 pM–1 μM. Hill-model dynamic range: 0.38 pM–17.1 nM;LOD: <1 pM; maximum sensitivity: 7.54 mV/decade; maximum response: 50.57 mV.	Cortisol calibration was performed primarily in PBS. Additional validation was conducted in biologically relevant buffers, including artificial sweat; native human sweat was not tested.	Real-time measurements consisted of five consecutive transistor scans at each cortisol concentration and showed stable, distinguishable responses. A numerical binding-response time and recovery time were not reported.	Sampling system NA. No integrated sweat-induction, collection, microfluidic transport, filling, or sample-renewal system was demonstrated.	Aptamer-mediated cortisol sensing was evaluated; analyte removal, sensor regeneration, bidirectional tracking, and regeneration-cycle retention NR.	Aptamer-functionalized transistors maintained electrical performance in physiological buffer for approximately 48–50 days and showed no significant decrease in cortisol sensitivity after 50 days in PBS. Devices operated under up to 50% strain; cortisol calibration under 25% strain was similar to that at 0% strain. More than 1 h of continuous bias-stress stability was reported, but extended biofluid signal drift during continuous cortisol monitoring was not evaluated.	No human or animal cortisol experiment, native-sweat measurement, exercise test, circadian monitoring, or acute-stress trajectory was performed.	Cortisol sensing, mechanical compliance, and buffer stability were characterized at the device level; native-sweat and on-body measurements were NR.
Pei et al. (2026) [21]	Reusable molecularly imprinted polymer cortisol sensor integrated with ECG, galvanic skin response, radial artery pulse, and skin-temperature monitoring	Tested range: 1 nM–10 μM in PBS and artificial sweat; sensitivity: 0.2447 μA/log(nM) in PBS and 0.24 μA/log(nM) in artificial sweat. Formal calculated LOD: NR.	Sweat; epidermal multimodal wearable system with wireless carbachol iontophoresis and integrated microfluidic collection	Cortisol binding response stabilized after 1 min, which was selected as the minimum incubation time. Electrochemical restoration returned the signal to its background level in approximately 55 s. These are sensor incubation and restoration times, respectively, and do not include sweat induction, chamber filling, or sample replacement.	The incubation chamber capacity was 8.4 μL. Wireless iontophoresis was applied for 5 min, and the chamber filled with sweat during the following approximately 5 min. Tested sample-volume loading of 0.075–0.375 μL/mm^2 produced no substantial signal change. Complete microfluidic replacement of an old sample with a new sample required 300 s.	Electrochemical chronoampero-metric restoration returned the MIP sensor to its background current in approximately 55 s. Ten restoration cycles produced consistent responses with <5% RSD. This regeneration of the sensing surface is distinct from the approximately 300-s microfluidic sample-replacement process.	The cortisol sensor retained approximately 98.3% of its signal after 1000 cycles of 30% bending and >96% after three weeks under ambient storage. Daily cortisol measurements and physiological-signal monitoring were demonstrated for 14 days, with a separate 72-h monitoring demonstration. Uninterrupted operational drift of the cortisol sensor NR.	Controlled stress experiments included 15 participants, with each participant completing two sessions. In representative traces, CPT increased cortisol from 86 to 104 nM, followed by a decline to 97 nM; a math quiz increased cortisol from 86 to 113 nM. A separate single-participant 24-h trace showed a morning peak of 105 nM, a decline to 79 nM after waking, an increase to 95 nM during a check-in meeting, an increase from 84 to 94 nM during running, and an increase to 107 nM while watching a horror movie. Stroop and morning-versus-afternoon results were presented graphically for multiple subjects.	Sweat-cortisol measurements were integrated with ECG, GSR, RAP, and skin temperature; incubation, electrochemical restoration, and microfluidic renewal occurred between cortisol readings.

Table S2. Participant characteristics and potential sources of interindividual variability.

Information	P1 - Undergraduate	P2 - Master's student	P3 - Ph.D. student
Age (years)	21	25	29
Gender	Female	Male	Female
Menstrual-cycle phase	Unsure	N/A	Luteal phase
Date of last menstrual period	Unsure	N/A	Unsure
Hormonal contraception	None	None	None
Active pills or placebo for oral contraceptive	N/A	N/A	N/A
Caffeine consumption	None	None	Yes - tea (6oz every morning)
Last meal/drink	Yogurt, granola, and banana at 8:00 am	One egg and one croissant at 8:30 am	None
Alcohol consumption	None	None	None
Nicotine/tobacco use	None	None	None
Hours of sleep	8 h	7 h	7 h
Sleep quality	Good	Good	Average
Unusually stressful event	None	None	None
Overall stress level (0-10)	3	3	8
Recent strenuous physical activity	Yes - 1.5 h of lacrosse at moderate intensity	None	None
Typical exercise per week	10 h	3 h	0 h
Trained athlete	Yes	No	No
BMI (kg/m2)	20.8	21.0	31.5
Prescription or over-the-counter medication	Yes - Enbrel, 50 mg	None	Yes - antibiotic for strep throat (name not recorded)

Note. Information was self-reported by participants. N/A, Not-applicable; BMI, body mass index. Items described as not recorded were unavailable in the source participant-information table.

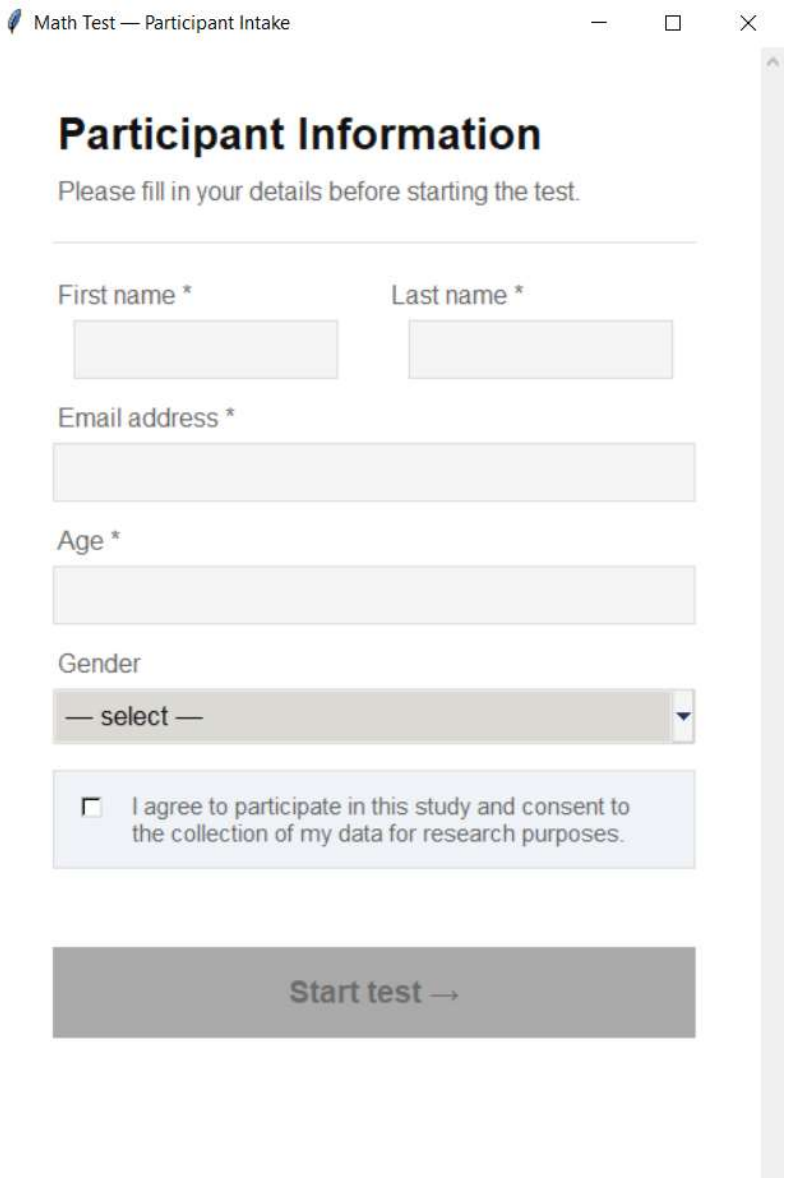


Figure S1. Participant-intake interface. Representative participant-information screen displayed by the computerized cognitive-task application before task initiation. All identifying fields are blank in the displayed example.

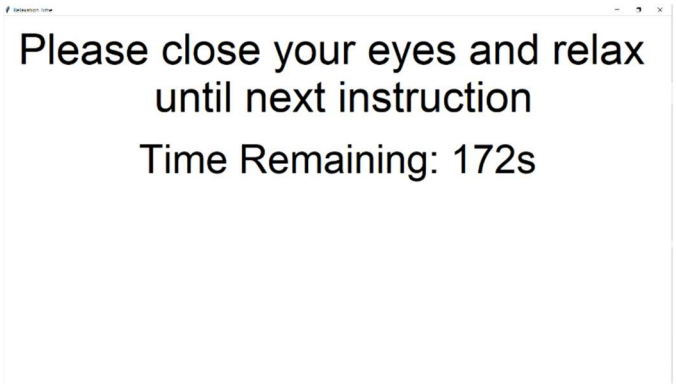
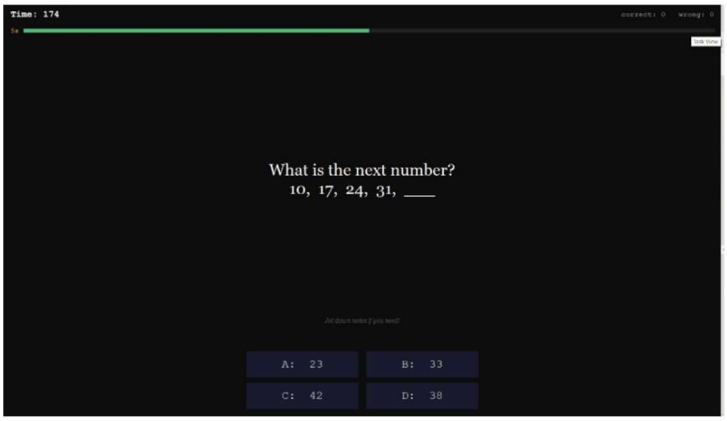


Figure S2. Pre-task relaxation screen. Representative screen displayed during the timed resting period preceding the computerized cognitive stress protocol.

a



b



c

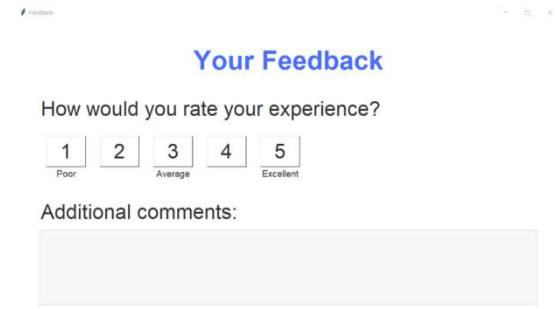


Figure S3. Computerized cognitive-task interfaces. Representative screens from the cognitive protocol: (a) timed mental-arithmetic task with multiple-choice responses and adaptive question difficulty; (b) color–word Stroop task, in which participants identified the displayed font color rather than the written color word; and (c) post-task feedback screen used to record the participant's experience rating and optional comments.

References

[1] R. M. Torrente-Rodríguez, J. Tu, Y. Yang, J. Min, M. Wang, Y. Song, Y. Yu, C. Xu, C. Ye, W. W. IsHak, W. Gao, *Matter* **2020**, *2*, 4 921–937.

[2] B. Wang, C. Zhao, Z. Wang, K.-A. Yang, X. Cheng, W. Liu, W. Yu, S. Lin, Y. Zhao, K. M. Cheung, H. Lin, H. Hojaiji, P. S. Weiss, M. N. Stojanović, A. J. Tomiyama, A. M. Andrews, S. Emaminejad, *Science Advances* **2022**, *8*.

[3] J. E. An, K. H. Kim, S. J. Park, S. E. Seo, J. Kim, S. Ha, J. Bae, O. S. Kwon, *ACS Sensors* **2022**, *7* 99.

[4] L. Fiore, V. Mazzaracchio, A. Serani, G. Fabiani, L. Fabiani, G. Volpe, D. Moscone, G. M. Bianco, C. Occhiuzzi, G. Marrocco, F. Arduini, *Sensors and Actuators B: Chemical* **2023**, *379* 133258.

[5] N. K. Singh, S. Chung, A. Chang, J. Wang, D. A. Hall, *Biosensors and Bioelectronics* **2023**, *227* 115097.

[6] M. Garg, H. Guo, E. Maclam, E. Zhanov, S. Samudrala, A. Pavlov, M. S. Rahman, M. Namkoong, J. P. Moreno, L. Tian, *ACS Applied Materials & Interfaces* **2024**, *16* 46113.

[7] Y. Chen, Z. He, Y. Wu, X. Bai, Y. Li, W. Yang, Y. Liu, R. Li, *Biosensors* **2025**, *15* 194.

[8] K. Liu, H. Wang, F. Zhu, Z. Chang, R. Du, Y. Deng, X. Qi, *ACS Nano* **2024**, *18* 14207.

[9] Y. Zhou, L. He, L. He, M. Zhang, M. Chen, Y. Wu, L. Qi, L. Qi, B. Zhang, X. Yang, X. He, K. Wang, *Biosensors and Bioelectronics* **2025**, *269* 116935.

[10] C. T. Sharkey, A. F. Aroche, I. G. Agusta, H. E. Nissan, T. Saha, S. Mukherjee, J. Twiddy, M. D. Dickey, O. D. Velev, M. A. Daniele, *Lab on a Chip* **2025**, *25* 4577.

[11] J. W. Kwak, T. Trinh, A. D. White, Y. Chen, N. Eckman, I. Jain, Y. Xu, N. Nguyen, D. Gopalan, Y. E. Kim, N. U. Kamat, J. R. Tumbleston, C. H. Park, A. Yoshikawa, J. Ji, M. T. Dulay, M. Eisenstein, E. A. Appel, J. Kim, J. M. DeSimone, H. T. Soh, *Advanced Materials* **2026**.

[12] S. Sheibani, L. Capua, S. Kamaei, S. S. A. Akbari, J. Zhang, H. Guérin, A. M. Ionescu, *Communications materials* **2021**, *2*.

[13] X. Mei, J. Yang, X. Yu, Z. Peng, G. Zhang, Y. Li, *Sensors and Actuators B: Chemical* **2023**, *381* 133451.

[14] Y. Cheng, S. Feng, Q. Ning, T. Li, H. Xu, Q. Sun, D. Cui, K. Wang, *Microsystems & Nanoengineering* **2023**, *9*, 1.

[15] S. Chakoma, X. Pei, H. Qin, A. Ghandehari, S. Najafikhoshnoo, J. Rajendran, R. Esfandyarpour, *Nano Research* **2024**, *17*, 8 7542–7556.

[16] N. I. Hossain, T. Noushin, S. Tabassum, *Scientific Reports* **2024**, *14*.

[17] C. Wang, Z. Wang, W. Wei, Z. Zhang, A. A. Li, G. Huang, X. Li, S. S. Ge, L. Zhou, H. Kong, *npj Flexible Electronics* **2024**, *8*.

[18] J. Tu, J. Yeom, J. C. Ulloa, S. A. Solomon, J. Min, W. Heng, G. Kim, J. Dao, R. Vemu, M. Pang, C. Wang, D.-H. Kim, W. Gao, *Science Advances* **2025**, *11*, 32.

[19] Y. Liu, X. Su, P. Fan, X. Liu, Y. Pan, J. Ping, *Science Bulletin* **2025**, *70* 2004.

[20] C. Zhao, Q. Liu, J.-Y. Chang, A. Patil, L. Michalek, Y. Wu, Y. Yuan, R. K. Mow, Y. Shi, Y. Yao, K.-J. Hsu, Y. Zheng, Z. Bao, *Science Advances* **2026**, *12*, 23.

[21] X. Pei, A. Ghandehari, S. Chakoma, J. Rajendran, J. A. Tavares-Negrete, R. Esfandyarpour, *Nature Communications* **2026**, *17*, 1150.